Recent Advances in Two-Dimensional Materials beyond Graphene

Ganesh R. Bhimanapati,[†] Zhong Lin,[‡] Vincent Meunier,[∥,■] Yeonwoong Jung,[§] Judy Cha,[⊥] Saptarshi Das,[#] Di Xiao,[▽] Youngwoo Son,[⊗] Michael S. Strano,[⊗] Valentino R. Cooper,[○] Liangbo Liang,[∥,■] Steven G. Louie,[¶,●] Emilie Ringe,[▼] Wu Zhou,[○] Steve S. Kim,[¥,∞] Rajesh R. Naik,[¥] Bobby G. Sumpter,[○] Humberto Terrones,[∥,■] Fengnian Xia,[⊥] Yeliang Wang,[+] Jun Zhu,[‡] Deji Akinwande,[◆] Nasim Alem,[†] Jon A. Schuller,[◇] Raymond E. Schaak,[×] Mauricio Terrones,[†,‡,×] and Joshua A. Robinson*[,†]

[†]Department of Materials Science and Engineering, Center for Two-Dimensional and Layered Materials, Pennsylvania State University, University Park, Pennsylvania 16802, United States, [‡]Department of Physics, Center for Two-Dimensional and Layered Materials, Pennsylvania State University, University Park, Pennsylvania 16802, United States, [§]Nanoscience Technology Center, Department of Materials Science and Engineering, University of Central Florida, Orlando, Florida 32826, United States, [⊥]Department of Mechanical Engineering and Material Science, Yale School of Engineering and Applied Sciences, New Haven, Connecticut 06520, United States, [∥]Department of Physics, Applied Physics, and Astronomy, Rensselaer Polytechnic Institute, Troy, New York 12180, United States, [■]Center for Nanophase Materials Sciences, Oak Ridge National Laboratory, Oak Ridge, Tennessee 37831, United States, [#]Birck Nanotechnology Center & Department of ECE, Purdue University, West Lafayette, Indiana 47907, United States, [▽]Department of Physics, Carnegie Mellon University, Pittsburgh, Pennsylvania 15213, United States, [⊗]Department of Chemical Engineering, Massachusetts Institute of Technology, Cambridge, Massachusetts 02139, United States, [○]Center for Nanophase Materials Sciences and Computer Science & Mathematics Division, Oak Ridge National Laboratory, Oak Ridge, Tennessee 37831, United States, [¶]Department of Physics, University of California at Berkeley, Berkeley, California 94720, United States, [¥]Air Force Laboratory, Materials & Manufacturing directorate, Wright-Patterson AFB, Dayton, Ohio 45433, United States, [∞]UES Inc., Beavercreek, Ohio 45432, United States, [±]Department of Electrical Engineering, Yale University, New Haven, Connecticut 06511, United States, [●]Lawrence Berkeley National Lab, Berkeley, California 94720, United States, [+]Beijing National Laboratory for Condensed Matter Physics, Institute of Physics, Chinese Academy of Sciences, Beijing 100190, China, [▼]Department of Materials Science & Nano Engineering, Rice University, Houston, Texas 77005, United States, [◆]Microelectronics Research Centre, The University of Texas at Austin, Austin, Texas 78758, United States, [◇]Electrical and Computer Engineering Department, University of California at Santa Barbara, Santa Barbara, California 93106, United States, and [×]Department of Chemistry and Materials Research Institute, Pennsylvania State University, University Park, Pennsylvania 16802, United States,

ABSTRACT The isolation of graphene in 2004 from graphite was a defining moment for the "birth" of a field: two-dimensional (2D) materials. In recent years, there has been a rapidly increasing number of papers focusing on non-graphene layered materials, including transition-metal dichalcogenides (TMDs), because of the new properties and applications that emerge upon 2D confinement. Here, we review significant recent advances and important new developments in 2D materials "beyond graphene". We provide insight into the theoretical modeling and understanding of the van der Waals (vdW) forces that hold together the 2D layers in bulk solids, as well as their excitonic properties and growth morphologies. Additionally, we highlight recent breakthroughs in TMD synthesis and characterization and discuss the newest families of 2D materials, including monoelement 2D materials (*i.e.*, silicene, phosphorene, *etc.*) and transition metal carbide- and carbon nitride-based MXenes. We then discuss the doping and functionalization of 2D materials beyond graphene that enable device applications, followed by advances in electronic, optoelectronic, and magnetic devices and theory. Finally, we provide perspectives on the future of 2D materials beyond graphene.

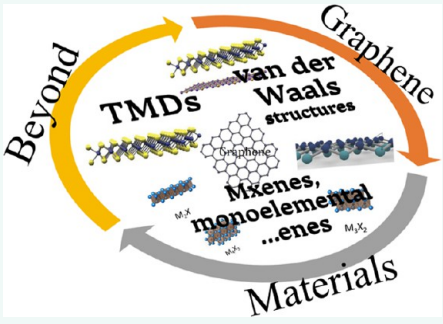

KEYWORDS: two-dimensional materials · graphene · heterostructures · transition metal dichalcogenide · phospherene · silicene · germanene · stanene · van der Waals epitaxy · van der Waals solid

Layered materials have existed for eons,[1] and have been studied scientifically for more than 150 years.[2] However, only recently[3] have we begun to realize the true potential of these systems for advanced technological applications. Each layered material, when thinned to its physical limits, exhibits novel properties different from its bulk counterpart. Therefore, at the physical limit these materials are referred to as two-dimensional (2D) materials. The most highly studied 2D material is graphene because of its exceptional electronic, optoelectronic, electrochemical and biomedical applications. Beyond graphene, there is a very wide spectrum of 2D electronic materials

* Address correspondence to jrobinson@psu.edu.

Received for review September 3, 2015 and accepted November 6, 2015.

Published online November 06, 2015
10.1021/acsnano.5b05556

that range from insulators to semiconductors to metals and even to superconductors. 2D materials research initially focused on graphene following the seminal paper by Novoselov and Geim,[3] but it was also demonstrated very early on that other 2D materials also possess exciting properties.[4] Following graphene, 2D hexagonal boron nitride (hBN) was theoretically predicted to induce a bandgap in graphene when graphene was deposited onto it.[5] This led to a significant increase in hBN experimental research, and ultimately to an understanding that hBN may be an ideal substrate for graphene electronics.[6] Rapidly following graphene and hBN, research on semiconducting 2D layers provided evidence that the band structure of a subset of the 2D materials family changes drastically as they are thinned to monolayer thickness.[7] Device fabrication further ignited the interest of many in the electronics community.[8] These novel semiconducting 2D materials, known as transition-metal dichalcogenides (TMDs), are now a primary focus of many researchers, as clearly evidenced by the publication record devoted to such materials (Figure 1). There are many layered materials that go beyond TMDs, including monochalcogenides (GaSe, *etc.*), monoelemental 2D semiconductors (silicene, phosphorene, germanene), and MXenes (Figure 1). Finally, the true potential of these layered materials may emerge from the ability to stack them, layer-by-layer in

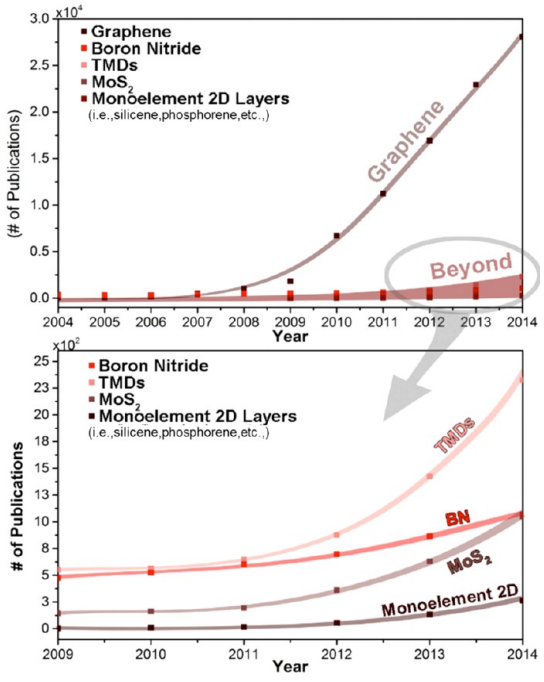

Figure 1. Publication trends in 2D materials beyond graphene. Source: Web of Science. Search index: [Title search (*x*) or title (*y*) and topic (*z*), where *x* = graphene, boron nitride, transition metal chalcogenides, molybdenum disulfide or monoelements (silicene, germanene, phosphorene, stanene or borophene), *y* = graphene or BN or TMDs or MoS_2) and *z* = graphene or boron nitride or transition metal chalcogenides (TMDs: MoS_2, WS_2, $MoSe_2$, WSe_2, TaS_2, $TaSe_2$, NbS_2), MoS_2 or monoelement 2D: silicene, germanene, stanene, borophene, phosphorene.].

VOCABULARY: **$(NH_4)_2MoS_4$** - ammonia tetra thiomolybdate; **2D** - two-dimensional; **3D** - three-dimensional; **ADF** - annular dark field; **Ag** - silver; **AHM, $(NH_4)_6Mo_7O_{24}\cdot 4H_2O$** - ammonium heptamolybdate; **ALD** - atomic layer deposition; **ARPES** - angle resolved photoemission spectroscopy; **Au** - gold; **$AuCl_3$** - gold chloride; **BP** - black phosphorus; **BV** - benxyl viologen; **C** - carbon; **CF_3** - carbon tetrafluoride radical; **CH_3** - methyl radical; **CL** - cathodoluminescence; **Cl** - chlorine atom; **Cl_2** - chlorine; **Co** - cobalt; **CrI_3** - chromium iodide; **$CrSiTe_3$** - chromium silicon telluride; **Cs_2CO_3** - cesium carbonate; **CVD** - chemical vapor deposition; **DCE** - 1,2-dichloroethane; **DF** - density functional; **DFPT** - density functional perturbation theory; **DFT** - density functional theory; **DMC** - diffusion quantum Monte Carlo; **DNA** - deoxy ribonucleic acid; **EELS** - electron energy loss spectroscopy; **EG** - epitaxial graphene; **FET** - field effect transistor; **GaAlAs** - gallium aluminum arsenide; **GaAs** - gallium arsenide; **GaN** - gallium nitride; **GaSe** - gallium selenide; **Ge** - germanium; **GW-BSE** - GW plus Bethe Salpeter equation; **H_2O** - water; **H_2S** - hydrogen sulfide; **hBN** - hexagonal boron nitride; **HF** - hydrogen fluoride; **$HfSe_2$** - halfnium selenide; **HRTEM** - high resolution transmission electron microscopy; **In_2Se_3** - indium selenide; **K** - potassium; **LED** - light emitting diodes; **Li** - lithium; **LSPR** - localized surface plasmon resonance; **LSPR** - localized surface plasmon resonance; **MBE** - molecular beam epitaxy; **Mn** - manganese; **Mo** - molybdenum; **$MoCl_5$** - molybdenum chloride; **MOCVD** - metal organic chemical vapor deposition; **MoO_3** - molybdenum(VI) oxide; **MoS_2** - molybdenum disulfide; **$MoSe_2$** - molybdenum diselenide; **Na** - sodium; **NADH** - nicotinamide adenine dinucleotide; **NbS_2** - niobium disulfide; **NH_2** - ammonia radical; **NO_2** - nitrogen dioxide; **O_2** - Oxygen; **OLED** - organic light emitting diode; **OTS** - Octadecyltrichlorosilane; **PDMS** - polydimethylsiloxane; **PEI** - polyethylenimine; **PL** - Photoluminescence; **PMMA** - poly methyl methacrylate; **PTAS** - perylene-3,4,9,10- tetracarboxylic acid tetrapotassium salt; **p-TSA** - *p*-toluene sulfonic acid; **PVA** - poly vinyl alcohol; **QC** - quantum chemical; **QFEG** - quasi-free-standing epitaxial graphene; **QSHE** - quantum spin hall effect; **S** - sulfur; **SAMs** - self-assembled monolayers; **SBs** - Schottky barriers; **Sc** - scandium; **Se** - selenium; **SERS** - surface enhanced Raman spectroscopy; **Si** - silicon; **SiC** - silicon carbide; **SiO_2** - silicon dioxide; **Sn** - tin; **SnS_2** - tin sulfide; **$SnSe_2$** - tin diselenide; **SO** - spin orbit; **SPR** - surface plasmon resonance; **STEM** - scanning transmission electron microscopy; **STM** - scanning tunneling microscopy; **STMDs** - semiconducting transition metal dichalcogenides; **STS** - scanning tunneling spectroscopy; **$TaSe_2$** - tantalum diselenide; **TCNQ** - 7,7,8,8- tetracyanoquinodimethane; **TEM** - transmission electron microscopy; **TFT** - thin film transistors; **TMDs** - transition metal dichalcogenides; **TOF-SIMS** - time-of-flight- secondary ion mass spectroscopy; **UHV** - ultra high vacuum; **vdW** - van der Waals; **W** - tungsten; **WO_3** - tungsten(VI) oxide; **WS_2** - tungsten disulfide; **WSe_2** - tungsten diselenide;

any desired sequence, to create novel three-dimensional (3D) architectures with entirely new functions.

In the following pages, we present a forward-looking review of recent advances in the field of 2D materials beyond graphene. Because the field is developing very rapidly, this review aims to summarize only the most recent advances in 2D theory, synthesis, characterization, and devices. Earlier developments were captured in prior reviews.[9−19]

MODELING GROWTH MORPHOLOGY

Growth of single-layer materials typically yields small (few to hundreds of micrometers) single crystals with well-defined shapes, typically triangular. At such length scales, the particle morphology can influence many of their properties; hence morphology becomes a key factor in engineering new nanostructures with controllable functions. In this section, tools that help understand, describe and potentially predict shape based on thermodynamic and kinetic arguments are discussed.

Analogous to the highly size- and shape-dependent localized surface plasmon resonance (LSPR) phenomenon in metallic nanostructures, the photoluminescence of graphene quantum dots has been shown to vary with size[20] and shape.[21] Also, analogous to metal nanocrystals, a number of approaches exist to understand morphology in terms of thermodynamic properties and/or growth kinetics. In crystals, the famous Wulff construction[22−24] and its twinned,[25] alloyed,[26] supported,[27,28] and kinetic[29,30] derivatives provide a full toolbox to understand the origin of the overall particle shape. Such constructions relate the relative expression of each crystallographic facet to its surface energy or growth velocity: the higher the surface energy, the least a facet is expressed, resulting in the dominant facet being that with the lowest energy. The direct analogue for 2D materials uses the edge energy or edge growth velocity. The higher the edge energy, the least likely it is to be present. Because these constructs relate easily observable and quantifiable values (relative surface expression) to important yet often intractable parameters (growth velocity, surface/interface energy), Wulff constructions are extremely helpful for interpreting and predicting experimental outcomes.

A number of novel 2D materials are generally more complex than graphene, and chemical termination now plays a significant role. In hBN, for example, zigzag edges can be B- or N-terminated while the composition of the armchair edge is stoichiometric. Controlling the chemical potential in the reaction leads to a continuous crystal shape transition from triangle to hexagon to inverted triangle, and a concurrent change of magnetic properties in embedded systems.[31] Preferential edge orientation and composition are also critical in the design of functional TMDs, where edges have been shown to dominate catalytic activity.[32,33] Finally, very recently Cao *et al.*[34] applied Wulff constructions to elucidate the shape, edge, and magnetism evolution of monolayer MoS_2 (Figure 2) as a function of chemical potential from the Mo-rich to the S-rich condition. The findings can be applied to explain extensive experimental observations about the morphology of MoS_2 domains. Much work remains to be done in understanding the composition (and properties) of the edges in 2D materials, and Wulff constructions applied in 2D seem to constitute an attractive approach that, with time, will move from a theory tool to a routine experimental data analysis approach.

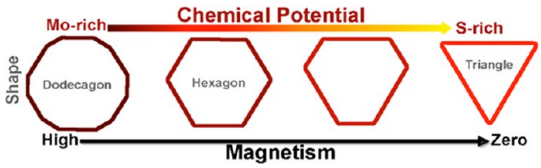

Figure 2. Simplified morphology and magnetism schematic of MoS_2 as a function of chemical potential (Mo to S-rich), calculated using Wulff constructions. Adapted from ref 34. Copyright 2015 American Chemical Society.

MODELING VDW INTERACTIONS IN LAYERED MATERIALS

The mechanical separation of graphite to produce single (or a few) layers of graphene is a profound illustration of the importance of vdW forces in defining the structure and function of 2D materials.[3] The enormous variability in stacking sequences of 2D layered materials and the closeness of their corresponding cohesive energies with those of dense structures further emphasizes the role vdW forces play in the design and discovery of new 2D materials.[35,36] As such, first-principles methods that can model dense and sparse matter on the same footing are paramount not only to the discovery and design of new 2D materials, but also for developing our understanding and control of growth morphology.

Advances in high performance computing and mathematical algorithms have made highly accurate diffusion quantum Monte Carlo (DMC) calculations (Figure 3) for interlayer binding energies in layered materials possible.[37,38] Such studies have allowed for an understanding of the intercalation of metal cations at the surface of or between carbon-based structures such as graphene bilayers,[37] thus representing a new era in our understanding of the electronic origins of dispersion interactions.

Despite the reliability and accuracy of quantum chemical (QC) and DMC calculations, DFT still remains the workhorse for exploring larger, more complex systems with significant atomic relaxations such as the dichalcogenides and related vdW-heterostructures, thus placing the focus on correcting current deficiencies within the method. New techniques run the gamut

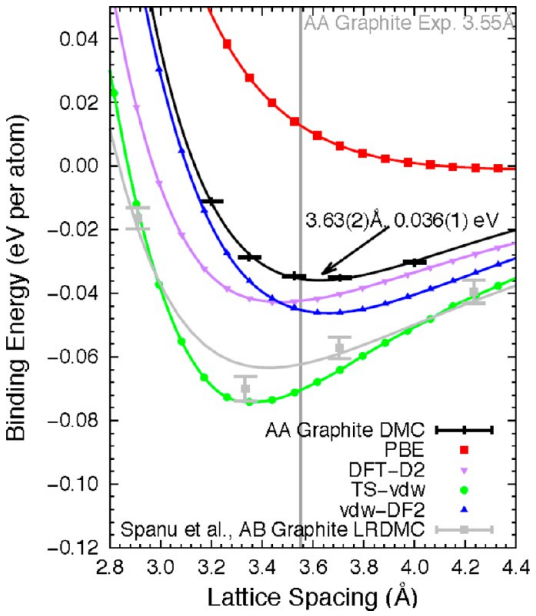

Figure 3. Calculated binding energies of AA stacked graphite as a function of interplanar lattice separation obtained from different density functionals and for DMC simulations. The self-consistent vdW functional vdw-DF2 shows good accuracy. Adapted with permission from ref 57, Copyright 2010 Materials Research Society.

from postprocessing, semiempirical, pairwise corrections[39−44] to the development of new, self-consistent, correlation functionals[45−52] and many-body approaches,[53−55] each having varying degrees of computational demands and transferability and with successive developments approaching chemical accuracy.[56−63]

These modern DFT-based approaches are now mature enough, that with proper caution, it is possible to use theory to explore the classes of layered materials where vdW interactions are intrinsically important, and thereby placing us on the verge of a new era in computational aided materials research. Such methods provide tools for the discovery of new 2D materials that have yet to be synthesized. Of fundamental importance is the ability to assess the energetic and dynamic stability of candidate materials. Recent efforts have demonstrated that the inclusion of dispersion interactions through a nonlocal correlation term (as is done in the Rutgers-Chalmers vdW density functional; vdW-DF[46−49]) can be critical in assessing these energies relative to bulk materials and can guide the discovery of novel 2D materials.[64−66] Related to this is the cleavability of a material, i.e., the ability to separate/isolate individual layers of a material. In most 2D materials, this is solely defined through the vdW interactions that occur between layers. Again, such methods are fundamental in computing the relevant energy scales involved in this interaction,[67,68] thus leading to the prediction of a candidate material for realizing 2D magnetism.[68]

As discussed in this review, the ability to grow novel 2D materials has seen tremendous progress over the past decade. In many cases, the substrate may have significant effects on the fundamental properties of the 2D materials. The incorporation of dispersion interactions with DFT has made it possible not only to more accurately study these effects, but also to discern which substrates can be used to control materials properties. A profound example of the effects of substrate on 2D material properties is silicene and germanene. Free standing silicene, like graphene, is predicted to have a Dirac cone band structure. Early angle resolved photoemission spectroscopy (ARPES) results for silicene on Ag(111)[69] suggested that the Dirac cone would remain despite the buckling of Si atoms. Subsequent theory was fundamental in demonstrating that in fact the linear bands were due to new states arising due to hybridization between Ag and silicene.[70] Since then, much effort has been placed on understanding the effects of different substrates on the electronic structure of 2D materials. Such efforts have relied on the inclusion of dispersion interactions in DFT approaches either through self-consistent methods (as in vdW-DF) or through additive terms (*e.g.*, the DFT-D2 assumes that the interactions between molecules or atoms are through the addition of semiempirical pairwise corrections (*e.g.*, Lennard-Jones type potentials) based on molecular C6 coefficients).[39−42,52] These methods have identified a number of suitable substrates for the growth of 2D materials that allow for better control of material properties.[71−73] In all cases, it has been demonstrated that growth on a vdW bonded material may be fruitful for truly retaining a 2D materials' free-standing properties. Furthermore, the role of dispersion interactions is invaluable. Not only is it useful for understanding the stability of a layered material adsorbed onto a substrate by dispersion interactions, but DFT methods which include dispersion interactions are now being employed to understand the fundamental interactions of precursor materials.[74,75] These can be used to optimize the growth process thus allowing for the controlled growth of new and interesting materials.

Regardless of which method is used for treating intermolecular vdW interactions, one thing is certain, the inclusion of vdW interactions is paramount to our ability to properly simulate and understand layered materials. Not only is this important for understanding binding, adsorption, and intercalation tin, but also when trying to understand relevant experimental signatures[76] due to interlayer lattice vibrational modes.[77−84] Thus, with continued progress in the development of first-principles methods that can accurately account for vdW interactions, it may be possible to truly discover and design novel 2D materials that may be experimentally realizable.

MODELING ELECTRON INTERACTIONS AND EXCITONIC EFFECTS IN 2D TMDS

An exciton describes a two-particle excitation with simultaneous creation of both an electron and a hole.

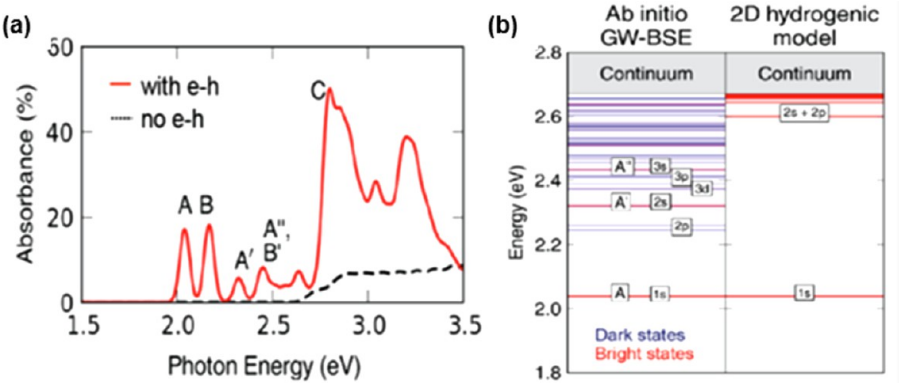

Figure 4. (a) Calculated absorbance of monolayer MoS_2 with (red line) and without (black dashed line) electron–hole interactions included, using the *ab initio* GW-BSE approach. A broadening of 20 meV is used to prepare the curves. There are three series of exciton states: A, B and C, and (b) energy levels of the A series excitons in monolayer MoS_2 from *ab initio* GW-BSE calculations (left panel) and from a 2D hydrogenic model (right panel). Adapted with permission from ref 58, Copyright 2009 *J. Phys. Org. Chem.*

Semiconducting TMD layers exhibit dramatically strong light-exciton interactions and greatly enhanced electron–electron interactions. Exciton binding energies in monolayer TMD materials can be hundreds of millielectronvolts (meV),[85−90] orders of magnitude larger than what is seen in typical bulk semiconductors. Such excitonic effects dominate the optical response in TMD mono- and few-layers, and create new opportunities for basic science studies and novel optoelectronic applications.

First-principles calculations based on the GW and GW plus Bethe Salpeter equation (GW-BSE) methods[91,92] on various quasi-2D TMDs (such as MoS_2, $MoSe_2$, and WSe_2) predicted that TMD monolayers can have multiple series of excitons, arising from different regions of the Brillouin zone, with binding energies in excess of 0.6 eV and unusual excitation spectra (optically bright and dark excited states of novel energy level and orbital-angular-momentum dependence) that cannot be explained by the usual 2D hydrogenic model (Figure 4a,b).[85,89,90] These extraordinary features originate from enhanced Coulomb interactions owing to reduced dimensionality and, importantly, an incomplete and strongly spatial-dependent screening in quasi-2D systems.[85,86,89,90] The *ab initio* calculations further revealed that, despite their large binding energies, the TMD excitons are of the Wannier type with wave functions that are very extended in real-space, but localized in k-space.[85]

The large exciton binding energy in monolayer $MoSe_2$ has been confirmed by combining scanning tunneling spectroscopy (STS), optical spectroscopy, and GW-BSE theory.[90] The electronic band gap is given by single-particle excitations (sum of the energy for creating an isolated electron and an isolated hole). Furthermore, two-photon excitation spectroscopy has been used to investigate the novel excitonic level structure of monolayer WS_2, including dark states.[89] These measurements probed the optically inactive exciton 2p and 3p excited states, and show excellent agreement with theoretical predictions,[89] both in their energies and ordering with respect to other orbital angular momentum exciton states. Another important and interesting aspect of the electronic and optical properties of TMD layers is that, owing to their quasi-2D atomic structure, they are very sensitive to environment screening. Both the electronic bandgaps and exciton binding energies can change substantially depending on the supporting substrates, as demonstrated in ref.[90]

LARGE-AREA, MORPHOLOGY-CONTROLLED SYNTHESIS OF TMDS

Two-dimensional TMDs have been realized by various synthetic methods, including vapor-phase chemical reactions, wet-chemical synthesis, and liquid exfoliations.[93−95] Vapor deposition techniques have been most extensively explored due to their potential for high scalability and morphological control. In this process, metal containing precursors [*e.g.*, MoO_3, WO_3, or $(NH_4)_2MoS_4$][95] are vaporized and reacted with chalcogen elements through vapor–solid reactions, leading to the growth of 2D TMDs on a substrate downstream. Most common procedures rely on the coevaporation of metal and chalcogen precursors both initially in solid phases. These techniques generally yield 2D TMDs with limited spatial homogeneity and uncontrolled morphologies due to the difficulty with controlling growth variables for vaporized reactants. Opposite to the commonly used solid-phase chalcogen elements, gas-phase chalcogen reactants such as hydrogen sulfide (H_2S) have been used to improve the scalability and uniformity of 2D MoS_2[19] Also, the synthesis of nanocrystalline 2D MoS_2 with controlled layer numbers has been demonstrated on the centimeter scale *via* the sulfurization of molybdenum chloride ($MoCl_5$) precursors[96] The success for the improved scalability is attributed to the balance control between the partial pressure of vaporized MoS_2 and its

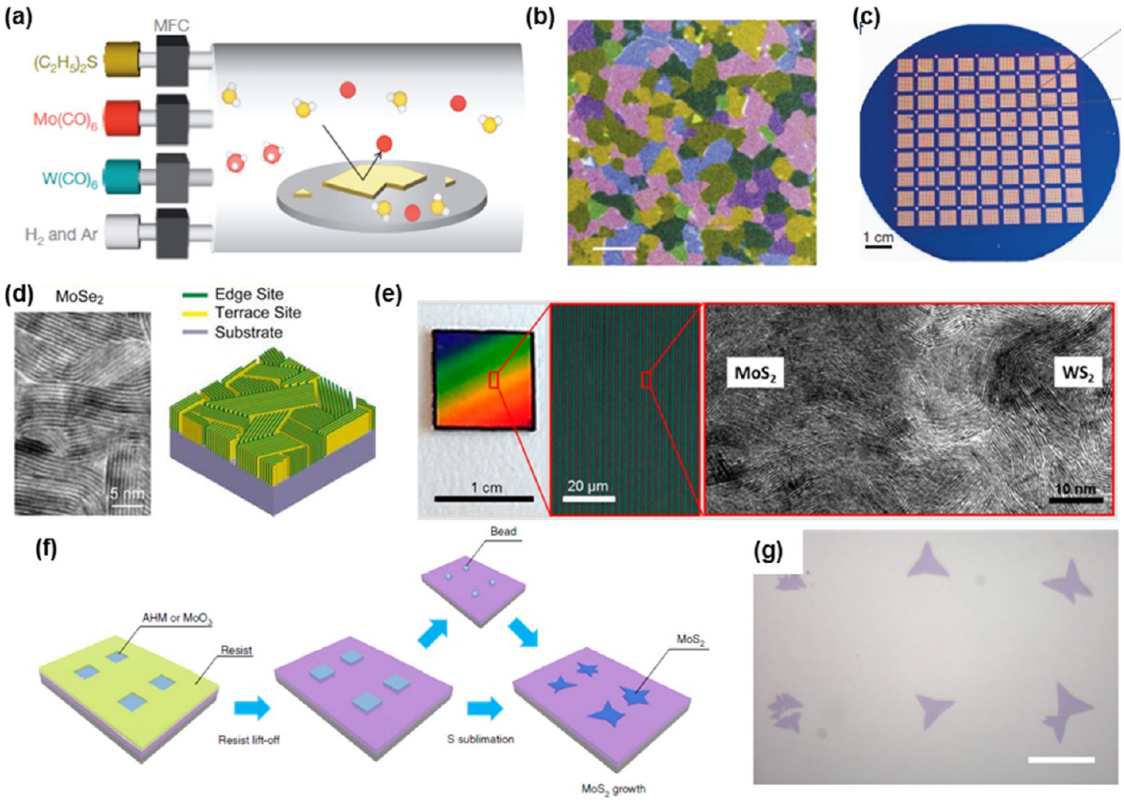

Figure 5. Synthesis of various 2D TMDs. (a) Schematic for the MOCVD process. Adapted with permission from ref 114. Copyright 2015 Nature Publishing Group. (b) False color dark-field TEM image showing continuous 2D monolayer MoS_2. Adapted with permission from ref 114. Copyright 2015 Nature Publishing Group). (c) Four-inch wafer scale batch fabrication of 2D monolayer MoS_2 electronic devices. Adapted with permission from ref 114. Copyright 2015 Nature Publishing Group. (d and e) Synthesis of 2D TMDs with vertically standing 2D layers. (d) 2D $MoSe_2$ with vertically standing 2D layers. Adapted with permission from ref 32. Copyright 2007 AAAS. (e) Large-scale controlled synthesis of 2D MoS_2/WS_2 with vertically standing 2D layers. Adapted with permission from ref 33. Copyright 2014 Royal Society of Chemistry. (f and g) Site-specific synthesis based on CVD processes on patterned seed layers. Adapted from ref 37. Copyright 20l4 American Chemical Society. (f) Schematics for synthesis and (g) site-specifically synthesized 2D MoS_2.

equilibrium pressure.[18] Moreover, predeposition of elemental metals on growth substrates and their subsequent reactions with chalcogen vapors have been demonstrated to yield large-area 2D TMDs.[97−104] The major advantage of this approach is the morphology and the coverage control of 2D TMDs enabled by metal deposition methods. The goal of uniformity was further extended *via* seed-promoting molecules such as perylene-3,4,9,10-tetracarboxylic acid tetra-potassium salt (PTAS).[105,106] The high solubility of PTAS in water enhances the seed solution to be uniformly distributed on hydrophilic substrate surfaces on a large scale. Another such technique to grow high quality, precisely doped electronic grade 2D materials with abrupt interfaces is through molecular beam epitaxy (MBE).[107−112] With the availability of *in situ* characterization during the growth, MBE particularly has an advantage of having precise thickness control and the ability to grow on 2D or 3D substrates. Finally, very recently, metal−organic CVD (MOCVD) based on gas-phase precursors[113−115] has proven that large-scale growth of 2D TMDs is readily achievable, with the most impressive demonstration being a 100 mm wafer of monolayer MoS_2 with uniform electrical properties (Figure 5a−c).[114] In addition to scalable growth, the synthesis of 2D TMDs with controlled orientation, layer number, chemical composition, and placement have been extensively pursued. CVD based on the thermal evaporation of elemental metal seed layers has demonstrated the growth of 2D TMDs in two distinct 2D layer orientations of vertical and horizontal (Figure 5d,e).[99,116,117] The thickness of the metal seed layers was identified to be the critical parameter to dictate the 2D layer growth orientation.[99] The chemical composition of 2D TMDs can also be controlled by simultaneously reacting multiple metal precursors with multiple chalcogen elements in vapor phases. For example, alloyed 2D monolayer of various compositions such as $Mo_xW_{1-x}S_2$[118,119] and MoS_xSe_{2-x}[120−122] have been synthesized, which present tunable band gap energies with varying ratios of elements. The control of the stoichiometric variations in MoS_2 have been demonstrated to provide tunable electrical and optical properties.[123−125] In addition to the chemical compositions control during growths, postgrowth processes have also been developed to convert the chemical composition of 2D TMDs after

their growths. For example, ion-exchange reactions have been applied to convert 2D MoS_2 into 2D $MoSe_2$, consequently tuning their opto-electrical properties.[126,127] Selective area growth of 2D materials has also recently been realized, in part, using a spin-coated ammonium heptamolybdate [AHM, $(NH_4)_6Mo_7O_{24}\cdot 4H_2O$] and pregrowth lithographic techniques to achieve site-specific, patterned growth of 2D MoS_2 (Figure 5f,g).[128] Finally, 2D MoS_2 with site-specifically controlled layer numbers has been demonstrated on a single SiO_2 growth substrate by modifying the surface properties of the SiO_2 *via* plasma etch treatments.[129] Despite the modest success in improving scalability and uniformity, the chemically synthesized large-area 2D TMDs at present still exhibit electrical properties far from what are demanded for realistic applications. For example, the room temperature field-effect-transistor (FET) mobility of state-of-the art 2D MoS_2 grown on a 4-in. wafer with uniform layer numbers is $\sim 30\ cm^2\ V^{-1}\ s^{-1}$,[114] an order-of-magnitude smaller than those of mechanically exfoliated materials. Such limitation is attributed to the defective nature of chemically synthesized materials: intrinsic defects (*e.g.*, vacancies) in individual 2D grains as well as interfacial defects (*e.g.*, grain boundaries) across individual 2D grains. Further information on the growth of different TMDs using different techniques is summarized in Table 1. Here, mechanical exfoliation includes scotch tape exfoliation and chemical vapor transport. Powder vaporization covers the general CVD techniques that are based on powder transport to grow 2D materials on various substrates.

SYNTHESIS OF 2D-TMD HETEROSTRUCTURES

Developing new hybrid materials by combining 2D layered materials in vertical stacks offers an enormous amount of possibilities to broaden the versatility of 2D materials, allowing for achieving superior and unusual material properties that cannot be obtained otherwise.[199] Thus, securing robust methods that enable controlled stacking of a variety of 2D materials with any desired combination and thicknesses will play a key role for 2D materials to be widely used, in particular, in transparent and flexible electronic and optoelectronic device applications. Many of these structures are summarized in Table 1, where a commonly used scheme to fabricate 2D heterostructures such as MoS_2/WSe_2,[140,142] MoS_2/WS_2,[200] $MoS_2/MoSe_2$,[201] and $MoSe_2/WSe_2$[202] is the mechanical transfer of separately exfoliated 2D crystals.[143,147,149,203] However, despite the relatively high quality crystals, the dry transfer method may not be suitable when sophisticated control of lattice orientation is required and can introduce various adsorbates, such as hydrocarbons, trapped between layers during the process that may deteriorate the interface quality between the layers.[204] As a result, it is very advantageous to develop techniques capable of directly synthesizing these heterostructures. Vertically stacked 2D TMD/graphene[180,181,187,205−207] heterostructures (Figure 6a−c) have been synthesized by the sequential growth of 2D TMDs on top of preexisting graphene (or hBN[208]). Additionally, a variety of 2D TMD-only heterostructures have also been demonstrated, including heterostructures with vertically standing 2D layers such as MoS_2/WS_2 (or $MoSe_2/WSe_2$) synthesized by the one-step sulfurization (or selenization) of elemental metals.[117,209] In-plane 2D heterostructures have been more challenging to synthesize as the formation of alloyed structures is thermodynamically favored. Recently, in-plane heterostructures in lateral and vertical orientations have been demonstrated by the sequential *in situ* vapor−solid reactions,[189,190] or by the coreaction of

TABLE 1. Table showing the diffreent TMDs Grown To-date Using Various Techniques[a,b]

Technique		Mono- and few-layer materials available to date					Achievements	Challenges
		Single phase TMD	*TMD alloy*	*Doped TMD*	*Vertical heterostructures*	*Lateral heterostructures*		
Top-down	Mechanical exfoliation (and CVT)	1T, 2H MoX_2 1T, 2H WX_2 BP,SnX_2, 1T, 2H $(Nb,Ti,Zr,Nb,Ta)X_2$	$Mo_xW_{1-x}S_2$ $Mo_xW_{1-x}Se_2$	Au-doped MoS_2, Re-doped MoS_2, Nb-doped MoS_2	2H (MoS_2-WS_2), 2H (MoS_2-WSe_2), 2H MoS_2-graphene, 2H WS_2-graphene, 2H MoX_2-hBN,2H WX_2-hBN, 2H WSe_2-1T $SnSe_2$, 2H MoS_2-BP	-	High crystallinity	Thickness control, yield, not scalable
	Liquid exfoliation	1T,2H MoX_2 1T,2H WX_2 2H TiS_2,2H TaS_2, $(Nb,Ti,Zr,Nb,Ta)X_2$	-	-	-	-	High scalability	Small crystallites, thickness control, yield.
Bottom- up	Powder Vaporization	1T, 2H MoX_2 1T, 2H WX_2	MoS_xSe_{2-x} $Mo_xW_{1-x}S_2$	Mn-doped MoS_2 Co-doped MoS_2	1T MoX_2-2H MoX_2, 2H MoX_2-2H WX_2,2H MoS_2-BP, 2H MoX_2-GR, 2H WX_2-GR, 2H MoS_2-2H WSe_2-GR, 2H WS_2-hBN, 2H MoS_2-SnS_2, 2H WS_2-SnS_2, 2H WSe_2-SnS_2	Graphene-hBN, 1T MoS_2-2H MoS_2, 2H MoS_2-WS_2 2H MoX_2-2H MoX_2 2H WX_2-2H WX_2	High scalability	Defect control, uniformity, stoichiometry control
	MOCVD	1T MoX_2, WX_2	-	-	MoS_2-WSe_2-graphene	-	High scalability	Defect control
	MBE	2H $MoSe_2$ 2H WSe_2 1T $PtSe_2$	-	-	$MoSe_2$-graphene	-	High scalability	Defect control, domain size

X- S,Se, BP- Black phosphorous, GR- graphene

[a] X, S, Se; BP, black phosphorus; GR, graphene ribbons. [b] References 7, 39, 90, 96, 99, 105, 106, 113, 114, 119, 121, 126, 130−198, 400.

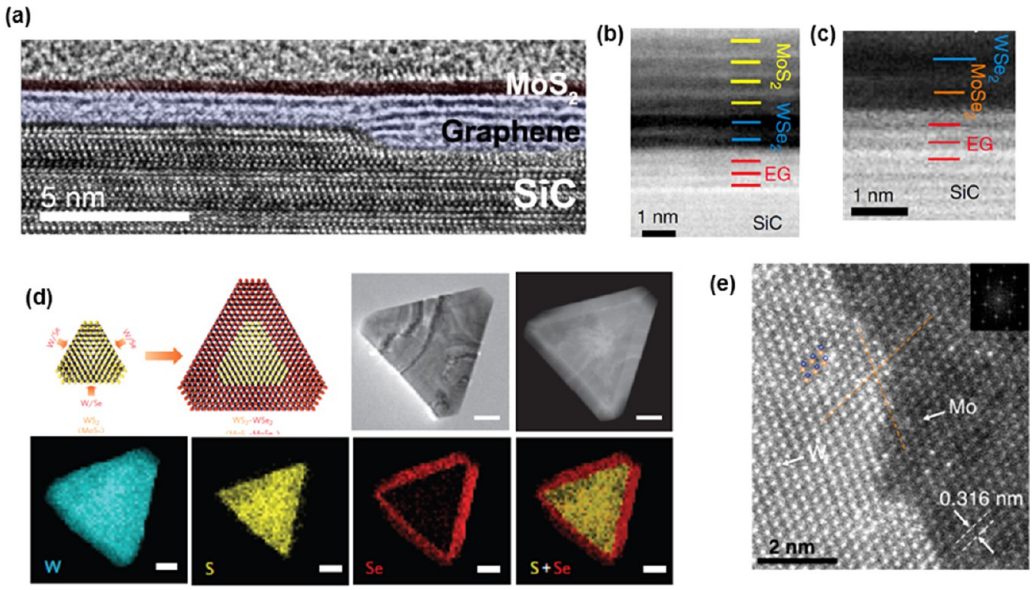

Figure 6. Synthesis of 2D TMD heterostructures. (a) Cross-sectional HRTEM of MoS_2/Quasi-free-standing epitaxial graphene (QFEG) showing the nucleation and subsequent lateral growth of MoS_2 on a SiC step edge covered with the top graphene layer is flat. (b and c) Scanning TEM images of stacked MoS_2−WSe_2−EG vertical stacked heterostructures showing pristine interfaces with no intermixing of Mo−W or S−Se after synthesis. (d) 2D monolayer MoS_2/WS_2 heterostructures with lateral hetero interfaces. Synthesis schematic and chemical composition analysis.[79] (e) HRTEM image showing the hetero interface of 2D monolayer MoS_2/WS_2. Adapted with permission from ref 81. Copyright 2013 American Physical Society.

Mo and W-containing precursors with chalcogens (Figure 6d,e).[173,175,190,210,211] Postgrowth processes based on ion-exchange reactions have also been employed to develop 2D heterostructures. For example, an exchange of Se ions with S ions on pre-existing $MoSe_2$ has been demonstrated to site-specifically convert $MoSe_2$ into MoS_2 realizing in-plane 2D $MoSe_2$/MoS_2 heterostructures.[127] Finally, the epitaxy of MoS_2, WS_2, and WSe_2 on SnS_2 microplates was also demonstrated under mild experimental conditions (450 °C for 2−6 min), using $MoCl_5$/S, WCl_6/S and Se as precursors, respectively.[188] Despite significant lattice mismatch at the interface with SnS_2, 15%, 16%, and 11% for MoS_2, WS_2, and WSe_2, respectively, the heterostructure can successfully form without a significant strain due to relatively weak vdW forces at the interface. At present, the synthesis of all the above-mentioned 2D heterostructures has been limited to very small areas. More effort should be focused in the direction to produce scaled-up 2D heterostructures while maintaining their atomically seamless heterointerfaces.

DOPING AND CHEMICAL FUNCTIONALIZATION OF TMDS

For versatile use of 2D materials in next-generation electronics and optoelectronics, development of controllable doping processes for tailoring their carrier types and Fermi levels is critical given the necessity of, for example, Schottky barrier modulation at TMD/metal junctions and realization of appropriate junctions. However, the traditional doping methods including dopant diffusion and ion-implantation used for conventional bulk semiconductors are not suitable for atomically thin 2D layers due to unavoidable crystal damage during the process. As a result, chemistries typically conducted on organic molecules and surfaces have thus been tried as a starting point for chemical functionalization in pursuit of simple and efficient routes for electronic and optical modulation. The motivations for chemical modification of 2D layers other than doping level tuning include opening an electronic band gap, charge storage, chemical and biological sensing, making new composite materials, and so on.

Similar to graphene,[212−214] various chemical approaches have been adopted to systematically tune electronic and optical characteristics of TMDs by modulation of the charge carrier type and concentration. These efforts have mostly been focused on single- and multilayers of MoS_2, $MoSe_2$, WS_2 and WSe_2, through physisorption of molecules,[215,216] metallic nanoparticles surface functionalization,[217,218] solution-based functionalization,[218−220] and plasma-assisted doping.[221,222] The molecular physisorption can offer wide-range control of charge density, thereby modulating optical properties such as the photoluminescence (PL) processes. Tongay *et al.*[216] have shown that the light emission efficiency in 2D TMDs (MoS_2, $MoSe_2$ and WSe_2) is largely modulated by charge transfer with physically adsorbed electronegative gaseous molecules including O_2 and H_2O, and over a 100-fold modulation in the efficiency was achieved, while inert gases have exhibited a negligible effect. Physisorbed O_2 and H_2O molecules electronically depleted n-type

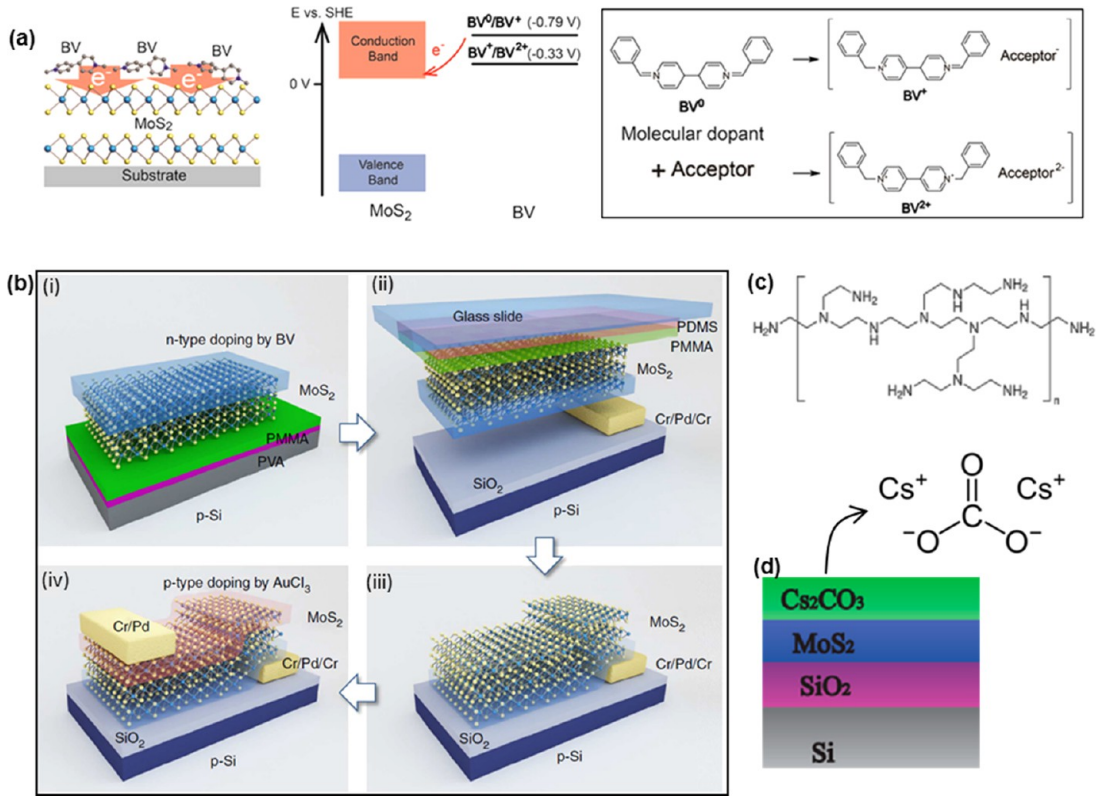

Figure 7. (a) Schematic of BV surface doping of MoS_2, an energy band diagram of MoS_2 and BV redox states, and redox reactions of the BV molecule when adsorbed on an acceptor material, MoS_2. Adapted from ref 223. Copyright 2014 American Chemical Society. (b) Fabrication of chemically doped vertical p−n homogeneous junction in a few-layer MoS_2 flake. (i) A MoS_2 flake was transferred on a PMMA/PVA/Si substrate, and then BV-doped and annealed. (ii) After dissolving the PVA layer in deionized water, the PMMA film supporting a MoS_2 flake was transferred to a PDMS/glass substrate. (iii) The MoS_2 flake was stamped on the SiO_2/Si substrate, and the n-doped surface was aligned with the Cr/Pd/Cr bottom electrode prepared in advance. (iv) After $AuCl_3$ doping and annealing, the vertical p−n junction in the MoS_2 flake was formed, followed by the deposition of a Cr/Pd top electrode. Adapted with permission from ref 224. Copyright 2015 Nature Publishing Group. (c) Structure of amine-rich PEI as n-type dopants for multilayer MoS_2 FETs. Adapted with permission from ref 219. Copyright 2013 IEEE. (d) Schematic illustration of the MoS_2 FET layout with Cs_2CO_3 film on top. Adapted from refs 217 and 229. Copyright 2014 and 2013, respectively, American Chemical Society.

materials such as MoS_2 and $MoSe_2$, and resulted in drastic enhancement in PL; however, in p-type WSe_2, the opposite effect was observed. NO_2 molecules can also be utilized as a p-type dopant for 2D TMDs. When WSe_2 is exposed to NO_2 environment in N_2 gas, NO_2 could physically and chemically adsorb on the WSe_2 surface and transfer electrons from WSe_2 due to its strong oxidizing property.[215] The doping effect on MoS_2 through electronic beam (e-beam) deposition of metallic nanoparticles of noble metals (Au, Ag, Pd, Pt) is also investigated where p-type doping was observed which exhibited increasing trend with metal work functions for varying dose of nanoparticles. In addition, Mouri *et al.*[218] used F_4TCNQ and 7,7,8,8-tetracyanoquinodimethane (TCNQ) as p-type chemical dopants, and nicotinamide adenine dinucleotide (NADH) as n-type dopants to effectively tune the PL of monolayer MoS_2; the enhancement in PL intensity was observed upon the adsorption of the p-type dopants, while the n-type dopants weakened the intensity. P-type dopants extract electrons from the MoS_2 such that the recombination of excitons becomes a dominant process instead of that of negative trions, while this switching of the mechanism is suppressed by n-type dopant molecules.[218]

Organic compounds, such as benzyl viologen (BV), can form an electron transfer complex to n-dope MoS_2 *via* surface charge transfer mechanism.[223,224] The BV-doped MoS_2 exhibits excellent stability in ambient air (with only a minimal change in the electrical characteristics after 9 days of air exposure), and an electron sheet density of $\sim 1.2 \times 10^{13}$ cm^{-2} is achieved that corresponds to the degenerate doping limit for MoS_2.[223] The neutral BV molecule transfers electrons to MoS_2, and eventually a two-electron transfer process is carried out between the two materials (Figure 7a). The doping process is reversible, which can be valuable not only for selective removal of the molecule for patterned doping, but also for the controlled modulation of charge carrier density, such that the BV molecules are removed from the MoS_2 surface by immersion in toluene; the transfer characteristics of BV-doped devices recover the original state before doping.[223] Multilayer MoS_2 is n-doped by *p*-toluene sulfonic acid (*p*-TSA),

which has been widely used for tailoring charge density of conducting polymers; Raman spectroscopy and electrical measurements indicate an n-type doping where the threshold voltage shifts toward more negative gate voltages as the time of exposure to p-TSA increases.[225] Controlled tuning of electronic and optical properties of TMD flakes can also be achieved by modifying SiO_2 substrates with functional self-assembled monolayers (SAMs) with different dipole moments, thereby tuning the charge redistribution between the substrates and the flakes.[220] Raman data and electrical characteristics of field effect transistors show that fluoroalkyltrichlorosilane-SAMs with a large positive dipole moment significantly reduce the intrinsic n-type characteristic of MoS_2 flakes (p-type doping), whereas 3-(trimethoxysilyl)-1-propanamine-SAMs improve the intrinsic n-type characteristic (n-type doping). In general, CH_3-terminated SAMs exhibit little influence on charge carrier density due to the slight dipole moments, while NH_2-/SH-SAMs with lone pair electrons and CF_3-SAMs possessing high electronegativity show electron- and hole-donating characteristics, respectively.[220]

A stable and tunable doping capability over a wide range, especially over the natural propensity of TMDs (n-type and p-type for MoS_2 and WSe_2, respectively), is critical to achieve practical junctions (*e.g.*, p−n, p−n−p, *etc.*), which are required as central building blocks of electronic and optoelectronic devices. Due to the strong propensity toward a certain doping type of TMDs, much effort has been focused on realizing p−n junctions based on vertical vdW heterostructures by stacking different TMDs of dissimilar types.[142,226] In order to develop a homogeneous p−n junction utilizing a single 2D material, Suh *et al.*[138] have demonstrated a vdW vertical p−n junction that is formed by stacking the hole-doped MoS_2 layer (p-type) with an undoped layer (n-type), which showed gate tunable current rectification. The p-doped MoS_2 is achieved through substitutional degenerate p-type doping of MoS_2 by incorporating niobium (Nb) to replace Mo atoms *via* a chemical vapor transport (CVT) method, in which stable doping is realized by covalent bonding in the crystal lattice. A similar approach was taken, but utilizing the surface charge transfer method, to form a vdW p−n junction. Here, the BV and $AuCl_3$ were used as n- and p-type dopants, respectively, to make MoS_2 behave as n- and p-type semiconductor materials (Figure 7b).[224] The hole-doping was enabled by spin-coating a $AuCl_3$ solution which is commonly used in graphene doping due to its large positive reduction potential where $AuCl_4^-$ in solution receives electrons from MoS_2 through surface charge transfer to form Au nanoaggregates.[227,228] Furthermore, a lateral MoS_2 p−n junction with a strong photo response was also demonstrated. By the degenerately hole-doping of partially masked MoS_2, the junction was formed at an interface between the doped and undoped crystal regions.[138] The partial masking of the MoS_2 surface was conducted by transfer of a hBN layer to protect the MoS_2 area underneath from doping.

The chemical and molecular modification of TMDs can also be utilized as a strategy to reduce both sheet and contact resistances of field effect transistors (FETs), providing a simple strategy to further optimize the performance of the devices utilizing 2D semiconductor layers. Du *et al.*[219] adopted amine-rich polyethylenimine (PEI, Figure 7c) as n-type dopants for multilayer MoS_2 FETs and showed that a 2.6 times reduction in sheet resistance and 1.2 times reduction in contact resistance have been achieved with a negative shift of the threshold voltage confirming n-type doping upon exposure to a PEI solution (Figure 7d). Doping schemes using metal atoms *via* surface charge transfer are also applicable to TMDs. In their work, Fang *et al.*[229] used K atoms to degenerately n-dope the source/drain contact regions of few-layer MoS_2 and WSe_2 nanosheets and achieved low contact resistances in their FET devices. Moreover, the work shows that n-type WSe_2 FETs can be enabled with high mobility comparable to those of previously reported p-type WSe_2 FETs by simply doping the contacts accordingly. However, this approach lacks air stability, limiting applicability of the method. K atoms become highly reactive upon exposure to ambient air and water molecules, leading to immediate oxidation of K, that the vacuum process is required.[229] Cl is also used to n-dope few-layer WS_2 and MoS_2. The exfoliated WS_2 or MoS_2 flakes were soaked in undiluted 1, 2 dichloroethane (DCE) at room temperature for more than 12 h and high doping density of 6.0×10^{11} and 9.2×10^{12} cm^{-2} were obtained, respectively.[230] A possible mechanism suggests that the doping may have been realized through the replacement of S vacancy with Cl atom.

In addition to the enhancement realized by the prior examples of degenerate chemical doping of TMDs, the development of robust and controllable nondegenerate doping schemes without crystal damage is crucial for designing TMDs-based electronic and optoelectronic devices, allowing for wide-range charge carrier density modulation. For this purpose Lin *et al.*[217] reported nondegenerate n-doping of monolayer MoS_2 *via* surface functionalization using cesium carbonate (Cs_2CO_3) (Figure 7d), which has previously been adopted as an electron injection material in organic light-emitting devices (OLEDs) and can induce n-type doping for organic semiconductors.[231,232] A controllable nondegenerate p-type doping technique was demonstrated on few-layer and bulk forms of WSe_2 by adjusting the concentration of octadecyltrichlorosilane (OTS).[233] This p-doping effect arises from the methyl ($-CH_3$) functional groups in OTS, which exhibit a positive dipole and consequently reduce the electron density in a WSe_2 crystal as the charge carriers are

accumulated at the interface between OTS and WSe_2. The doping concentration achieved with varying OTS concentration ranged from 1.6×10^{10} to 3.0×10^{11} cm^{-2}, which is in the nondegenerate regime.

RAMAN SPECTROSCOPY OF SEMICONDUCTING TRANSITION METAL DICHALCOGENIDES (STMDS)

Raman spectroscopy plays an important role in the characterization of STMDs since it is not destructive and provides useful information about the structure of monolayers, number of layers, stacking and defects. MoS_2, $MoSe_2$, WS_2, and WSe_2 share the same trigonal prismatic (or 2H) structure belonging to the same space group $P63/mmc$ (D_{6h}^4 in Shöenflies notation). However, for few layer STMDs, the structure possesses a different symmorphic space group depending on the number of layers. For odd numbers of layers, the point group symmetry in the unit cell is D_{3h}, and for even numbers of layers, it becomes D_{3d}. The symmetry considerations mentioned above are useful to perform theoretical Raman spectroscopy of STMDs from first-principles using density functional perturbation theory DFPT[234,235] and compare with the experimental results. The Raman spectrum of bulk trigonal prismatic STMDs exhibits three active signals at high frequencies named E_{1g}, E^1_{2g}, and A_{1g}. The polarization tension corresponding to E_{1g} renders this mode invisible in the commonly used backscattering geometry.[236,237] The E_{1g} and E^1_{2g} are in-plane modes and the A_{1g} is an out-of-plane mode. These three modes become E″, E′, and A'_1 for a system with odd number of layers, and E^2_g, E^1_g, and A_{1g} for an even number of layers, respectively.[238] As the number of layers increase, the in-plane modes shift to lower frequencies and the out of plane modes shift to higher frequencies;[239] this behavior has been confirmed theoretically in trigonal TMDs.[238,240] Interestingly, a second-order Raman resonance process has been identified in monolayer WS_2 with a laser excitation of 514.5 nm involving the longitudinal acoustic mode (LA) at the M point in the Brillouin zone LA(M), allowing the clear differentiation of monolayer and few layer systems. Here also the theoretical approach based on first-principles calculations agrees with the experiment.[241] Moreover, DFPT simulations demonstrate that few layered STMDs exhibit an additional first-order Raman out-of-plane mode, which it is not active in the monolayer and bulk, that involves the vibration of the transition metal atom and is named A'^2_1 or A^2_{1g} depending on whether the layers are odd or even.[238] Figure 8 shows the experimental Raman spectra for few layered WSe_2, including the bulk, in which a new Raman active mode appears around 310 cm^{-1}, confirming the theoretical results obtained from DFPT.

In addition to the high-frequency intralayer modes discussed above, low-frequency interlayer modes have recently begun to attract increasing attention. For high-frequency intralayer modes, which involve vibrations from the intralayer chemical bonds, the restoring forces are dominated by the strength of these intralayer chemical bonds instead of the interlayer vdW interactions. Consequently, there are great limitations for them as unambiguous thickness indicators. In stark contrast, low-frequency interlayer modes (including in-plane shear modes and out-of-plane breathing modes) correspond to layer−layer vibrations with each layer moving as a whole unit, and hence, their frequencies are solely determined by the interlayer vdW restoring forces. Both experimental and theoretical works have demonstrated their promising potential as effective indicators of layer thickness of 2-D crystals, including STMDs.[77−84] Furthermore, a recent work using ultra-low-frequency Raman spectroscopy and first-principles Raman simulations revealed that low-frequency interlayer Raman modes also could be fingerprints of the layer−layer stacking configurations for bilayer and trilayer $MoSe_2$ and WSe_2.[235] The results could be extended to other family members of STMDs.

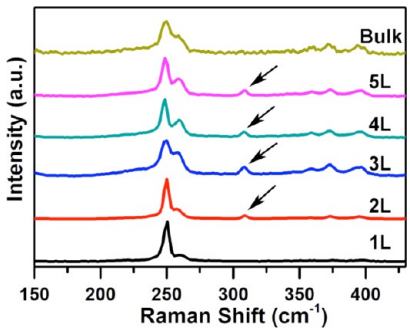

Figure 8. Experimental Raman spectra of WSe_2 with different layers (N = 1−5) including bulk taken with 514.5 nm excitation wavelength. The black arrows show a new Raman active mode, which appears in few layer materials but is not present in the monolayer nor in bulk. Adapted with permission from ref 238. Copyright 2014 Nature Publishing Group.

Theoretical methods have gone beyond simply providing understanding by not only explaining observations already made, but by predicting the behavior of possible new 2D arrangements such as heterolayer systems composed of sandwiching different STMDs; this is the case for heterostructures of MoS_2 and WS_2, which actually have been synthesized.[242] The Raman simulations reveal that depending on the stacking order of the layers, the Raman spectrum exhibits unique features in both frequency and intensity that can be used for identification.[243] There are unresolved challenges that need further experimental and theoretical efforts to resolve, including the role of the different defects in the Raman spectrum of STMDs. In this context, recently an exfoliated MoS_2 monolayer has been exposed to Mn^+ ions to generate defects, finding that the LA(M) signal increases as the density of defects increases, thus showing an analogy of the LA(M) peak to the D peak in graphene.[244]

SCANNING TRANSMISSION ELECTRON MICROSCOPY (STEM) OF TMDS

Perhaps one of the most powerful techniques to probe the electronic, chemical, and structural properties of 2D materials is scanning transmission electron microscopy (STEM). Instead of using a broad stationary beam as in TEM, STEM uses a highly focused electron beam for imaging and analysis, where the e-beam can be rastered across the sample or parked precisely at selected positions. Several STEM based techniques have proven useful for 2D materials characterization. Annular dark field (ADF) imaging, also known as Z-contrast imaging, reveals atomic-scale structural information with atomic number contrast.[245,246] Electron energy-loss spectroscopy (EELS) can provide chemical, bonding and electronic structure information and can be used to measure local optical properties of the material.[247]

Importantly, one must consider that electron beam−sample interactions can trigger transformations and transition dynamics in 2D crystals. Although triggered by the electrons, such transition dynamics reveal the atomistic mechanisms by which crystals can evolve, and defects and edges can be created and transformed in a variety of 2D structures such as graphene[248−253] and hBN.[254−258] These studies show interplay of knock-on damage and ionization damage taking place in 2D crystals under the electron beam. Thus, a low accelerating voltage (30−120 keV) is often necessary to minimize knock-on damage, and low-dose analysis is usually preferred. Fortunately, with the latest aberration-corrected STEM capabilities, the above-mentioned imaging and spectroscopy analysis can all be performed at atomic resolution with single atom sensitivity even at low accelerating voltage.[259−262]

The main advantages of STEM over TEM are (i) multiple imaging and spectroscopy signals can be acquired simultaneously, allowing for direct correlation of the structural and spectroscopic information;[247,263−267] (ii) the atomic number contrast information in ADF images provides a feasible way to perform image-based atom-by-atom chemical analysis[268] and to quantify the thickness of the 2D TEM samples;[269] and (iii) the ability to precisely control the position of the electron beam enables local spectroscopic analysis from individual atoms and controllable structural modification/manipulation of the material at designated regions.

While detailed image simulation is often necessary for quantitative interpretation of HRTEM images, the interpretation of STEM ADF images is straightforward: the bright atoms in the ADF image always correspond to atoms in the thin sample. This important feature has enabled direct identification of all the carbon atom positions in bilayer graphene, which in turn defines the stacking order and the structure of stacking boundaries in bilayer graphene.[245,246] More importantly, the ADF image intensity, to a first approximation, is proportional to the square of the atomic number, *i.e.* heavier atoms display higher image intensity. By quantifying the ADF image intensity at each atomic position, atom-by-atom chemical analysis has been first demonstrated on monolayer h-BN with carbon and oxygen impurities,[268] and soon became one of the most powerful tools for characterizing defects in 2D materials. For example, using quantitative STEM-ADF imaging, Zhou *et al.* reported the first systematic study of intrinsic structural defects in CVD-grown monolayer MoS_2, including point defects (vacancies, antisite defects, and adatoms, Figure 9a), grain boundaries, and edges.[269] This study verified some of the theoretically proposed grain boundary configurations,[270,271] and also identified two types of 60° grain boundaries with predicted metallic behavior, as shown in Figure 9b,c. Similar structural defects were also observed in other TMD monolayers,[167] and the relative population of different point defects is sensitive to the growth method for MoS_2 monolayers.[272] Furthermore, dopant distributions in W-doped and Se-doped MoS_2 monolayers can be automatically mapped out with almost 100% detection efficiency, by applying atom-finding scripts to atomically resolved ADF images and filtering out distinct intensity ranges due to the presence of dopant atoms (Figure 9d, e).[133,170] In bilayer MoS_2, the dopant distribution can even be mapped out layer-by-layer.[170] Such analysis serves as a highly efficient and accurate measurement of the local composition for electron-beam sensitive TMD layers. Atom-by-atom chemical analysis *via* STEM-ADF imaging has also helped to study the structural epitaxy and chemical intermixing at lateral WS_2/MoS_2 heterostructure interfaces,[173,175] and impurity configurations in monolayer graphene.[265,273−275]

Even though the temporal resolution is lower than that in TEM imaging, the chemical information contained in the ADF images has made sequential STEM imaging a particularly powerful method for exploring defect dynamics at the atomic scale *via* energy transfer from the electron beam. By combining *in situ* heating and electron irradiation, Suenaga and co-workers have observed the phase transformation between the semiconducting 2H and metallic 1T phases in monolayer MoS_2 at the atomic scale (Figure 9f), and they showed that the size of the 1T domains in the 2H matrix can be controlled by adjusting the electron dose.[267] In a more recent study, Lin *et al.* showed that electron irradiation can generate Se vacancies in monolayer $MoSe_2$, and the segregation of Se vacancies under energy transfer from the electron beam can subsequently trigger the nucleation and growth of inversion domains in $MoSe_2$, connecting to the pristine lattice *via* conductive 60° grain boundaries (Figure 9g).[276] Such *in situ* defect dynamics studies can help to

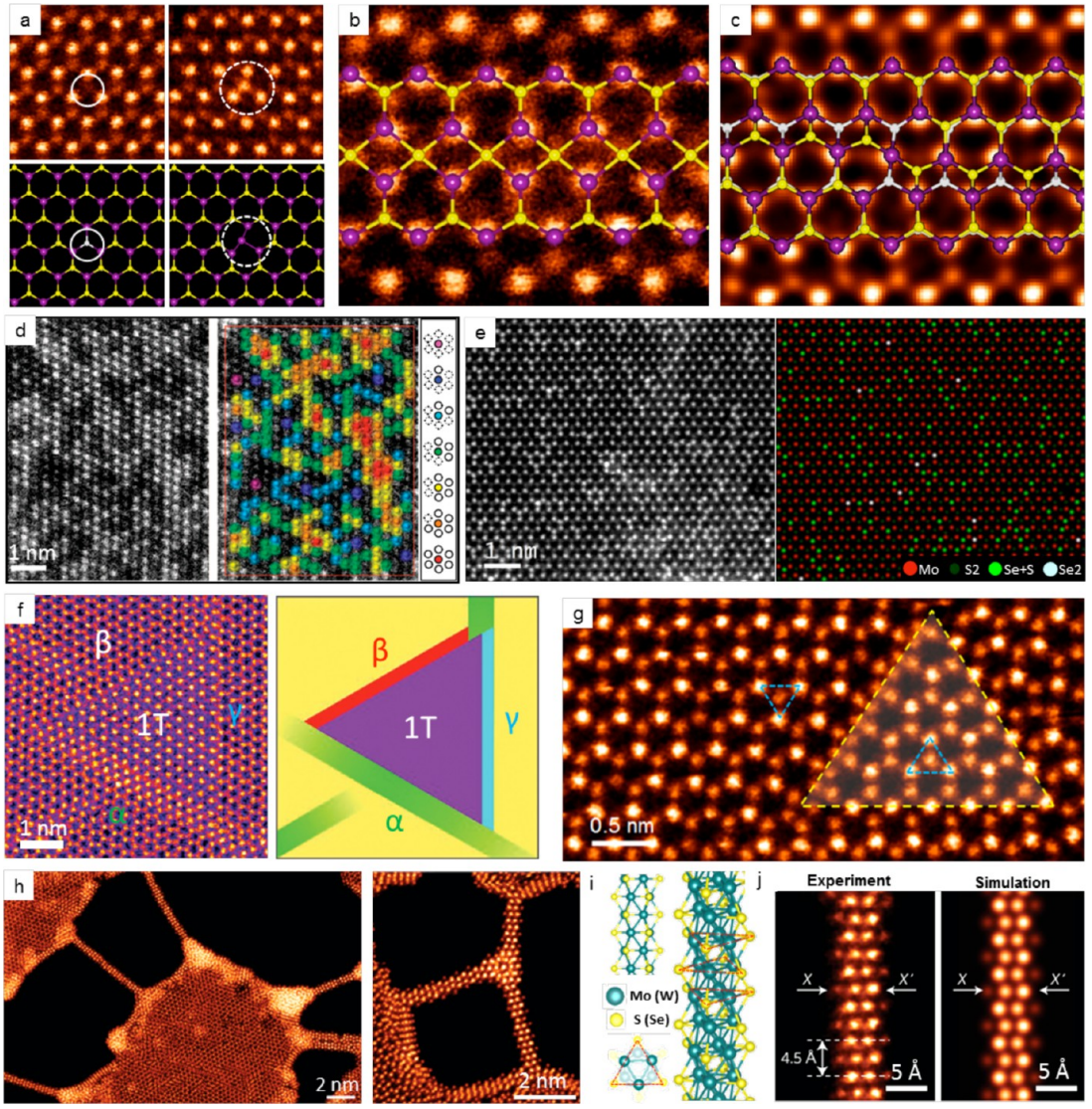

Figure 9. Characterization and engineering of defects in TMD atomic layers. (a) STEM ADF images and the corresponding atomic models of S vacancy and MoS_2 antisite defect in monolayer MoS_2. Adapted from ref 269. Copyright 2013 American Chemical Society. (b and c) ADF images of two types of 60° grain boundaries in monolayer MoS_2 with structural models overlaid Adapted from ref 269. Copyright 2013 American Chemical Society. (d) ADF image and the corresponding doping behavior analysis of a W-doped MoS_2 monolayer Adapted with permission from ref 133. Copyright 2013 Nature Publishing Group. (e) ADF image and the corresponding dopant distribution map of a Se-doped MoS_2 monolayer. Adapted from ref 170. Copyright 2014 American Chemical Society. (f) ADF image and a schematic of a 1T domain in a 2H MoS_2 monolayer, induced by the electron beam under *in situ* heating. Adapted with permission from ref 267. Copyright 2014 Nature Publishing Group. (g) ADF image of an inversion domain in a 2H $MoSe_2$ monolayer induced by the electron beam. Adapted from ref 276. Copyright 2015 American Chemical Society. (h) Sub-nanometer MoSe nanowire array and junctions created within a $MoSe_2$ monolayer using an electron beam. (i) The atomic structure model of the MX nanowire. (j) Comparison of the experimental and simulated ADF images of the MoSe nanowire created by electron beam. Adapted with permission from ref 277. Copyright 2014 Nature Publishing Group.

understand the structural evolution of the material under external excitation, *e.g.*, energy transfer *via* thermal annealing.

When the electron−sample interaction is controlled, the electron beam in STEM can also be used to create new nanostructures at designated regions in the sample. In a recent study, Lin *et al.* used the focused electron beam in STEM to generate holes at preselected regions in TMD monolayers, and demonstrated that under continuous electron irradiation the nanoribbons confined by two adjacent holes can eventually collapse into subnm-wide highly stable metallic MX nanowires with robust self-adapted junctions to the TMD monolayers (Figure 9h−j).[277] Such ultrasmall MX nanowires can be fabricated across a wide range of TMD monolayer systems, and patterning these nanowires or creating complex nanowire junctions were also demonstrated *via* precise control of the e-beam position on the samples. This study points to a promising possibility that multiple devices may be fabricated in a single TMD monolayer and that a focused e-beam system could subsequently be applied to sculpt these

MX nanowires to produce lateral interconnects between different devices.

The recent development of monochromatic STEM-EELS instrumentation has made it possible to measure phonon modes from 2D materials[278] and to map out excitons at a lateral TMD heterostructure with subwavelength spatial resolution.[279] Besides EELS, cathodoluminescence (CL) can also serve as a low-background technique to probe properties such as bandgap and plasmon resonances. SEM-CL has conventionally been used in several light-emitting interfaces and materials such as GaN, GaAs, and GaAlAs.[280,281] Recently, BN nanostructures were characterized with CL and showed a strong luminescence peak at 5.33 eV, confirming a UV bandgap.[282] Given advances in detection and collection schemes, STEM-CL is now possible and much remains to be unraveled about the local bandgap variations in 2D materials.

2D ELECTRONICS AND OPTOELECTRONICS

2D materials are being extensively investigated as the channel materials for next generation FETs owing to their ultrathin body nature that allows aggressive scaling down to atomic dimensions. One of the major challenges that needs to be resolved in this context is the source/drain contact formation since it limits the ultimate performance of these 2D FETs.[283−287] Note that in conventional Si FETs a substitutional doping scheme is adopted in order to minimize the contact resistance and tune the carrier type (electron or hole). However, the absence of a sustainable doping scheme for 2D materials necessitates the use of metals with different work functions to achieve the same objective. Since metal−2D contacts are characterized by Schottky barriers (SBs), one has to minimize the height and width of the SB to improve the current transmission. This was achieved through Sc[285] and MoO_x[284] contacts for n-type and p-type MoS_2 FETs, respectively, whereas graphene contacts were used for WSe_2 FETs[283,286] since the Fermi level of graphene can be tuned through electrostatic gating. As noted previously in the Doping and Chemical Functionalization of TMDs section, various routes have been explored for chemical doping of the TMDs to achieve improved device performance. In addition, recently phase engineering was applied to selectively induce the metallic 1T phase at the source and the drain contact regions of a MoS_2 FET,[287,288] which showed significant performance improvement. In general, MoS_2 and $MoSe_2$ FETs[8,289,290] have been found to be dominated by electron transport, whereas WS_2 and WSe_2 FETs[291−293] are mostly ambipolar (presence of both electron and hole branches in the current transport). This observation is related to the pinning of metal Fermi levels close to a certain energy in the bandgap of the channel material irrespective of the work functions of the metals.[294] For Mo-based chalcogenides, the pinning occurs near the conduction band edge, whereas for W-based chalcogenides, the pinning occurs close to the midgap. FETs based on several other metal chalcogenides like SnS_2, $HfSe_2$, GaS, In_2Se_3 and many more have also been demonstrated.[295−298]

Benchmarking the carrier mobility (Figure 10a) of various 2D materials provides evidence that the TMDs exhibit only a modest mobility compared to phosphorene and graphene.[299] The relatively low mobility values of the STMDs point to a high density of midgap localized states caused by disorder.[293] Potential candidates are metal and chalcogen vacancies, divacancies, dislocations, and molecules and atoms bonded or adsorbed onto the exfoliated sheets.[269,300−302] However, it is encouraging to note that the FETs based on various 2D materials are being implemented in different components of an integrated circuit like the digital inverters[182,303,304] (Figure 10b), analog amplifiers[305−307] (Figure 10c), and memory transistor.[308] 2D materials also show promise for thin film transistor (TFT) technologies.[299] The two most desirable features of the TFTs, mechanical flexibility and optical transparency, are naturally inherited by the 2D materials owing to their vdW epitaxy and atomically thin body. In fact, high performance TFTs based on MoS_2, WSe_2, and black phosphorus (Figure 10d,e) have already been demonstrated.[150,286,307,309] In particular, flexible black phosphorus FETs can endure many thousands, perhaps millions, of bending cycles that is only limited by the substrate, gate dielectric and contact interface. Figure 10e shows robust black phosphorus FET electrical properties at the measurement limit of 5000 bending cycles at 1% strain. Finally, the high surface to volume ratio of the 2D materials makes them ideal for sensor and detector applications as well. For example, MoS_2 and WS_2 FETs have been successfully employed for toxic gas sensing, protein and pH sensing and label free detection of biomolecules (Figure 10f).[310−312] The extraordinary light absorption capability and current conversion efficiency of the 2D materials also pave their way as energy harvesting devices.[313]

2D materials also provide an enormous scope to study the fundamental principles of light absorption and emission in atomically thin materials with the ultimate goal to realize high performance optoelectronic devices like light emitting diodes (LEDs), photodetectors, lasers, and optical cavities, among others.[146,148,315−319] The first generation of 2D phototransistors demonstrated photoresponsivity on the order of ∼120 mA/W in spite of being severely limited by the contact resistance.[317] This issue was resolved in low contact resistance monolayer WSe_2 phototransistors resulting in photoresponsivity as high as $\sim 1.8 \times 10^5$ A/W.[319] Finally, when high mobility graphene was combined with high photoresponsive MoS_2 in a hybrid graphene−MoS_2 phototransistor, record high room

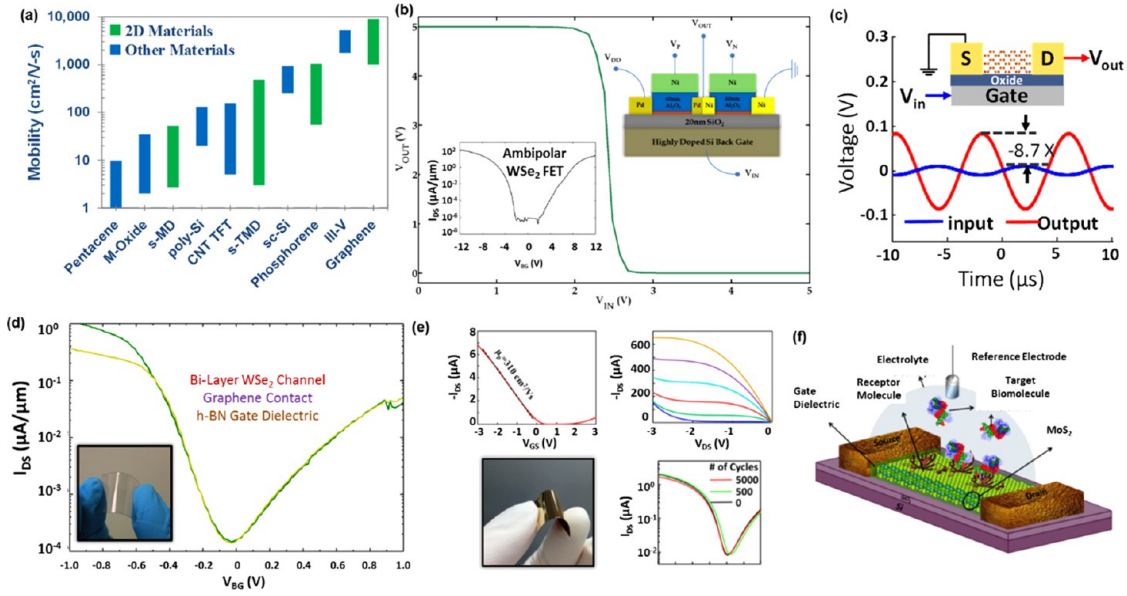

Figure 10. Potential Applications for 2D Materials. (a) Room temperature experimental mobility benchmarking for different semiconducting materials. Adapted with permission from ref 299. Copyright 2014 Nature Publishing Group. (b) A high gain digital inverter based on WSe_2 ambipolar FET. Adapted with permission from refs 303, 304, and 314. Copyright 2014 American Chemical Society, AIP Publishing LLC, and American Chemical Society, respectively. (c) An analog small signal amplifier based on black phosphorus FET. Adapted with permission from refs 305−307. Copyright 2015 IEEE, 2013 AIP Publishing LLC, and 2015 American Chemical Society, respectively. (d) An all 2D thin film transistor for flexible electronics. Adapted from ref 286. Copyright 2014 American Chemical Society. (e) A flexible BP FET showing robust performance at 5000 bending cycles at 1.5% strain. Adapted from refs 150, 307, and 309. Copyright 2013, 2015, and 2013, respectively, American Chemical Society. (f) A biosensor based on MoS_2 FET. Adapted with permission from refs 310−312. Copyright 2014 Nature Publishing Group, American Chemical Society, and John Wiley & Sons, respectively.

temperature photoresponsivity of $\sim 5 \times 10^8$ A/W was obtained.[146] WSe_2 p−n photodiodes having two local bottom gates with different gate dielectrics produced photodetection efficiencies up to 320 mA/W, which is comparable to state of the art commercial silicon photodetectors for green light.[148]

2D layered-material optoelectronic devices are likely to leverage integration with optical cavities and other photonic architectures as well.[320] In a solar cell or photodetector, for instance, it is crucial to absorb large fractions of light in potentially atomically thick materials. The simplest such architectures are based on the "Salisbury screen" concept and comprise an absorbing layered material placed a quarter wavelengths from a reflecting ground plane. Such cavities can indeed support perfect absorption even at monolayer thicknesses, but only in a narrow wavelength band defined by a Fabry−Perot resonance.[321] More broadband enhancement of light absorption in ultrathin films is possible in plasmonic[322] or dielectric gap-mode[323] architectures. In applying these concepts to 2D layered-materials, however, one must be careful to consider the presence of optical anisotropies. Both plasmonic and dielectric gap-mode architectures predominantly exhibit enhancement of out-of-plane oriented electric fields.[324] This anisotropy in field enhancements stems from a fundamental property of electromagnetics: the difference between continuity conditions for parallel ($E_{\parallel,1} = E_{\parallel,2}$) and perpendicular ($\varepsilon_{\perp,1}E_{\perp,1} = \varepsilon_{\perp,2}E_{\perp,2}$) electric fields. As a result, many photonic architectures are incompatible with layered materials, which typically exhibit absorption only for in-plane (*i.e.*, parallel) oriented electric fields.[325] Similar anisotropies were recently demonstrated in photoluminescence from MoS_2 excitons[326] and must be taken into account when designing photonic architectures for enhancing light emission.[327−330] In other cases, optical anisotropies in layered materials can enable novel optical phenomena. For instance, boron nitride anisotropies lead to naturally occurring hyperbolic dispersion,[331,332] the basis of many metamaterial technologies.[333]

BEYOND TMDS: MONOELEMENTAL 2D MATERIALS—GROUP III, IV, AND V "...ENES"

Among the elemental 2D layered materials, the most famous is, of course, graphene (monolayer of graphitic carbon). But there are a host of other elemental 2D materials that have also gained interest in recent years. These include borophene, silicene, germanene, stanene, and phosphorene, which are the monolayer versions of boron, silicon, germanium, tin, and black phosphorus, respectively. While borophene (Figure 11a) was only proposed very recently,[334] Wen *et al.*[335] systematically investigated main group IV structures in 1D, 2D, and 3D using DFT and concluded that carbon is the only group IV element to form sp^2 hybrid orbitals due to the adequate overlap between neighboring p orbitals.

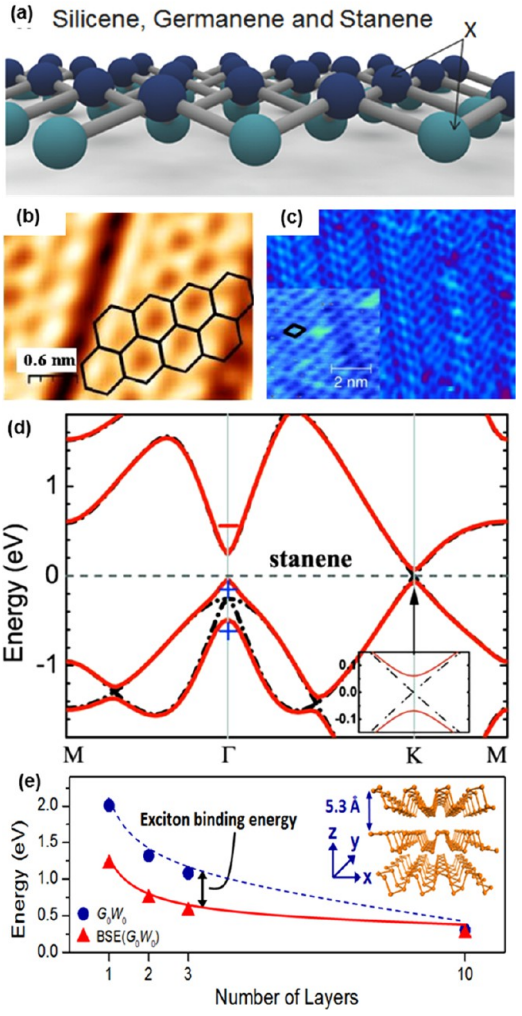

Figure 11. (a) Crystal structure model showing buckled hexagonal 2D sheets composed of a single element of Si, Ge, or Sn. False colors are used to indicate atomic planes at different heights. Adapted with permission from ref 337. Copyright 2015 John Wiley & Sons, Inc. (b) STM image of silicon nanoribbons with the honeycomb structural model overlaid. Adapted with permission from ref 341. Copyright 2010 AIP Publishing LLC. (c) STM image of Germanene, a novel two-dimensional germanium allotrope akin to graphene and silicene. The inset shows a zoomed-in image with a unit cell of a modulated supercell marked by a black diamond. Adapted with permission from ref 346. Copyright 2014 IOP Publishing. (d) Calculated band structure of Stanene.[338] (Large-gap quantum spin hall insulators in tin films.) (e) Calculated electronic [G_0W_0] and optical BSE(G_0W_0) bandgap of black phosphorus as a function of layer number. The energy difference represents the exciton binding energy. Adapted with permission from refs 365 and 419. Copyright 2014 American Physical Society.

It is therefore not surprising that atomically flat structures made of Si, Ge, Sn, or Pb are not stable and have never been observed in nature. However, Cahangirov[336] reported stable 2D, slightly buckled (beta-type) honeycomb structures of silicene and germanene. In spite of this clear departure from graphene chemistry, other atomic layer structures are named in a way similar to that used for carbon sp^2 layers: Si, Ge, and Sn forming structures known as silicene, germanene, and stanene (or tinene) (Figure 11a). Quite remarkably, the atomic corrugation preserves the presence of linearly crossing electron bands at the Fermi energy, indicating that electrons in silicene and germanene behave as massless Fermions, similar to electrons in graphene.

Planar allotropes of C, Si, Ge, and Sn follow the hexagonal honeycomb structure of graphene.[337] However, in contrast to graphene which features sp^2 hybridization, Si, Ge, and Sn tend to favor sp^3 bonding, thereby leading to buckled structures.[338,339] However, in each case, the monolayer structures are, in their stable configurations, made up of hexagons in an exactly 3-fold binding configuration. The hexagons can be found in a number of three-dimensional configurations, with a preference for a chairlike arrangement,[339] and a specific buckling parameter δ varies from 0.0 nm (C), 0.045 nm (Si), 0.069 nm (Ge), and 0.029 nm (Sn), according to a first-principles study.[340]

Silicene, germanene, and stanene do not form bulk layered structures, thereby barring the possibility of using exfoliation methods to isolate their single layer structures. Therefore, synthesis methods must rely on other techniques such as epitaxial surface growth. This way, monolayers of silicene on Ir (111), Ag(110) and Ag(111) were recently reported (Figure 10b).[69,341−344] In addition, experimental evidence for germanene have been provided recently by Davila *et al.*[345] while Bampoulis *et al.*[346] reported an experimental study of germanene growth on Ge(110) to show the hexagonal lattice to have a 0.02 nm corrugation in the vertical direction (Figure 11c). This corrugation is significantly smaller than the theoretical one reported for single layers, as could be expected for a structure overlaid on a substrate. Note that other techniques were developed to synthesize germanene on a variety of substrates, such as Au,[347] GaAs,[348] and Pt.[350]

Experimental evidence indicates that silicene overlaid on silver presents Fermi velocities similar to that of graphene and low energy electrons behave as massless Dirac Fermions.[349,351] Germanene and stanene are predicted to possess massless Dirac Fermions and a behavior similar to that of silicene.[352,353] While silicene, germanene, and stanene present a massless Dirac Fermion behavior similar to graphene, they also present significant and noteworthy spin orbit (SO) coupling.[337,354] The larger ionic mass of Si compared to that of C renders SO coupling more marked compared to graphene, leading to an experimentally observable SO band gap of 1.55 meV.[355] Further, the even more massive Ge's SO band gap is predicted to be as high as 23.9 meV.[355] This large SO coupling makes these structures potentially very attractive for applications such as the quantum spin Hall effect (QSHE).

Tin-based atomic monolayers have been studied less broadly than their Si and Ge counterpart. The name of the pristine layer based on one monolayer of tin atoms is not unique. Some authors employ the

English-based name 'tin', while other sticks to the conventional Latin root 'stannum'. In each case, the root is combined with the usual suffix used in graphene[338,340,356] It follows, therefore, that the literature on Sn atomic layer materials includes reference to both "stanene" or "stanene" and "tinene". However, it seems that the accepted convention of using Latin etymology tends to favor the former over the latter. Single layer stanene has been recently grown epitaxially by molecular beam epitaxy as confirmed by atomic and electronic characterization using scanning tunneling microscopy and angle-resolved photoemission spectroscopy.[357] In addition, while experiments have not been able to confirm it yet, first-principles calculations predict that two-dimensional tin films are QSH insulators with sizable SO bulk gap of 0.3 eV, sufficiently large for practical applications at room temperature (Figure 11d).[338]

Moving one column over from the group IV elements, we find phosphorus. Recently, black phosphorus (or "phosphorene" at the monolayer limit) (Figure 11a) has attracted significant attention as an emerging 2D material due to its unique properties compared with well-explored graphene and TMDs such as MoS_2 and WSe_2.[358−362] In bulk form, this monoelemental layered structure is a semiconductor with a bandgap of 0.3 eV[363] that is highly anisotropic,[363] leading to distinctively different optical and electronic properties along different crystalline directions.[361,362,364] Black phosphorus also follows a similar scaling rule as most other semiconducting 2D materials, where the electronic (optical) bandgap increases from 0.3 eV in bulk to 1.3 eV at the monolayer limit (Figure 11e).[243,365] Moreover, as in other 2D materials, excitons dominate the optical responses in mono- and few-layer black phosphorus; however, light emission from excitons is linearly polarized along the light effective mass direction (*x*-direction).[365−367] The large energy tuning range and highly anisotropic properties may be utilized to construct photonic devices such as photodetectors, modulators, and polarizers in a broad wavelength range from mid-infrared to visible. Another interesting property of black phosphorus is its high carrier mobility,[368] making it promising for high frequency electronics applications.[369] Due to its anisotropic band structure, the measured mobility along light effective mass (*x*-direction) is usually around two times larger than that in heave effective mass (*y*-direction).[361,362] Theoretical investigations show that the intrinsic hole mobility of few-layer (1−5 layers) black phosphorus can exceed 5000 $cm^2/(V\ s)$ even at room temperature, while the electron mobility of few-layer black phosphorus is around 1000 $cm^2/(V\ s)$.[364] Reported carrier mobility of few-layer black phosphorus is much lower.[361,362] Development of surface protection scheme utilizing atomic layer deposition (ALD) oxide or layered hBN may ultimately lead to high mobility, few-layer black phosphorus suitable for electronic applications.[370]

BEYOND TMDS: MXENES

Another developing class of 2D materials is based on the transition metal carbides or carbon nitrides, described as "MXenes".[371−373] MXenes are produced usually by etching out a layer (A) from a 3D structure consisting of MAX, where M is an early transition metal, A is a group III or IV element, and X is carbon or nitrogen.[374−376] Several techniques to selectively remove "A" include heating under vacuum,[377] heating in molten salts[378,379] and molten metals, and selective etching using strong etchants such as Cl_2[380,381] and HF.[382] MXenes synthesized to date include Ti_3C_2, Ti_2C, Nb_2C, V_2C, $Ti_3C_2T_x$, Ti_2CT_x, V_2CT_x, Nb_2CT_x, $Nb_4C_3T_x$, and $Ta_4C_3T_x$, where T_x represents surface functional groups (O, OH and F).[372,375,376] Most of the MXenes have a layer thickness of less than 1 nm, which can be used to form 3D structures of tens of micrometers. The distance between the MXene sheets can be controlled by carefully choosing the starting MAX compound and the cations. Generally, MXenes are mechanically strong materials as these are composed of mostly M−C or M−N bonds, which are some of the strongest bonds known.[383] These MXenes have been effectively used as electrode materials for supercapacitors,[384] fuel cell applications,[385,386] and energy storage applications[387,388] (Li-, Na-, and K-batteries) because of the low metal diffusion barrier at the surface and the high metallic conductivity.

WHAT IS NEXT?

Even though remarkable and extraordinary advances in 2D materials research continues to emerge, there is still much to learn about controlling defects, understanding the impact of substrate, and developing means for controlled doping, which underpin future technologies. Continued advancement in the main themes of this review—theory, synthesis, characterization, and devices—will be critical as we move forward in 2D materials science and technology.

Theory. Two significant gaps must be addressed to enable more rapid progress for designing low-dimensional materials with desired optoelectronic, magnetic, multiferroic, and other properties. First, there is an urgent need for reliable computational techniques that accurately (and rapidly) address the complex functionalities that provide the precision necessary for discriminating between closely competing behaviors, and that are capable of achieving the length scales necessary to bridge across features such as grain boundaries and composition gradients. The large length and time scales, as well as finite temperatures, make even DFT calculations for investigating materials under device-relevant conditions prohibitively expensive. Grain boundaries, extended defects and complex heterostructures further complicate this issue. Second, there is a need to take full advantage of all of the

information contained in experimental data to provide input into computational methods, which ultimately will help to predict new materials and understand their behavior. Such efforts include integrating data efficiently from different characterization techniques to provide a more complete perspective on materials structure and function.

Synthesis. Synthetic efforts ultimately must lead to the combination of atomic-level precision with wafer-level scalability during materials growth. For the synthesis of individual 2D TMDs, CVD conditions should be optimized and controlled to grow large crystalline grains (ideally, only single-crystalline grains) with minimum defect concentration on technologically relevant length scales. With these achievements, the electrical properties of chemically synthesized 2D TMDs should become comparable to those of their mechanically exfoliated analogues. For the growth of 2D TMD heterostructures, new approaches must be developed to enable the rational and scalable integration of multiple 2D TMDs while maintaining atomically seamless heterointerfaces. Such atomic-level control of structural and compositional variations would promise exciting new quantum physics and would also open up opportunities for a wide range of unconventional applications in electronics, optics and optoelectronics. Ultimately, the large-scale synthesis of 2D TMDs with tailored materials properties has the potential to enable the production of novel integrated circuits based on the electronic devices at the ultimate size limit, which function in highly predicted manners. Beyond TMDs, significant efforts must be undertaken for monoelemental 2D materials synthesis to facilitate large-area growth on insulating substrates, with *in situ* capping capabilities. Currently, most monoelemental layers are grown on conducting substrates, which requires subsequent transfer processes; the environmental sensitivity of these materials has hindered the speed of their advancement relative to graphene or the TMDs, even though they could be better suited for specific electronic applications.

Biofunctionalization. Biofunctionalization of graphene was a major focus for a variety of applications,[389] and the integration of nongraphene 2D materials is expected to benefit various biochemical, biological, and biomedical applications due to their capability to exhibit wide band gaps for applications ranging from FETs to light emissive quantum platelets. Recent work from Banerjee *et al.*[311] demonstrated MoS_2 FET based biomolecular detection and contrasted its sensing performance to a graphene FET. However, there are numerous challenges ahead for effectively interfacing the emerging 2D materials with biomolecules and operating the biofunctionalized 2D materials devices in biological fluids, such as buffer, serum, sweat, saliva, *etc*. First and foremost, chemical stability, specifically the air, moisture, and oxidation stability, should be explored to ensure the integrity of 2D materials throughout the interfacing process with biomolecules. Second, the plasmonic characteristics of 2D materials should be investigated thoroughly to provide for SPR-, LSPR-, and SERS-based optical pathway in investigating bio-2D materials interaction as well as its use as a plasmonic sensing platform. Third, increasing the number of 2D materials material formulations and processing conditions is required. For example, graphene exhibits unparalleled processing methods originating from its abundance in chemical/physical growth, exfoliation, oxidation, and reduction. The resulting hydrophobicity, water solubility, organic phase, and separation methods enables one to investigate the feasibility of graphene in many applications including 3D printing ink for tissue engineering scaffolds,[390] localized reduction of fluorinated graphene to form nano stripped graphene channel,[391] and encapsulating membrane for *in situ* monitoring of DNA−DNA hybridization in real time.[392] Further bandgap engineering tools, bio/chemical reactivity, nanosized patterning, and selective atomistic passivation for the 2D materials can be additional challenges that need to be addressed to aid in advancing their biological/biomedical applications.

Characterization. It will be important to continue pushing the limit of low-voltage low-dose STEM imaging for 2D materials that are sensitive to the electron beam. A growing effort that combines high-resolution STEM analysis with *in situ* microscopy techniques is enabling researchers to study the structural changes of materials under external excitations or under relevant working conditions. Future studies will provide valuable insights into understanding the failure mechanisms of 2D devices under extreme working conditions or due to aging.[393] Efforts should also be made to correlate atomic-scale structural information obtained from electron microscopy studies with optical spectroscopy characterization and device performance, enabled by performing all studies on the same regions of the samples or ultimately on a working device. As instrument stability and collection performance improves, correlated STEM-CL, EELS and conventional PL studies of 2D materials will unravel fascinating properties, in particular at the edges, boundaries, and interfaces. In parallel, interesting work will continue to emerge on exploring new defect structures and 2D nanostructures[277,394,395] using the electron beam as an energy source to excite the 2D material specimen.[396]

Surface sensitive characterization technique such as time-of-flight secondary ion mass spectroscopy (TOF-SIMS) is a recently emerging tool for identifying impurities of 2D materials at the atomic level, especially with its high sensitivity of about parts per billion (ppb)-level detection. Recently, TOF-SIMS demonstrated unprecedented ability to depth profile graphene/hBN

heterostructures, clearly showing the interfacial carbonaceous materials that result from the mechanical stacking process,[397] as well as delineating dopant locations in Mn-doped MoS_2 monolayers.[174] As a result, TOF-SIMS should be given serious consideration for nanoscale chemical analysis of these materials. Another technique, scanning tunneling microscopy (STM), has proven to be one of the most powerful research tools, enabling investigations of the morphology and local properties of novel 2D materials, such as silicene, germanene, and TMDs.[344,350] For 2D materials on solid surfaces, complicated superstructures due to modification from the substrate lattice are often present, and STM imaging is very effective in identifying such superstructures *via* Moire patterns. The height profiles of STM images can be further used to reveal the vertical corrugation of buckled 2D atomic layers.[69,398] Recent studies have also been focused on epitaxial growth of MX_2 materials on metal substrates inside the UHV STM chamber and *in situ* STM analysis of the geometric features of the as-grown epitaxial MX_2 atomic layers.[401] Future STM efforts on 2D materials could include continuity of 2D sheets at step edges of the substrates and the local element-doping or defects at the atomic scale, as well as related quantum interference. STM combined with other techniques (such as excitation sources from external optical, magnetic, electric field) will be very powerful for investigating the fundamental properties of these materials as well as substrate-modified new phenomena.

Devices. One of the highly promising future directions for electronic and optoelectronic devices based on 2D materials emerges from the vertical stacking of different 2D systems.[190,399−402] Such heterojunction devices already exhibit novel tunneling phenomena,[149,187] diode rectification,[403] tunable photovoltaic effect,[141] significantly enhanced photosensitivity,[146] superior light emission[318] and decent quantum efficiency.[313] Piezotronics is an equally promising field of research for 2D materials given recent breakthroughs. For example, a finite and zero piezoelectric response were observed in MoS_2 when the layer number was switched between odd and even, respectively; this is in sharp contrast to bulk piezoelectric materials.[404] This oscillation is due to the breaking and recovery of the inversion symmetry of the 2D crystal. A piezoelectric coefficient of $e_{11} = 2.9 \times 10^{-10}$ C m^{-1} has been reported for free-standing monolayer MoS_2. 2D materials also provide a platform to replace charge-based devices. In this context, valleytronics is a recent development requiring that the conduction/valence bands of a material have two or more minima at equal energies but at different positions in momentum space. Monolayer MoS_2, which has two energy-degenerate valleys at both the conduction and valence band edges, is a promising material for valleytronics.[405,406] It has been experimentally demonstrated that optical pumping with circularly polarized light can achieve a valley polarization of 30% in pristine monolayer MoS_2.[406]

2D Magnets. Since the initial discovery of graphene, the family of 2D materials has grown considerably with new additions such as hBN and TMDs. Conspicuously missing in the current material line up are 2D magnets, crucial for the development of spintronic applications. Furthermore, the successful fabrication of a 2D magnet would significantly advance our understanding of low-dimensional magnetism. There have been various theoretical proposals on how to realize 2D magnets, which generally fall into three categories. The first is to dope transition metal elements into a nonmagnetic parent compound. For example, it was predicted that in graphene/transition-metal hybrid systems the exchange interaction between metal clusters strongly depends on gate voltage, opening up the exciting possibility for achieving strong and reproducible magnetoelectric effects.[407] Doping transition metals into dichalcogenides has also been recently experimentally studied,[174] but the predicted Curie temperature is well below room temperature.[407] Another interesting possibility is intercalated compounds[408,409] such as $Cr_{1/3}NbS_2$, a helical magnet in its bulk form.[410] The second route is to explore the strong van Hove singularity often found in 2D materials, which could lead to a Stoner-type magnetic instability. In monolayer GaSe, hole doping could induce tunable ferromagnetism and half metallicity, and the averaged electron spin magnetic moment can be as large as close to 1.0 μ_B/carrier.[411,412] The third route is *via* layered vdW crystals which are intrinsically magnetic. In this regard, transition metal trichalcogenides such as CrI_3[68] and $CrSiTe_3$[413,414] constitute an attractive family of materials. These materials are known to exhibit a large variety of magnetic phases in their bulk form,[415] making them ideal candidates for exfoliated 2D magnets. Interesting properties such as coupled spin and valley degrees of freedom have also been predicted for monolayers of these materials.[416] Furthermore, it was shown that strain can be an effective knob for tuning the magnetic properties of these compounds.[417,418] With so many possible options, the race to realize the first 2D magnet will surely bring new and exciting opportunities to the fast expanding field of 2D materials.

Conflict of Interest: The authors declare no competing financial interest.

Acknowledgment. This review was developed out of the workshop "Beyond Graphene: From Atoms to Applications", hosted by the Penn State Center for Two-Dimensional and Layered Materials on May 11−12, 2015 with sponsorship from Corning, Inc., Kyma Technologies, FEI, and Oak Ridge Associated Universities (ORAU). Support was also provided by the Penn State Materials Research Institute and Center for Nanoscale Science. J.A.R. and M.T. also wish to acknowledge Rosemary Bittel for logistical support. Finally, the authors would like to acknowledge those agencies who have funded their research in 2D materials: NSF, DOE, DARPA, STARnet, NYStar, ONR, DTRA, AFRL, ARO, AFOSR.

REFERENCES AND NOTES

1. Golden, J.; McMillan, M.; Downs, R. T.; Hystad, G.; Goldstein, I.; Stein, H. J.; Zimmerman, A.; Sverjensky, D. A.; Armstrong, J. T.; Hazen, R. M. Rhenium Variations in Molybdenite (MoS2): Evidence for Progressive Subsurface Oxidation. *Earth Planet. Sci. Lett.* **2013**, *366*, 1–5.
2. Brodie, B. C. On the Atomic Weight of Graphite. *Philos. Trans. R. Soc. London* **1859**, *149*, 249–259.
3. Novoselov, K. S.; Geim, A. K.; Morozov, S. V.; Jiang, D.; Zhang, Y.; Dubonos, S. V.; Grigorieva, I. V.; Firsov, A. A. Electric Field Effect in Atomically Thin Carbon Films. *Science (Washington, DC, U. S.)* **2004**, *306*, 666–669.
4. Novoselov, K. S.; Jiang, D.; Schedin, F.; Booth, T. J.; Khotkevich, V. V.; Morozov, S. V.; Geim, a K. Two-Dimensional Atomic Crystals. *Proc. Natl. Acad. Sci. U. S. A.* **2005**, *102*, 10451–10453.
5. Giovannetti, G.; Khomyakov, P.; Brocks, G.; Kelly, P.; van den Brink, J. Substrate-Induced Band Gap in Graphene on Hexagonal Boron Nitride: Ab Initio Density Functional Calculations. *Phys. Rev. B: Condens. Matter Mater. Phys.* **2007**, *76*, 073103.
6. Dean, C. R.; Young, A. F.; Meric, I.; Lee, C.; Wang, L.; Sorgenfrei, S.; Watanabe, K.; Taniguchi, T.; Kim, P.; Shepard, K. L.; et al. Boron Nitride Substrates for High-Quality Graphene Electronics. *Nat. Nanotechnol.* **2010**, *5*, 722–726.
7. Mak, K. F.; Lee, C.; Hone, J.; Shan, J.; Heinz, T. F. Atomically Thin MoS2: A New Direct-Gap Semiconductor. *Phys. Rev. Lett.* **2010**, *105*, 136805.
8. Radisavljevic, B.; Radenovic, a; Brivio, J.; Giacometti, V.; Kis, a. Single-Layer MoS2 Transistors. *Nat. Nanotechnol.* **2011**, *6*, 147–150.
9. Chen, Y.; Tan, C.; Zhang, H.; Wang, L. Two-Dimensional Graphene Analogues for Biomedical Applications. *Chem. Soc. Rev.* **2015**, *44*, 2681–2701.
10. Kim, S. J.; Choi, K.; Lee, B.; Kim, Y.; Hong, B. H. Materials for Flexible, Stretchable Electronics: Graphene and 2D Materials. *Annu. Rev. Mater. Res.* **2015**, *45*, 63–84.
11. Rao, C. N. R.; Maitra, U. Inorganic Graphene Analogs. *Annu. Rev. Mater. Res.* **2015**, *45*, 29–62.
12. Das, S.; Robinson, J. a; Dubey, M.; Terrones, H.; Terrones, M. Beyond Graphene: Progress in Novel Two-Dimensional Materials and van Der Waals Solids. *Annu. Rev. Mater. Res.* **2015**, *45*, 1–27.
13. Kannan, P. K.; Late, D. J.; Morgan, H.; Rout, C. S. Recent Developments in 2D Layered Inorganic Nanomaterials for Sensing. *Nanoscale* **2015**, *7*, 13293–13312.
14. Lotsch, B. V. Vertical 2D Heterostructures. *Annu. Rev. Mater. Res.* **2015**, *45*, 85–109.
15. Wang, H.; Yuan, H.; Sae Hong, S.; Li, Y.; Cui, Y. Physical and Chemical Tuning of Two-Dimensional Transition Metal Dichalcogenides. *Chem. Soc. Rev.* **2015**, *44*, 2664–2680.
16. Jariwala, D.; Sangwan, V. K.; Lauhon, L. J.; Marks, T. J.; Hersam, M. C. Emerging Device Applications for Semiconducting Two-Dimensional Transition Metal Dichalcogenides. *ACS Nano* **2014**, *8*, 1102–1120.
17. Fiori, G.; Bonaccorso, F.; Iannaccone, G.; Palacios, T.; Neumaier, D.; Seabaugh, A.; Banerjee, S. K.; Colombo, L. Electronics Based on Two-Dimensional Materials. *Nat. Nanotechnol.* **2014**, *9*, 768–779.
18. Xu, X.; Yao, W.; Xiao, D.; Heinz, T. F. Spin and Pseudospins in Layered Transition Metal Dichalcogenides. *Nat. Phys.* **2014**, *10*, 343–350.
19. Voiry, D.; Mohite, A.; Chhowalla, M. Phase Engineering of Transition Metal Dichalcogenides. *Chem. Soc. Rev.* **2015**, *44*, 2702–2712.
20. Peng, J.; Gao, W.; Gupta, B. K.; Liu, Z.; Romero-Aburto, R.; Ge, L.; Song, L.; Alemany, L. B.; Zhan, X.; Gao, G.; et al. Graphene Quantum Dots Derived from Carbon Fibers. *Nano Lett.* **2012**, *12*, 844–849.
21. Kim, S.; Hwang, S. W.; Kim, M.-K.; Shin, D. Y.; Shin, D. H.; Kim, C. O.; Yang, S. B.; Park, J. H.; Hwang, E.; Choi, S.-H.; et al. Anomalous Behaviors of Visible Luminescence from Graphene Quantum Dots: Interplay between Size and Shape. *ACS Nano* **2012**, *6*, 8203–8208.
22. Dinghas, A. Uber Einen Geometrischen Sat von Wulff Fur Die Gleichgewitchtsform von Kristallen. *Z. Kristallogr. - Cryst. Mater.* **1943**, *105*, 304–314.
23. von Laue, M. Der Wulffsche Satz Fur Die Gleichgewichtsform von Kristallen. *Z. Kristallogr. - Cryst. Mater.* **1943**, *105*, 124–133.
24. Wulff, G. On the Question of Speed of Growth and Dissolution of Crystal Surfaces. *Z. Kristallogr. - Cryst. Mater.* **1901**, *34*, 449–530.
25. Marks, L. D. Modified Wulff MTP. *Philos. Mag. A* **1984**, *49*, 81.
26. Ringe, E.; Van Duyne, R. P.; Marks, L. D. Wulff Construction for Alloy Nanoparticles. *Nano Lett.* **2011**, *11*, 3399–3403.
27. Winterbottom, W. L. Equilibrium Shape of a Small Particle in Contact with a Foreign Substrate. *Acta Metall.* **1967**, *15*, 303.
28. Zia, R. K. P.; Avron, J. E.; Taylor, J. E. The Summertop Construction: Crystals in a Corner. *J. Stat. Phys.* **1988**, *50*, 727–736.
29. Frank, F. C. In *Growth and Perfection of Crystals*; Doremus, R. H., Roberts, B. W., Tumbull, D., Eds.; Wiley: New York, 1958.
30. Ringe, E.; Van Duyne, R. P.; Marks, L. D. Kinetic and Thermodynamic Modified Wulff Constructions for Twinned Nanoparticles. *J. Phys. Chem. C* **2013**, *117*, 15859–15870.
31. Liu, Y.; Bhowmick, S.; Yakobson, B. I. BN White Graphene with "Colorful" Edges: The Energies and Morphology. *Nano Lett.* **2011**, *11*, 3113–3116.
32. Jaramillo, T. F.; Jørgensen, K. P.; Bonde, J.; Nielsen, J. H.; Horch, S.; Chorkendorff, I. Identification of Active Edge Sites for Electrochemical H2 Evolution from MoS2 Nanocatalysts. *Science (Washington, DC, U. S.)* **2007**, *317*, 100–102.
33. Zhang, J.; Najmaei, S.; Lin, H.; Lou, J. MoS2 Atomic Layers with Artificial Active Edge Sites as Transparent Counter Electrodes for Improved Performance of Dye-Sensitized Solar Cells. *Nanoscale* **2014**, *6*, 5279–5283.
34. Cao, D.; Shen, T.; Liang, P.; Chen, X.; Shu, H. Role of Chemical Potential in Flake Shape and Edge Properties of Monolayer MoS2. *J. Phys. Chem. C* **2015**, *119*, 4294–4301.
35. Kobayashi, K.; Watanabe, K.; Taniguchi, T. First-Principles Study of Various Hexagonal BN Phases. *J. Phys. Soc. Jpn.* **2007**, *76*, 104707.
36. Friend, R. H.; Yoffe, A. D. Electronic-Properties of Intercalation Complexes of the Transition-Metal Dichalcogenides. *Adv. Phys.* **1987**, *36*, 1–94.
37. Ganesh, P.; Kim, J.; Park, C.; Yoon, M.; Reboredo, F. A.; Kent, P. R. C. Binding and Diffusion of Lithium in Graphite: Quantum Monte Carlo Benchmarks and Validation of van Der Waals Density Functional Methods. *J. Chem. Theory Comput.* **2014**, *10*, 5318–5323.
38. Spanu, L.; Sorella, S.; Galli, G. Nature and Strength of Interlayer Binding in Graphite. *Phys. Rev. Lett.* **2009**, *103*, 196401.
39. Grimme, S. Accurate Description of van Der Waals Complexes by Density Functional Theory Including Empirical Corrections. *J. Comput. Chem.* **2004**, *25*, 1463.
40. Grimme, S. Semiempirical GGA-Type Density Functional Constructed with a Long-Range Dispersion Correction. *J. Comput. Chem.* **2006**, *27*, 1787–1799.
41. Grimme, S.; Antony, J.; Ehrlich, S.; Krieg, H. A Consistent and Accurate Ab Initio Parametrization of Density Functional Dispersion Correction (DFT-D) for the 94 Elements H-Pu. *J. Chem. Phys.* **2010**, *132*, 154104.
42. Grimme, S.; Antony, J.; Schwabe, T.; Muck-Lichtenfeld, C. Density Functional Theory with Dispersion Corrections for Supramolecular Structures, Aggregates, and Complexes of (bio)organic Molecules. *Org. Biomol. Chem.* **2007**, *5*, 741.
43. Grimme, S.; Muck-Lichtenfeld, C.; Antony, J. Noncovalent Interactions between Graphene Sheets and in Multishell (Hyper)Fullerenes. *J. Phys. Chem. C* **2007**, *111*, 11199–11207.

44. Tkatchenko, A.; Scheffler, M. Accurate Molecular van Der Waals Interactions from Ground-State Electron Density and Free-Atom Reference Data. *Phys. Rev. Lett.* **2009**, *102*, 73005.
45. Berland, K.; Chakarova-Kack, S. D.; Cooper, V. R.; Langreth, D. C.; Schroder, E. A van Der Waals Density Functional Study of Adenine on Graphene: Single-Molecular Adsorption and Overlayer Binding. *J. Phys.: Condens. Matter* **2011**, *23*, 135001.
46. Dion, M.; Rydberg, H.; Schröder, E.; Langreth, D. C.; Lundqvist, B. I. Van Der Waals Density Functional for General Geometries. *Phys. Rev. Lett.* **2004**, *92*, 246401.
47. Lee, K.; Murray, É. D.; Kong, L.; Lundqvist, B. I.; Langreth, D. C. A Higher-Accuracy van Der Waals Density Functional. *Phys. Rev. B: Condens. Matter Mater. Phys.* **2010**, *82*, 81101.
48. Thonhauser, T.; Cooper, V. R.; Li, S.; Puzder, A.; Hyldgaard, P.; Langreth, D. C. Van Der Waals Density Functional: Self-Consistent Potential and the Nature of the van Der Waals Bond. *Phys. Rev. B: Condens. Matter Mater. Phys.* **2007**, *76*, 125112.
49. Vydrov, O. A.; Van Voorhis, T. Implementation and Assessment of a Simple Nonlocal van Der Waals Density Functional. *J. Chem. Phys.* **2010**, *132*, 164113.
50. Vydrov, O. A.; Van Voorhis, T. Nonlocal van Der Waals Density Functional Made Simple. *Phys. Rev. Lett.* **2009**, *103*, 63004.
51. Vydrov, O. A.; Wu, Q.; Van Voorhis, T. Self-Consistent Implementation of a Nonlocal van Der Waals Density Functional with a Gaussian Basis Set. *J. Chem. Phys.* **2008**, *129*, 014106.
52. Grimme, S. Density Functional Theory with London Dispersion Corrections. *Wiley Interdiscip. Rev. Mol. Sci.* **2011**, *1*, 211–228.
53. DiStasio, R. A., Jr.; Gobre, V. V.; AlexandreTkatchenko, A. Many-Body van Der Waals Interactions in Molecules and Condensed Matter. *J. Phys.: Condens. Matter* **2014**, *26*, 213202.
54. Tkatchenko, A.; Ambrosetti, A.; DiStasio, R. A. Interatomic Methods for the Dispersion Energy Derived from the Adiabatic Connection Fluctuation-Dissipation Theorem. *J. Chem. Phys.* **2013**, *138*, 74106.
55. Tkatchenko, A.; Alfe, D.; Kim, K. S. First-Principles Modeling of Non-Covalent Interactions in Supramolecular Systems: The Role of Many-Body Effects. *J. Chem. Theory Comput.* **2012**, *8*, 4317.
56. Berland, K.; Cooper, V. R.; Lee, K.; Schröder, E.; Thonhauser, T.; Hyldgaard, P.; Lundqvist, B. I. Van Der Waals Forces in Density Functional Theory: A Review of the vdW-DF Method. *Rep. Prog. Phys.* **2015**, *78*, 66501.
57. Tkatchenko, A.; Romaner, L.; Hofmann, O. T.; Zojer, E.; Ambrosch-Draxl, C.; Scheffler, M. Van Der Waals Interactions Between Organic Adsorbates and at Organic/Inorganic Interfaces. *MRS Bull.* **2010**, *35*, 435.
58. Johnson, E. R.; Mackie, I. D.; DiLabio, G. A. Dispersion Interactions in Density-Functional Theory. *J. Phys. Org. Chem.* **2009**, *22*, 1127.
59. Cooper, V. R.; Kong, L.; Langreth, D. C.; Landau, D. P.; Lewis, S. P.; Schuttler, H. B. Computing Dispersion Interactions in Density Functional Theory. *Phys. Procedia* **2010**, *3*, 1417–1430.
60. Klimes, J.; Michaelides, A. Perspective: Advances and Challenges in Treating van Der Waals Dispersion Forces in Density Functional Theory. *J. Chem. Phys.* **2012**, *137*, 120901.
61. Tkatchenko, A. Current Understanding of Van Der Waals Effects in Realistic Materials. *Adv. Funct. Mater.* **2015**, *25*, 2054–2061.
62. Grafenstein, J.; Cremer, D. An Efficient Algorithm for the Density-Functional Theory Treatment of Dispersion Interactions. *J. Chem. Phys.* **2009**, *130*, 124105.
63. Burns, L. A.; Vazquez-Mayagoitia, A.; Sumpter, B. G.; Sherrill, C. D. Density-Functional Approaches to Noncovalent Interactions: A Comparison of Dispersion Corrections (DFT-D), Exchange-Hole Dipole Moment (XDM) Theory, and Specialized Functionals. *J. Chem. Phys.* **2011**, *134*, 84107.
64. Fang, C.; Van Blaaderen, A.; Van Huis, M. a. Two-Dimensional Hydrous Silica: Nanosheets and Nanotubes Predicted from First-Principles Simulations. *J. Phys. Chem. C* **2015**, *119*, 14343–14350.
65. Zhuang, H. L.; Hennig, R. G. Computational Identification of Single-Layer CdO for Electronic and Optical Applications. *Appl. Phys. Lett.* **2013**, *103*, 212102.
66. Zhuang, H. L.; Hennig, R. G. Electronic Structures of Single-Layer Boron Pnictides. *Appl. Phys. Lett.* **2012**, *101*, 153109.
67. Zhuang, H. L.; Hennig, R. G. Computational Search for Single-Layer Transition-Metal Dichalcogenide Photocatalysts. *J. Phys. Chem. C* **2013**, *117*, 20440–20445.
68. McGuire, M. A.; Dixit, H.; Cooper, V. R.; Sales, B. C. Coupling of Crystal Structure and Magnetism in the Layered, Ferromagnetic Insulator CrI3. *Chem. Mater.* **2015**, *27*, 612–620.
69. Vogt, P.; De Padova, P.; Quaresima, C.; Avila, J.; Frantzeskakis, E.; Asensio, M. C.; Resta, A.; Ealet, B.; Le Lay, G. Silicene: Compelling Experimental Evidence for Graphenelike Two-Dimensional Silicon. *Phys. Rev. Lett.* **2012**, *108*, 155501.
70. Cahangirov, S.; Audiffred, M.; Tang, P.; Iacomino, A.; Duan, W.; Merino, G.; Rubio, A. Electronic Structure of Silicene on Ag(111): Strong Hybridization Effects. *Phys. Rev. B: Condens. Matter Mater. Phys.* **2013**, *88*, 035432.
71. Li, L.; Zhao, M. First-Principles Identifications of Superstructures of Germanene on Ag(111) Surface and H-BN Substrate. *Phys. Chem. Chem. Phys.* **2013**, *15*, 16853–16863.
72. Liu, H.; Gao, J.; Zhao, J. Silicene on Substrates: A Way to Preserve or Tune Its Electronic Properties. *J. Phys. Chem. C* **2013**, *117*, 10353–10359.
73. Ramirez-Torres, A.; Le, D.; Rahman, T. S.; Li, L.; Zhao, M. Effect of Monolayer Supports on the Electronic Structure of Single-Layer MoS_2. *IOP Conf. Ser.: Mater. Sci. Eng.* **2014**, *118*, 012011.
74. Hwang, J.; Kim, M.; Campbell, D.; Alsalman, H. a; Kwak, J. Y.; Shivaraman, S.; Woll, A. R.; Singh, A. K.; Hennig, R. G.; Gorantla, S.; et al. Van Der Waals Epitaxial Growth of Graphene on Sapphire by Chemical Vapor Deposition without a Metal Catalyst. *ACS Nano* **2013**, *7*, 385–395.
75. Liu, L.; Siegel, D. A.; Chen, W.; Liu, P.; Guo, J.; Duscher, G.; Zhao, C.; Wang, H.; Wang, W.; Bai, X.; et al. Unusual Role of Epilayer−substrate Interactions in Determining Orientational Relations in van Der Waals Epitaxy. *Proc. Natl. Acad. Sci. U. S. A.* **2014**, *111*, 16670–16675.
76. Dichalcogenides, M.; Yuan, J.; Najmaei, S.; Zhang, Z.; Zhang, J.; Lei, S.; Ajayan, P. M. Photoluminescence Quenching and Charge Transfer in Arti Fi Cial Heterostacks of Monolayer Transition Black Phosphorus. *ACS Nano* **2015**, *9*, 555–563.
77. Ling, X.; Liang, L.; Huang, S.; Puretzky, A. A.; Geohegan, D. B.; Sumpter, B. G.; Kong, J.; Meunier, V.; Dresselhaus, M. S. Low-Frequency Interlayer Breathing Modes in Few-Layer Black Phosphorus. *Nano Lett.* **2015**, *15*, 4080–4088.
78. Dong, S.; Zhang, A.; Liu, K.; Ji, J.; Ye, Y. G.; Luo, X. G.; Chen, X. H.; Ma, X.; Jie, Y.; Zhang, Q. Collective Compression Mode and Strong Interlayer Coupling in Atomically Thin Black Phosphorus. **2015**, *arXiv:1503.06577* .
79. Luo, X.; Lu, X.; Koon, G. K. W.; Castro Neto, A. H.; Özyilmaz, B.; Xiong, Q.; Quek, S. Y. Large Frequency Change with Thickness in Interlayer Breathing Mode-Significant Interlayer Interactions in Few Layer Black Phosphorus. *Nano Lett.* **2015**, *15*, 3931–3938.
80. Tan, P. H.; Han, W. P.; Zhao, W. J.; Wu, Z. H.; Chang, K.; Wang, H.; Wang, Y. F.; Bonini, N.; Marzari, N.; Pugno, N.; et al. The Shear Mode of Multilayer Graphene. *Nat. Mater.* **2012**, *11*, 294–300.
81. Zhang, X.; Han, W. P.; Wu, J. B.; Milana, S.; Lu, Y.; Li, Q. Q.; Ferrari, A. C.; Tan, P. H. Raman Spectroscopy of Shear and Layer Breathing Modes in Multilayer MoS2. *Phys. Rev. B: Condens. Matter Mater. Phys.* **2013**, *87*, 115413.

82. Zhao, H.; Wu, J.; Zhong, H.; Guo, Q.; Wang, X.; Xia, F.; Yang, L.; Tan, P.-H.; Wang, H. Interlayer Interactions in Anisotropic Atomically-Thin Rhenium Diselenide. **2015**, *arXiv1504.07664* .
83. Zhao, Y.; Luo, X.; Li, H.; Zhang, J.; Araujo, P. T.; Gan, C. K.; Wu, J.; Zhang, H.; Quek, S. Y.; Dresselhaus, M. S.; et al. Interlayer Breathing and Shear Modes in Few-Trilayer MoS2 and WSe2. *Nano Lett.* **2013**, *13*, 1007–1015.
84. Zhao, Y.; Luo, X.; Zhang, J.; Wu, J.; Bai, X.; Wang, M.; Jia, J.; Peng, H.; Liu, Z.; Quek, S. Y.; et al. Interlayer Vibrational Modes in Few-Quintuple-Layer Bi2Te3 and Bi2Se3 Two-Dimensional Crystals: Raman Spectroscopy and First-Principles Studies. *Phys. Rev. B: Condens. Matter Mater. Phys.* **2014**, *90*, 245428.
85. Qiu, D. Y.; da Jornada, F. H.; Louie, S. G. Optical Spectrum of MoS2: Many-Body Effects and Diversity of Exciton States. *Phys. Rev. Lett.* **2013**, *111*, 216805.
86. Chernikov, A.; Berkelbach, T. C.; Hill, H. M.; Rigosi, A.; Li, Y.; Aslan, O. B.; Reichman, D. R.; Hybertsen, M. S.; Heinz, T. F. Exciton Binding Energy and Nonhydrogenic Rydberg Series in Monolayer WS2. *Phys. Rev. Lett.* **2014**, *113*, 76802.
87. He, K.; Kumar, N.; Zhao, L.; Wang, Z.; Mak, K. F.; Zhao, H.; Shan, J. Tightly Bound Excitons in Monolayer WSe2. *Phys. Rev. Lett.* **2014**, *113*, 26803.
88. Ramasubramaniam, A. Large Excitonic Effects in Monolayers of Molybdenum and Tungsten Dichalcogenides. *Phys. Rev. B: Condens. Matter Mater. Phys.* **2012**, *86*, 115409.
89. Ye, Z.; Cao, T.; O'Brien, K.; Zhu, H.; Yin, X.; Wang, Y.; Louie, S. G.; Zhang, X. Probing Excitonic Dark States in Single-Layer Tungsten Disulphide. *Nature* **2014**, *513*, 214–218.
90. Ugeda, M. M.; Bradley, A. J.; Shi, S.-F.; da Jornada, F. H.; Zhang, Y.; Qiu, D. Y.; Ruan, W.; Mo, S.-K.; Hussain, Z.; Shen, Z.-X.; et al. Giant Bandgap Renormalization and Excitonic Effects in a Monolayer Transition Metal Dichalcogenide Semiconductor. *Nat. Mater.* **2014**, *13*, 1091–1095.
91. Hybertsen, M. S.; Louie, S. G. Electron Correlation in Semiconductors and Insulators: Band Gaps and Quasiparticle Energies. *Phys. Rev. B: Condens. Matter Mater. Phys.* **1986**, *34*, 5390–5413.
92. Rohlfing, M.; Louie, S. G. Electron-Hole Excitations and Optical Spectra from First Principles. *Phys. Rev. B: Condens. Matter Mater. Phys.* **2000**, *62*, 4927–4944.
93. Chhowalla, M.; Shin, H. S.; Eda, G.; Li, L.-J.; Loh, K. P.; Zhang, H. The Chemistry of Two-Dimensional Layered Transition Metal Dichalcogenide Nanosheets. *Nat. Chem.* **2013**, *5*, 263–275.
94. Lv, R.; Robinson, J. a; Schaak, R. E.; Sun, D.; Sun, Y.; Mallouk, T. E.; Terrones, M. Transition Metal Dichalcogenides and beyond: Synthesis, Properties, and Applications of Single- and Few-Layer Nanosheets. *Acc. Chem. Res.* **2015**, *48*, 56–64.
95. Shi, Y.; Li, H.; Li, L.-J. Recent Advances in Controlled Synthesis of Two-Dimensional Transition Metal Dichalcogenides via Vapour Deposition Techniques. *Chem. Soc. Rev.* **2015**, *44*, 2744–2756.
96. Yu, Y.; Li, C.; Liu, Y.; Su, L.; Zhang, Y.; Cao, L. Controlled Scalable Synthesis of Uniform, High-Quality Monolayer and Few-Layer MoS2 Films. *Sci. Rep.* **2013**, *3*, 1866.
97. Lee, Y.; Lee, J.; Bark, H.; Oh, I.-K.; Ryu, G. H.; Lee, Z.; Kim, H.; Cho, J. H.; Ahn, J.-H.; Lee, C. Synthesis of Wafer-Scale Uniform Molybdenum Disulfide Films with Control over the Layer Number Using a Gas Phase Sulfur Precursor. *Nanoscale* **2014**, *6*, 2821–2826.
98. Gatensby, R.; McEvoy, N.; Lee, K.; Hallam, T.; Berner, N. C.; Rezvani, E.; Winters, S.; O'Brien, M.; Duesberg, G. S. Controlled Synthesis of Transition Metal Dichalcogenide Thin Films for Electronic Applications. *Appl. Surf. Sci.* **2014**, *297*, 139–146.
99. Jung, Y.; Shen, J.; Liu, Y.; Woods, J. M.; Sun, Y.; Cha, J. J. Metal Seed Layer Thickness-Induced Transition From Vertical to Horizontal Growth of MoS 2 and WS 2. *Nano Lett.* **2014**, *14*, 6842.
100. Muratore, C.; Hu, J. J.; Wang, B.; Haque, M. a.; Bultman, J. E.; Jespersen, M. L.; Shamberger, P. J.; McConney, M. E.; Naguy, R. D.; Voevodin, a. a. Continuous Ultra-Thin MoS2 Films Grown by Low-Temperature Physical Vapor Deposition. *Appl. Phys. Lett.* **2014**, *104*, 261604.
101. Serrao, C. R.; Diamond, A. M.; Hsu, S.-L.; You, L.; Gadgil, S.; Clarkson, J.; Carraro, C.; Maboudian, R.; Hu, C.; Salahuddin, S. Highly Crystalline MoS2 Thin Films Grown by Pulsed Laser Deposition. *Appl. Phys. Lett.* **2015**, *106*, 052101.
102. Browning, P.; Eichfeld, S.; Zhang, K.; Hossain, L.; Lin, Y.-C.; Wang, K.; Lu, N.; Waite, A. R.; Voevodin, A. A.; Kim, M.; et al. Large-Area Synthesis of WSe2 from WO3 by Selenium−oxygen Ion Exchange. *2D Mater.* **2015**, *2*, 014003.
103. Jin, Z.; Shin, S.; Kwon, D. H.; Han, S.-J.; Min, Y.-S. Novel Chemical Route for Atomic Layer Deposition of MoS2 Thin Film on SiO2/Si Substrate. *Nanoscale* **2014**, *6*, 14453–14458.
104. Tarasov, A.; Campbell, P. M.; Tsai, M.-Y.; Hesabi, Z. R.; Feirer, J.; Graham, S.; Ready, W. J.; Vogel, E. M. Highly Uniform Trilayer Molybdenum Disulfide for Wafer-Scale Device Fabrication. *Adv. Funct. Mater.* **2014**, *24*, 6389–6400.
105. Lee, Y. H.; Yu, L.; Wang, H.; Fang, W.; Ling, X.; Shi, Y.; Lin, C.-T.; Huang, J. K.; Chang, M. T.; Chang, C. S.; et al. Synthesis and Transfer of Single-Layer Transition Metal Disulfides on Diverse Surfaces. *Nano Lett.* **2013**, 1852.
106. Ling, X.; Lee, Y.; Lin, Y.; Fang, W.; Yu, L.; Dresselhaus, M. S.; Kong, J. Role of the Seeding Promoter in MoS2 Growth by Chemical Vapor Deposition. *Nano Lett.* **2014**, *14*, 464.
107. Vishwanath, S.; Liu, X.; Rouvimov, S.; Mende, P. C.; Azcatl, A.; McDonnell, S.; Wallace, R. M.; Feenstra, R. M.; Furdyna, J. K.; Jena, D.; et al. Comprehensive Structural and Optical Characterization of MBE Grown $MoSe_2$ on Graphite, CaF_2 and Graphene. *2D Mater.* **2015**, *2*, 024007.
108. Chiappe, D.; Scalise, E.; Cinquanta, E.; Grazianetti, C.; Van Den Broek, B.; Fanciulli, M.; Houssa, M.; Molle, A. Two-Dimensional Si Nanosheets with Local Hexagonal Structure on a MoS 2 Surface. *Adv. Mater.* **2014**, *26*, 2096–2101.
109. Liu, H.; Jiao, L.; Yang, F.; Cai, Y.; Wu, X.; Ho, W.; Gao, C.; Jia, J.; Wang, N.; Fan, H.; et al. Dense Network of One-Dimensional Midgap Metallic Modes in Monolayer MoSe2 and Their Spatial Undulations. *Phys. Rev. Lett.* **2014**, *113*, 066105.
110. Yue, R.; Barton, A. T.; Zhu, H.; Azcatl, A.; Pena, L. F.; Wang, J.; Peng, X.; Lu, N.; Cheng, L.; Addou, R.; et al. HfSe2 Thin Films: 2D Transition Metal Dichalcogenides Grown by Molecular Beam Epitaxy. *ACS Nano* **2015**, *9*, 474–480.
111. Liu, H. J.; Jiao, L.; Xie, L.; Yang, F.; Chen, J. L.; Ho, W. K.; Gao, C. L.; Jia, J. F.; Cui, X. D.; Xie, M. H. Molecular-Beam Epitaxy of Monolayer and Bilayer WSe2: A Scanning Tunneling Microscopy/spectroscopy Study and Deduction of Exciton Binding Energy. *2D Mater.* **2015**, *2*, 34004.
112. Barton, a. T.; Yue, R.; Anwar, S.; Zhu, H.; Peng, X.; McDonnell, S.; Lu, N.; Addou, R.; Colombo, L.; Kim, M. J.; et al. Transition Metal Dichalcogenide and Hexagonal Boron Nitride Heterostructures Grown by Molecular Beam Epitaxy. *Microelectron. Eng.* **2015**, *147*, 306–309.
113. Eichfeld, S. M.; Hossain, L.; Lin, Y.-C.; Piasecki, A. F.; Kupp, B.; Birdwell, A. G. G.; Burke, R. A.; Lu, N.; Peng, X.; Li, J.; et al. Highly Scalable, Atomically Thin WSe2 Grown via Metal-Organic Chemical Vapor Deposition. *ACS Nano* **2015**, *9*, 2080–2087.
114. Kang, K.; Xie, S.; Huang, L.; Han, Y.; Huang, P. Y.; Mak, K. F.; Kim, C.-J.; Muller, D.; Park, J. High-Mobility Three-Atom-Thick Semiconducting Films with Wafer-Scale Homogeneity. *Nature* **2015**, *520*, 656–660.
115. Kranthi Kumar, V.; Dhar, S.; Choudhury, T. H.; Shivashankar, S. A.; Raghavan, S. A Predictive Approach to CVD of Crystalline Layers of TMDs: The Case of MoS2. *Nanoscale* **2015**, *7*, 7802–7810.
116. Kong, D.; Wang, H.; Cha, J. J.; Pasta, M.; Koski, K. J.; Yao, J.; Cui, Y. Synthesis of MoS2 and MoSe2 Films with Vertically Aligned Layers. *Nano Lett.* **2013**, *13*, 1341.
117. Jung, Y.; Shen, J.; Sun, Y.; Cha, J. J.; Engineering, M.; Science, M.; Haven, N.; States, U.; Haven, W. Chemically Synthesized Heterostructures of Two-Dimensional

Dichalcogenides with Vertically. *ACS Nano* **2014**, *8*, 9550–9557.
118. Liu, H.; Antwi, K. K. A.; Chua, S.; Chi, D. Vapor-Phase Growth and Characterization of Mo(1-x)W(x)S2 ($0 \leq X \leq 1$) Atomic Layers on 2-Inch Sapphire Substrates. *Nanoscale* **2014**, *6*, 624–629.
119. Chen, Y.; Xi, J.; Dumcenco, D. O.; Liu, Z.; Suenaga, K.; Wang, D.; Al, C. E. T. Tunable Band Gap Photoluminescence from Atomically Thin Transition-Metal Dichalcogenide Alloys. *ACS Nano* **2013**, *7*, 4610–4616.
120. Li, H.; Zhang, Q.; Duan, X.; Wu, X.; Fan, X.; Zhu, X.; Zhuang, X.; Hu, W.; Zhou, H.; Pan, A.; et al. Lateral Growth of Composition Graded Atomic Layer MoS2(1-x)Se2x Nanosheets. *J. Am. Chem. Soc.* **2015**, *137*, 5284–5287.
121. Mann, J.; Ma, Q.; Odenthal, P. M.; Isarraraz, M.; Le, D.; Preciado, E.; Barroso, D.; Yamaguchi, K.; Palacio, G.; von, S.; Andrew, N.; et al. 2-Dimensional Transition Metal Dichalcogenides with Tunable Direct Band Gaps: MoS2(1-x)Se2x Monolayers. *Adv. Mater.* **2014**, *26*, 1399–1404.
122. Klee, V.; Preciado, E.; Barroso, D.; Nguyen, A. E.; Lee, C.; Erickson, K. J.; Triplett, M.; Davis, B.; Lu, I.-H.; Bobek, S.; et al. Superlinear Composition-Dependent Photocurrent in CVD-Grown Monolayer MoS $_{2(1-x)}$ Se $_{2\ x}$ Alloy Devices. *Nano Lett.* **2015**, *15*, 2612–2619.
123. Kim, I. S.; Sangwan, V. K.; Jariwala, D.; Wood, J. D.; Park, S.; Chen, K.-S.; Shi, F.; Ruiz-Zepeda, F.; Ponce, A.; Jose-Yacaman, M.; et al. Influence of Stoichiometry on the Optical and Electrical Properties of Chemical Vapor Deposition Derived MoS2. *ACS Nano* **2014**, *8*, 10551–10558.
124. Sangwan, V. K.; Jariwala, D.; Kim, I. S.; Chen, K.-S.; Marks, T. J.; Lauhon, L. J.; Hersam, M. C. Gate-Tunable Memristive Phenomena Mediated by Grain Boundaries in Single-Layer MoS2. *Nat. Nanotechnol.* **2015**, *10*, 403–406.
125. Bilgin, I.; Liu, F.; Vargas, A.; Winchester, A.; Man, M. K. L.; Upmanyu, M.; Dani, K.; Gupta, G.; Talapatra, S.; Mohite, A. D.; et al. Chemical Vapor Deposition Synthesized Atomically-Thin Molybdenum Disulfide with Opto-electronic-Grade Crystalline Quality. *ACS Nano* **2015**, *9*, 8822–8832.
126. Ma, Q.; Isarraraz, M.; Wang, C. S.; Preciado, E.; Klee, V.; Bobek, S.; Yamaguchi, K.; Li, E.; Odenthal, P. M.; Ariana, N.; et al. Postgrowth Tuning of the Bandgap of Single-Layer Molybdenum Disulfide Films by Sulfur/Selenium Exchange. *ACS Nano* **2014**, *8*, 4672–4677.
127. Mahjouri-Samani, M.; Lin, M.-W.; Wang, K.; Lupini, A. R.; Lee, J.; Basile, L.; Boulesbaa, A.; Rouleau, C. M.; Puretzky, A. a.; Ivanov, I. N.; et al. Patterned Arrays of Lateral Heterojunctions within Monolayer Two-Dimensional Semiconductors. *Nat. Commun.* **2015**, *6*, 7749.
128. Han, G. H.; Kybert, N. J.; Naylor, C. H.; Lee, B. S.; Ping, J.; Park, J. H.; Kang, J.; Lee, S. Y.; Lee, Y. H.; Agarwal, R.; et al. Seeded Growth of Highly Crystalline Molybdenum Disulphide Monolayers at Controlled Locations. *Nat. Commun.* **2015**, *6*, 6128.
129. Jeon, J.; Jang, S. K.; Jeon, S. M.; Yoo, G.; Jang, Y. H.; Park, J.-H.; Lee, S. Layer-Controlled CVD Growth of Large-Area Two-Dimensional MoS2 Films. *Nanoscale* **2015**, *7*, 1688–1695.
130. Frindt, R. F. Single Crystals of MoS2 Several Molecular Layers Thick. *J. Appl. Phys.* **1966**, *37*, 1928–1929.
131. Zhao, W.; Ghorannevis, Z.; Chu, L.; Toh, M.; Kloc, C.; Tan, P.-H.; Eda, G. Evolution of Electronic Structure in Atomically Thin Sheets of WS2 and WSe2. *ACS Nano* **2013**, *7*, 791–797.
132. Tonndorf, P.; Schmidt, R.; Bottger, P.; Zhang, X.; Borner, J.; Liebig, A.; Albrecht, M.; Kloc, C.; Gordan, O.; Zahn, D. R.; et al. Photoluminescence Emission and Raman Response of Monolayer MoS(2), MoSe(2), and WSe(2). *Opt. Express* **2013**, *21*, 4908–4916.
133. Dumcenco, D. O.; Kobayashi, H.; Liu, Z.; Huang, Y.-S.; Suenaga, K. Visualization and Quantification of Transition Metal Atomic Mixing in Mo1-xWxS2 Single Layers. *Nat. Commun.* **2013**, *4*, 1351.
134. Tongay, S.; Narang, D. S.; Kang, J.; Fan, W.; Ko, C.; Luce, A. V.; Wang, K. X.; Suh, J.; Patel, K. D.; Pathak, V. M. Two-Dimensional Semiconductor Alloys: Monolayer $Mo_{1-x}W_xSe_2$. *Appl. Phys. Lett.* **2014**, *104*, 012101.
135. Zhang, M.; Wu, J.; Zhu, Y.; Dumcenco, D. O.; Hong, J.; Mao, N.; Deng, S.; Chen, Y.; Yang, Y.; Jin, C.; et al. Two-Dimensional Molybdenum Tungsten Diselenide Alloys: Photoluminescence, Raman Scattering, and Electrical Transport. *ACS Nano* **2014**, *8*, 7130–7137.
136. Lin, Y. C.; Dumcenco, D. O.; Komsa, H. P.; Niimi, Y.; Krasheninnikov, A. V.; Huang, Y. S.; Suenaga, K. Properties of Individual Dopant Atoms in Single-Layer MoS2: Atomic Structure, Migration, and Enhanced Reactivity. *Adv. Mater.* **2014**, *26*, 2857–2861.
137. Laskar, M. R.; Nath, D. N.; Ma, L.; Lee, E. W., II; Lee, C. H.; Kent, T.; Yang, Z.; Mishra, R.; Roldan, M. A.; Idrobo, J.-C. P-Type Doping of MoS2 Thin Films Using Nb. *Appl. Phys. Lett.* **2014**, *104*, 92104.
138. Suh, J.; Park, T.-E.; Lin, D.-Y.; Fu, D.; Park, J.; Jung, H. J.; Chen, Y.; Ko, C.; Jang, C.; Sun, Y.; et al. Doping against the Native Propensity of MoS2: Degenerate Hole Doping by Cation Substitution. *Nano Lett.* **2014**, *14*, 6976–6982.
139. Hong, X. P.; Kim, J.; Shi, S. F.; Zhang, Y.; Jin, C. H.; Sun, Y. H.; Tongay, S.; Wu, J. Q.; Zhang, Y. F.; Wang, F. Ultrafast Charge Transfer in Atomically Thin MoS2/WS2 Heterostructures. *Nat. Nanotechnol.* **2014**, *9*, 682–686.
140. Fang, H.; Battaglia, C.; Carraro, C.; Nemsak, S.; Ozdol, B.; Kang, J. S.; Bechtel, H. A.; Desai, S. B.; Kronast, F.; Unal, A. A.; et al. Strong Interlayer Coupling in van Der Waals Heterostructures Built from Single-Layer Chalcogenides. *Proc. Natl. Acad. Sci. U. S. A.* **2014**, *111*, 6198–6202.
141. Furchi, M. M.; Pospischil, A.; Libisch, F.; Burgdoerfer, J.; Mueller, T. Photovoltaic Effect in an Electrically Tunable van Der Waals Heterojunction. *Nano Lett.* **2014**, *14*, 4785–4791.
142. Lee, C.-H.; Lee, G.-H.; van der Zande, A. M.; Chen, W.; Li, Y.; Han, M.; Cui, X.; Arefe, G.; Nuckolls, C.; Heinz, T. F.; et al. Atomically Thin P−n Junctions with van Der Waals Heterointerfaces. *Nat. Nanotechnol.* **2014**, *9*, 676–681.
143. Bertolazzi, S.; Krasnozhon, D.; Kis, A. Nonvolatile Memory Cells Based on MoS2/Graphene Heterostructures. *ACS Nano* **2013**, *7*, 3246–3252.
144. Britnell, L.; Ribeiro, R. M.; Eckmann, A.; Jalil, R.; Belle, B. D.; Mishchenko, A.; Kim, Y.-J.; Gorbachev, R. V.; Georgiou, T.; Morozov, S. V.; et al. Strong Light-Matter Interactions in Heterostructures of Atomically Thin Films. *Science (Washington, DC, U. S.)* **2013**, *340*, 1311–1314.
145. Choi, M. S.; Lee, G.-H.; Yu, Y.-J.; Lee, D.-Y.; Lee, S. H.; Kim, P.; Hone, J.; Yoo, W. J. Controlled Charge Trapping by Molybdenum Disulphide and Graphene in Ultrathin Heterostructured Memory Devices. *Nat. Commun.* **2013**, *4*, 1624.
146. Roy, K.; Padmanabhan, M.; Goswami, S.; Sai, T. P.; Ramalingam, G.; Raghavan, S.; Ghosh, A. Graphene-MoS2 Hybrid Structures for Multifunctional Photoresponsive Memory Devices. *Nat. Nanotechnol.* **2013**, *8*, 826–830.
147. Yu, W. J.; Li, Z.; Zhou, H.; Chen, Y.; Wang, Y.; Huang, Y.; Duan, X. Vertically Stacked Multi-Heterostructures of Layered Materials for Logic Transistors and Complementary Inverters. *Nat. Mater.* **2013**, *12*, 246–252.
148. Yu, W. J.; Liu, Y.; Zhou, H.; Yin, A.; Li, Z.; Huang, Y.; Duan, X. Highly Efficient Gate-Tunable Photocurrent Generation in Vertical Heterostructures of Layered Materials. *Nat. Nanotechnol.* **2013**, *8*, 952–958.
149. Georgiou, T.; Jalil, R.; Belle, B. D.; Britnell, L.; Gorbachev, R. V.; Morozov, S. V.; Kim, Y.-J.; Gholinia, A.; Haigh, S. J.; Makarovsky, O.; et al. Vertical Field-Effect Transistor Based on Graphene-WS2 Heterostructures for Flexible and Transparent Electronics. *Nat. Nanotechnol.* **2013**, *8*, 100–103.
150. Lee, G. H.; Yu, Y. J.; Cui, X.; Petrone, N.; Lee, C. H.; Choi, M. S.; Lee, D. Y.; Lee, C.; Yoo, W. J.; Watanabe, K.; et al. Flexible and Transparent MoS2 Field-Effect Transistors on Hexagonal Boron Nitride-Graphene Heterostructures. *ACS Nano* **2013**, *7*, 7931–7936.

151. Coleman, J. N.; Lotya, M.; O'Neill, A.; Bergin, S. D.; King, P. J.; Khan, U.; Young, K.; Gaucher, A.; De, S.; Smith, R. J.; et al. Two-Dimensional Nanosheets Produced by Liquid Exfoliation of Layered Materials. *Science (Washington, DC, U. S.)* **2011**, *331*, 568–571.
152. Varrla, E.; Backes, C.; Paton, K. R.; Harvey, A.; Gholamvand, Z.; McCauley, J.; Coleman, J. N. Large-Scale Production of Size-Controlled MoS2 Nanosheets by Shear Exfoliation. *Chem. Mater.* **2015**, *27*, 1129–1139.
153. Yu, X.; Prevot, M. S.; Guijarro, N.; Sivula, K. Self-Assembled 2D WSe2 Thin Films for Photoelectrochemical Hydrogen Production. *Nat. Commun.* **2015**, *6*, 7596.
154. Wu, S.; Huang, C.; Aivazian, G.; Ross, J. S.; Cobden, D. H.; Xu, X. Vapor-Solid Growth of High Optical Quality MoS2Monolayers with Near-Unity Valley Polarization. *ACS Nano* **2013**, *7*, 2768–2772.
155. Lin, Z.; Thee, M. T.; Elias, A. L.; Feng, S. M.; Zhou, C. J.; Fujisawa, K.; Perea-Lopez, N.; Carozo, V.; Terrones, H.; Terrones, M. Facile Synthesis of MoS2 and MoXW1-xS2 Triangular Monolayers. *APL Mater.* **2014**, *2*, 92514.
156. Clark, G.; Wu, S.; Rivera, P.; Finney, J.; Nguyen, P.; Cobden, D. H.; Xu, X. Vapor-Transport Growth of High Optical Quality WSe2Monolayers. *APL Mater.* **2014**, *2*, 101101.
157. Wang, X.; Feng, H.; Wu, Y.; Jiao, L. Controlled Synthesis of Highly Crystalline MoS2 Flakes by Chemical Vapor Deposition. *J. Am. Chem. Soc.* **2013**, *135*, 5304–5307.
158. Ji, Q.; Zhang, Y.; Gao, T.; Zhang, Y.; Ma, D.; Liu, M.; Chen, Y.; Qiao, X.; Tan, P.-H.; Kan, M.; et al. Epitaxial Monolayer MoS2 on Mica with Novel Photoluminescence. *Nano Lett.* **2013**, *13*, 3870–3877.
159. van der Zande, A. M.; Huang, P. Y.; Chenet, D. a; Berkelbach, T. C.; You, Y.; Lee, G.-H.; Heinz, T. F.; Reichman, D. R.; Muller, D. a; Hone, J. C. Grains and Grain Boundaries in Highly Crystalline Monolayer Molybdenum Disulphide. *Nat. Mater.* **2013**, *12*, 554–561.
160. Kong, D.; Wang, H.; Cha, J. J.; Pasta, M.; Koski, K. J.; Yao, J.; Cui, Y. Synthesis of MoS2 and MoSe2 Films with Vertically Aligned Layers. *Nano Lett.* **2013**, *13*, 1341–1347.
161. Gutierrez, H. R.; Perea-Lopez, N.; Elias, A. L.; Berkdemir, A.; Wang, B.; Lv, R.; Lopez-Urias, F.; Crespi, V. H.; Terrones, H.; Terrones, M. Extraordinary Room-Temperature Photoluminescence in Triangular WS2Monolayers. *Nano Lett.* **2013**, *13*, 3447–3454.
162. Zhang, Y.; Zhang, Y.; Ji, Q.; Ju, J.; Yuan, H.; Shi, J.; Gao, T.; Ma, D.; Liu, M.; Chen, Y.; et al. Controlled Growth of High-Quality Monolayer WS2 Layers on Sapphire and Imaging Its Grain Boundary. *ACS Nano* **2013**, *7*, 8963–8971.
163. Elías, A. L.; Perea-López, N.; Castro-Beltrán, A.; Berkdemir, A.; Lv, R.; Feng, S.; Long, A. D.; Hayashi, T.; Kim, Y. A.; Endo, M.; et al. Controlled Synthesis and Transfer of Large-Area WS2 Sheets: From Single Layer to Few Layers. *ACS Nano* **2013**, *7*, 5235–5242.
164. Peimyoo, N.; Shang, J.; Cong, C.; Shen, X.; Wu, X.; Yeow, E. K. L.; Yu, T. Nonblinking, Intense Two-Dimensional Light Emitter: Mono Layer WS2 Triangles. *ACS Nano* **2013**, *7*, 10985–10994.
165. Cong, C.; Shang, J.; Wu, X.; Cao, B.; Peimyoo, N.; Qiu, C.; Sun, L.; Yu, T. Synthesis and Optical Properties of Large-Area Single-Crystalline 2D Semiconductor WS2Monolayer from Chemical Vapor Deposition. *Adv. Opt. Mater.* **2014**, *2*, 131–136.
166. Wang, X.; Gong, Y.; Shi, G.; Chow, W. L.; Keyshar, K.; Ye, G.; Vajtai, R.; Lou, J.; Liu, Z.; Ringe, E.; et al. Chemical Vapor Deposition Growth of Crystalline Mono Layer MoSe2. *ACS Nano* **2014**, *8*, 5125–5131.
167. Lu, X.; Utama, M. I. B.; Lin, J.; Gong, X.; Zhang, J.; Zhao, Y.; Pantelides, S. T.; Wang, J.; Dong, Z.; Liu, Z.; et al. Large-Area Synthesis of Monolayer and Few-Layer MoSe2 Films on SiO2 Substrates. *Nano Lett.* **2014**, *14*, 2419–2425.
168. Okada, M.; Sawazaki, T.; Watanabe, K.; Taniguch, T.; Hibino, H.; Shinohara, H.; Kitaura, R. Direct Chemical Vapor Deposition Growth of WS2 Atomic Layers on Hexagonal Boron Nitride. *ACS Nano* **2014**, *8*, 8273–8277.
169. Huang, J.-K.; Pu, J.; Hsu, C.-L.; Chiu, M.-H.; Juang, Z.-Y.; Chang, Y.-H.; Chang, W.-H.; Iwasa, Y.; Takenobu, T.; Li, L.-J. Large-Area Synthesis of Highly Crystalline WSe2Monolayers and Device Applications. *ACS Nano* **2014**, *8*, 923–930.
170. Gong, Y.; Liu, Z.; Lupini, A. R.; Shi, G.; Lin, J.; Najmaei, S.; Lin, Z.; Elías, A. L.; Berkdemir, A.; You, G.; et al. Band Gap Engineering and Layer-by-Layer Mapping of Selenium-Doped Molybdenum Disulfide. *Nano Lett.* **2014**, *14*, 442–449.
171. Su, S.-H.; Hsu, Y.-T.; Chang, Y.-H.; Chiu, M.-H.; Hsu, C.-L.; Hsu, W.-T.; Chang, W.-H.; He, J.-H.; Li, L.-J. Band Gap-Tunable Molybdenum Sulfide Selenide Monolayer Alloy. *Small* **2014**, *10*, 2589–2594.
172. Li, H.; Duan, X.; Wu, X.; Zhuang, X.; Zhou, H.; Zhang, Q.; Zhu, X.; Hu, W.; Ren, P.; Guo, P.; et al. Growth of Alloy MoS2xSe2(1-X) Nanosheets with Fully Tunable Chemical Compositions and Optical Properties. *J. Am. Chem. Soc.* **2014**, *136*, 3756–3759.
173. Huang, C.; Wu, S.; Sanchez, A. M.; Peters, J. J. P.; Beanland, R.; Ross, J. S.; Rivera, P.; Yao, W.; Cobden, D. H.; Xu, X. Lateral Heterojunctions within Monolayer MoSe2-WSe2 Semiconductors. *Nat. Mater.* **2014**, *13*, 1096–1101.
174. Zhang, K.; Feng, S.; Wang, J.; Azcatl, A.; Lu, N.; Addou, R.; Wang, N.; Zhou, C.; Lerach, J. O.; Bojan, V.; et al. Manganese Doping of Monolayer MoS2: The Substrate Is Critical. *Nano Lett.* **2015**, *15*, 6586.
175. Gong, Y. J.; Lin, J. H.; Wang, X. L.; Shi, G.; Lei, S. D.; Lin, Z.; Zou, X. L.; Ye, G. L.; Vajtai, R.; Yakobson, B. I.; et al. Vertical and in-Plane Heterostructures from WS2/MoS2Monolayers. *Nat. Mater.* **2014**, *13*, 1135–1142.
176. Chiu, M. H.; Li, M. Y.; Zhang, W.; Hsu, W. T.; Chang, W. H.; Terrones, M.; Terrones, H.; Li, L. J. Spectroscopic Signatures for Interlayer Coupling in MoS2-WSe2 van Der Waals Stacking. *ACS Nano* **2014**, *8*, 9649–9656.
177. Gong, Y.; Lei, S.; Ye, G.; Li, B.; He, Y.; Keyshar, K.; Zhang, X.; Wang, Q.; Lou, J.; Liu, Z.; et al. Two-Step Growth of Two-Dimensional WSe2/MoSe2 Heterostructures. *Nano Lett.* **2015**, *15*, 6135–6141.
178. Deng, Y.; Luo, Z.; Conrad, N. J.; Liu, H.; Gong, Y.; Najmaei, S.; Ajayan, P. M.; Lou, J.; Xu, X.; Ye, P. D. Black Phosphorus-Monolayer MoS2 van Der Waals Heterojunction P-N Diode. *ACS Nano* **2014**, *8*, 8292–8299.
179. Ago, H.; Endo, H.; Solís-Fernández, P.; Takizawa, R.; Ohta, Y.; Fujita, Y.; Yamamoto, K.; Tsuji, M.; Solis-Fernandez, P.; Takizawa, R.; et al. Controlled van Der Waals Epitaxy of Monolayer MoS2 Triangular Domains on Graphene. *ACS Appl. Mater. Interfaces* **2015**, *7*, 5265–5273.
180. Lin, Y.-C.; Lu, N.; Perea-Lopez, N.; Li, J.; Lin, Z.; Peng, X.; Lee, C. H.; Sun, C.; Calderin, L.; Browning, P. N.; et al. Direct Synthesis of van Der Waals Solids. *ACS Nano* **2014**, *8*, 3715–3723.
181. Azizi, A.; Eichfeld, S.; Geschwind, G.; Zhang, K.; Jiang, B.; Mukherjee, D.; Hossain, L.; Piasecki, A. F.; Kabius, B.; Robinson, J. A.; et al. Freestanding van Der Waals Heterostructures of Graphene and Transition Metal Dichalcogenides. *ACS Nano* **2015**, *9*, 4882–4890.
182. Yu, L.; Kong, J.; Wang, H. Graphene/MoS2 Hybrid Technology for Large-Scale Two- Dimensional Electronics. *Nano Lett.* **2014**, *14*, 3055–3063.
183. McCreary, K. M.; Hanbicki, A. T.; Robinson, J. T.; Cobas, E.; Culbertson, J. C.; Friedman, A. L.; Jernigan, G. G.; Jonker, B. T. Large-Area Synthesis of Continuous and Uniform MoS2Monolayer Films on Graphene. *Adv. Funct. Mater.* **2014**, *24*, 6449–6454.
184. Zhang, W.; Chuu, C.-P.; Huang, J.-K.; Chen, C.-H.; Tsai, M.-L.; Chang, Y.-H.; Liang, C.-T.; Chen, Y.-Z.; Chueh, Y.-L.; He, J.-H. Ultrahigh-Gain Photodetectors Based on Atomically Thin Graphene-MoS_2 Heterostructures. *Sci. Rep.* **2014**, *4*, 3826.
185. Shim, G. W.; Yoo, K.; Seo, S.-B.; Shin, J.; Jung, D. Y.; Kang, I.-S.; Ahn, C. W.; Cho, B. J.; Choi, S.-Y. Large-Area Single-Layer MoSe2 and Its van Der Waals Heterostructures. *ACS Nano* **2014**, *8*, 6655–6662.
186. Li, B.; Huang, L.; Zhong, M.; Huo, N.; Li, Y.; Yang, S.; Fan, C.; Yang, J.; Hu, W.; Wei, Z. Synthesis and Transport Properties of Large-Scale Alloy Co0. 16Mo0. 84S2 Bilayer Nanosheets. *ACS Nano* **2015**, *9*, 1257–1262.

187. Lin, Y.-C.; Ghosh, R. K.; Addou, R.; Lu, N.; Eichfeld, S. M.; Zhu, H.; Li, M.-Y.; Peng, X.; Kim, M. J.; Li, L.-J.; et al. Atomically Thin Resonant Tunnel Diodes Built from Synthetic van Der Waals Heterostructures. *Nat. Commun.* **2015**, *6*, 7311.
188. Zhang, X.; Meng, F.; Christianson, J. R.; Arroyo-Torres, C.; Lukowski, M. A.; Liang, D.; Schmidt, J. R.; Jin, S. Vertical Heterostructures of Layered Metal Chalcogenides by van Der Waals Epitaxy. *Nano Lett.* **2014**, *14*, 3047–3054.
189. Duan, X.; Wang, C.; Shaw, J. C.; Cheng, R.; Chen, Y.; Li, H.; Wu, X.; Tang, Y.; Zhang, Q.; Pan, A.; et al. Lateral Epitaxial Growth of Two-Dimensional Layered Semiconductor Heterojunctions. *Nat. Nanotechnol.* **2014**, *9*, 1024–1030.
190. Li, M.-Y.; Shi, Y.; Cheng, C.-C.; Lu, L.-S.; Lin, Y.-C.; Tang, H.-L.; Tsai, M.-L.; Chu, C.-W.; Wei, K.-H.; He, J.-H.; et al. Epitaxial Growth of a Monolayer WSe2-MoS2 Lateral P-N Junction with an Atomically Sharp Interface. *Science (Washington, DC, U. S.)* **2015**, *349*, 524–528.
191. Lehtinen, O.; Komsa, H. P.; Pulkin, A.; Whitwick, M. B.; Chen, M. W.; Lehnert, T.; Mohn, M. J.; Yazyev, O. V.; Kis, A.; et al. Atomic Scale Microstructure and Properties of Se-Deficient Two-Dimensional MoSe2. *ACS Nano* **2015**, *9*, 3274–3283.
192. Zhang, Y.; Chang, T.-R.; Zhou, B.; Cui, Y.-T.; Yan, H.; Liu, Z.; Schmitt, F.; Lee, J.; Moore, R.; Chen, Y.; et al. Direct Observation of the Transition from Indirect to Direct Bandgap in Atomically Thin Epitaxial MoSe2. *Nat. Nanotechnol.* **2014**, *9*, 111–115.
193. Liu, H.; Zheng, H.; Yang, F.; Jiao, L.; Chen, J.; Ho, W.; Gao, C.; Jia, J.; Xie, M. Line and Point Defects in MoSe2 Bilayer Studied by Scanning Tunneling Microscopy and Spectroscopy. *ACS Nano* **2015**, *9*, 6619–6625.
194. Jiao, L.; Liu, H. J.; Chen, J. L.; Yi, Y.; Chen, W. G.; Cai, Y.; Wang, J. N.; Dai, X. Q.; Wang, N.; Ho, W. K.; et al. Molecular-Beam Epitaxy of Monolayer MoSe2: Growth Characteristics and Domain Boundary Formation. *New J. Phys.* **2015**, *17*, 53023.
195. Yu, Y.; Yang, F.; Lu, X. F.; Yan, Y. J.; Cho, Y.-H.; Ma, L.; Niu, X.; Kim, S.; Son, Y.-W.; Feng, D.; et al. Gate-Tunable Phase Transitions in Thin Flakes of 1T-TaS2. *Nat. Nanotechnol.* **2015**, *10*, 270–276.
196. Zeng, Z.; Tan, C.; Huang, X.; Bao, S.; Zhang, H. Growth of Noble Metal Nanoparticles on Single-Layer TiS2 and TaS2 Nanosheets for Hydrogen Evolution Reaction. *Energy Environ. Sci.* **2014**, *7*, 797–803.
197. Renteria, J.; Samnakay, R.; Jiang, C.; Pope, T. R.; Goli, P.; Yan, Z.; Wickramaratne, D.; Salguero, T. T.; Khitun, A. G.; Lake, R. K.; et al. All-Metallic Electrically Gated 2H-TaSe2 Thin-Film Switches and Logic Circuits. *J. Appl. Phys.* **2014**, *115*, 034305.
198. Lv, R.; Robinson, J. a; Schaak, R. E.; Sun, D.; Sun, Y.; Mallouk, T. E.; Terrones, M. Transition Metal Dichalcogenides and beyond: Synthesis, Properties, and Applications of Single- and Few-Layer Nanosheets. *Acc. Chem. Res.* **2015**, *48*, 56–64.
199. Geim, A. K.; Grigorieva, I. V. Van Der Waals Heterostructures. *Nature* **2013**, *499*, 419.
200. Tongay, S.; Fan, W.; Kang, J.; Park, J.; Koldemir, U.; Suh, J.; Narang, D. S.; Liu, K.; Ji, J.; Li, J.; et al. Tuning Interlayer Coupling in Large-Area Heterostructures with CVD-Grown MoS2 and WS2Monolayers. *Nano Lett.* **2014**, *14*, 3185–3190.
201. Ceballos, F.; Bellus, M. Z.; Chiu, H.-Y.; Zhao, H. Ultrafast Charge Separation and Indirect Exciton Formation in a MoS2−MoSe2 van Der Waals Heterostructure. *ACS Nano* **2014**, *8*, 12717–12724.
202. Rivera, P.; Schaibley, J. R.; Jones, A. M.; Ross, J. S.; Wu, S.; Aivazian, G.; Klement, P.; Seyler, K.; Clark, G.; Ghimire, N. J. Observation of Long-Lived Interlayer Excitons in Monolayer $MoSe_2-WSe_2$ Heterostructures. *Nat. Commun.* **2015**, *6*, 6242.
203. Dean, C. R.; Young, A. F.; MericI; LeeC; WangL; SorgenfreiS; WatanabeK; TaniguchiT; KimP; Shepard, K. L.; et al. Boron Nitride Substrates for High-Quality Graphene Electronics. *Nat. Nanotechnol.* **2010**, *5*, 722–726.
204. Haigh, S. J.; Gholinia, A.; Jalil, R.; Romani, S.; Britnell, L.; Elias, D. C.; Novoselov, K. S.; Ponomarenko, L. A.; Geim, A. K.; Gorbachev, R. Cross-Sectional Imaging of Individual Layers and Buried Interfaces of Graphene-Based Heterostructures and Superlattices. *Nat. Mater.* **2012**, *11*, 764–767.
205. Ago, H.; Endo, H.; Solís-Fernández, P.; Takizawa, R.; Ohta, Y.; Fujita, Y.; Yamamoto, K.; Tsuji, M. Controlled van Der Waals Epitaxy of Monolayer MoS2 Triangular Domains on Graphene. *ACS Appl. Mater. Interfaces* **2015**, *7*, 5265–5273.
206. Lin, Y.-C.; Chang, C.-Y. S.; Ghosh, R. K.; Li, J.; Zhu, H.; Addou, R.; Diaconescu, B.; Ohta, T.; Peng, X.; Lu, N.; et al. Atomically Thin Heterostructures Based on Single-Layer Tungsten Diselenide and Graphene. *Nano Lett.* **2014**, *14*, 6936–6941.
207. Shi, Y.; Zhou, W.; Lu, A.-Y.; Fang, W.; Lee, Y.-H.; Hsu, A. L.; Kim, S. M.; Kim, K. K.; Yang, H. Y.; Li, L.-J.; et al. Van Der Waals Epitaxy of MoS2 Layers Using Graphene As Growth Templates. *Nano Lett.* **2012**, *12*, 2784–2791.
208. Wang, S.; Wang, X.; Warner, J. H. All Chemical Vapor Deposition Growth of MoS2:h-BN Vertical van Der Waals Heterostructures. *ACS Nano* **2015**, *9*, 5246–5254.
209. Yu, J. H.; Lee, H. R.; Hong, S. S.; Kong, D.; Lee, H.-W.; Wang, H.; Xiong, F.; Wang, S.; Cui, Y. Vertical Heterostructure of Two-Dimensional MoS2 and WSe2 with Vertically Aligned Layers. *Nano Lett.* **2015**, *15*, 1031–1035.
210. Yu, Y.; Hu, S.; Su, L.; Huang, L.; Liu, Y.; Jin, Z.; Purezky, A. A.; Geohegan, D. B.; Kim, K. W.; Zhang, Y.; et al. Equally Efficient Interlayer Exciton Relaxation and Improved Absorption in Epitaxial and Nonepitaxial MoS2/WS2 Heterostructures. *Nano Lett.* **2015**, *15*, 486.
211. Heo, H.; Sung, J. H.; Jin, G.; Ahn, J.-H.; Kim, K.; Lee, M.-J.; Cha, S.; Choi, H.; Jo, M.-H. Rotation-Misfit-Free Heteroepitaxial Stacking and Stitching Growth of Hexagonal Transition-Metal Dichalcogenide Monolayers by Nucleation Kinetics Controls. *Adv. Mater.* **2015**, *27*, 3803–3810.
212. Craciun, M. F.; Khrapach, I.; Barnes, M. D.; Russo, S. Properties and Applications of Chemically Functionalized Graphene. *J. Phys.: Condens. Matter* **2013**, *25*, 423201.
213. Kuila, T.; Bose, S.; Mishra, A. K.; Khanra, P.; Kim, N. H.; Lee, J. H. Chemical Functionalization of Graphene and Its Applications. *Prog. Mater. Sci.* **2012**, *57*, 1061–1105.
214. Georgakilas, V.; Otyepka, M.; Bourlinos, A. B.; Chandra, V.; Kim, N.; Kemp, K. C.; Hobza, P.; Zboril, R.; Kim, K. S. Functionalization of Graphene: Covalent and Non-Covalent Approaches, Derivatives and Applications. *Chem. Rev.* **2012**, *112*, 6156–6214.
215. Fang, H.; Chuang, S.; Chang, T. C.; Takei, K.; Takahashi, T.; Javey, A. High-Performance Single Layered WSe2 P-FETs with Chemically Doped Contacts. *Nano Lett.* **2012**, *12*, 3788–3792.
216. Tongay, S.; Zhou, J.; Ataca, C.; Liu, J.; Kang, J. S.; Matthews, T. S.; You, L.; Li, J.; Grossman, J. C.; Wu, J. Broad-Range Modulation of Light Emission in Two-Dimensional Semiconductors by Molecular Physisorption Gating. *Nano Lett.* **2013**, *13*, 2831–2836.
217. Lin, J. D.; Han, C.; Wang, F.; Wang, R.; Xiang, D.; Qin, S.; Zhang, X.-A.; Wang, L.; Zhang, H.; Wee, A. T. S.; et al. Electron-Doping-Enhanced Trion Formation in Monolayer Molybdenum Disulfide Functionalized with Cesium Carbonate. *ACS Nano* **2014**, *8*, 5323–5329.
218. Mouri, S.; Miyauchi, Y.; Matsuda, K. Tunable Photoluminescence of Monolayer MoS2 via Chemical Doping. *Nano Lett.* **2013**, *13*, 5944–5948.
219. Du, Y.; Liu, H.; Neal, A. T.; Si, M.; Ye, P. D. Molecular Doping of Multilayer MoS2 Field-Effect Transistors: Reduction in Sheet and Contact Resistances. *IEEE Electron Device Lett.* **2013**, *34*, 1328–1330.
220. Li, Y.; Xu, C.-Y.; Hu, P.; Zhen, L. Carrier Control of MoS2 Nanoflakes by Functional Self-Assembled Monolayers. *ACS Nano* **2013**, *7*, 7795–7804.
221. Wi, S.; Kim, H.; Chen, M.; Nam, H.; Guo, L. J.; Meyhofer, E.; Liang, X. Enhancement of Photovoltaic Response in Multilayer MoS2 Induced by Plasma Doping. *ACS Nano* **2014**, *8*, 5270–5281.

222. Chen, M.; Nam, H.; Wi, S.; Ji, L.; Ren, X.; Bian, L.; Lu, S.; Liang, X. Stable Few-Layer MoS2 Rectifying Diodes Formed by Plasma-Assisted Doping. *Appl. Phys. Lett.* **2013**, *103*, 142110.
223. Kiriya, D.; Tosun, M.; Zhao, P.; Kang, J. S.; Javey, A. Air-Stable Surface Charge Transfer Doping of MoS2 by Benzyl Viologen. *J. Am. Chem. Soc.* **2014**, *136*, 7853–7856.
224. Li, H.-M.; Lee, D.; Qu, D.; Liu, X.; Ryu, J.; Seabaugh, A.; Yoo, W. J. Ultimate Thin Vertical P-N Junction Composed of Two-Dimensional Layered Molybdenum Disulfide. *Nat. Commun.* **2015**, *6*, 6564.
225. Andleeb, S.; Singh, A. K.; Eom, J. Chemical Doping of MoS2Multilayer by P-Toluene Sulfonic Acid. *Sci. Technol. Adv. Mater.* **2015**, *16*, 35009.
226. Cheng, R.; Li, D.; Zhou, H.; Wang, C.; Yin, A.; Jiang, S.; Liu, Y.; Chen, Y.; Huang, Y.; Duan, X. Electroluminescence and Photocurrent Generation from Atomically Sharp WSe2/MoS2 Heterojunction P−n Diodes. *Nano Lett.* **2014**, *14*, 5590–5597.
227. Shi, Y.; Kim, K. K.; Reina, A.; Hofmann, M.; Li, L.-J.; Kong, J. Work Function Engineering of Graphene Electrode via Chemical Doping. *ACS Nano* **2010**, *4*, 2689–2694.
228. Shin, H.-J.; Choi, W. M.; Choi, D.; Han, G. H.; Yoon, S.-M.; Park, H.-K.; Kim, S.-W.; Jin, Y. W.; Lee, S. Y.; Kim, J. M.; et al. Control of Electronic Structure of Graphene by Various Dopants and Their Effects on a Nanogenerator. *J. Am. Chem. Soc.* **2010**, *132*, 15603–15609.
229. Fang, H.; Tosun, M.; Seol, G.; Chang, T. C.; Takei, K.; Guo, J.; Javey, A. Degenerate N-Doping of Few-Layer Transition Metal Dichalcogenides by Potassium. *Nano Lett.* **2013**, *13*, 1991–1995.
230. Yang, L.; Majumdar, K.; Liu, H.; Du, Y.; Wu, H.; Hatzistergos, M.; Hung, P. Y.; Tieckelmann, R.; Tsai, W.; Hobbs, C.; et al. Chloride Molecular Doping Technique on 2D Materials: WS2 and MoS2. *Nano Lett.* **2014**, *14*, 6275–6280.
231. Huang, J.; Xu, Z.; Yang, Y. Low-Work-Function Surface Formed by Solution-Processed and Thermally Deposited Nanoscale Layers of Cesium Carbonate. *Adv. Funct. Mater.* **2007**, *17*, 1966–1973.
232. Wu, C.-I.; Lin, C.-T.; Chen, Y.-H.; Chen, M.-H.; Lu, Y.-J.; Wu, C.-C. Electronic Structures and Electron-Injection Mechanisms of Cesium-Carbonate-Incorporated Cathode Structures for Organic Light-Emitting Devices. *Appl. Phys. Lett.* **2006**, *88*, 152104.
233. Kang, D.-H.; Shim, J.; Jang, S. K.; Jeon, J.; Jeon, M. H.; Yeom, G. Y.; Jung, W.-S.; Jang, Y. H.; Lee, S.; Park, J.-H. Controllable Nondegenerate P-Type Doping of Tungsten Diselenide by Octadecyltrichlorosilane. *ACS Nano* **2015**, *9*, 1099–1107.
234. Refson, K.; Tulip, P. R.; Clark, S. J. Variational Density-Functional Perturbation Theory for Dielectrics and Lattice Dynamics. *Phys. Rev. B: Condens. Matter Mater. Phys.* **2006**, *73*, 155114.
235. Puretzky, A. A.; Liang, L.; Li, X.; Xiao, K.; Wang, K.; Mahjouri-Samani, M.; Basile, L.; Idrobo, J. C.; Sumpter, B. G.; Meunier, V.; et al. Low-Frequency Raman Fingerprints of Two-Dimensional Metal Dichalcogenide Layer Stacking Configurations. *ACS Nano* **2015**, *9*, 6333–6342.
236. Sekine, T.; Izumi, M.; Nakashizu, T.; Uchinokura, K.; Matsuura, E. Raman-Scattering and Ifrared Reflectance in 2H-MoSe2. *J. Phys. Soc. Jpn.* **1980**, *49*, 1069–1077.
237. Wieting, T. J.; Verble, J. L. Infrared and Raman Studies of Long-Wavelenght Optical Phonons in Hexagonal MoS2. *Phys. Rev. B* **1971**, *3*, 4286.
238. Terrones, H.; Del Corro, E.; Feng, S.; Poumirol, J. M.; Rhodes, D.; Smirnov, D.; Pradhan, N. R.; Lin, Z.; Nguyen, M. A. T.; Elias, A. L.; et al. New First Order Raman-Active Modes in Few Layered Transition Metal Dichalcogenides. *Sci. Rep.* **2014**, *4*, 4215.
239. Lee, C.; Yan, H.; Brus, L. E.; Heinz, T. F.; Hone, J.; Ryu, S. Anomalous Lattice Vibrations of Single- and Few-Layer MoS2. *ACS Nano* **2010**, *4*, 2695–2700.
240. Luo, X.; Zhao, Y.; Zhang, J.; Toh, M.; Kloc, C.; Xiong, Q.; Quek, S. Y. Effects of Lower Symmetry and Dimensionality on Raman Spectra in Two-Dimensional WSe2. *Phys. Rev. B: Condens. Matter Mater. Phys.* **2013**, *88*, 195313.
241. Berkdemir, A.; Gutierrez, H. R.; Botello-Mendez, A. R.; Perea-Lopez, N.; Elias, A. L.; Chia, C.-I.; Wang, B.; Crespi, V. H.; Lopez-Urias, F.; Charlier, J.-C.; et al. Identification of Individual and Few Layers of WS2 Using Raman Spectroscopy. *Sci. Rep.* **2013**, *3*, 1755.
242. Gong, Y. J.; Lin, J. H.; Wang, X. L.; Shi, G.; Lei, S. D.; Lin, Z.; Zou, X. L.; Ye, G. L.; Vajtai, R.; Yakobson, B. I.; et al. Vertical and in-Plane Heterostructures from WS2/MoS2Monolayers. *Nat. Mater.* **2014**, *13*, 1135–1142.
243. Liang, L. B.; Meunier, V. First-Principles Raman Spectra of MoS2, WS2 and Their Heterostructures. *Nanoscale* **2014**, *6*, 5394–5401.
244. Mignuzzi, S.; Pollard, A. J.; Bonini, N.; Brennan, B.; Gilmore, I. S.; Pimenta, M. A.; Richards, D.; Roy, D. Effect of Disorder on Raman Scattering of Single-Layer MoS2. *Phys. Rev. B: Condens. Matter Mater. Phys.* **2015**, *91*, 195411.
245. Lin, J.; Fang, W.; Zhou, W.; Lupini, A. R.; Idrobo, J. C.; Kong, J.; Pennycook, S. J.; Pantelides, S. T. AC/AB Stacking Boundaries in Bilayer Graphene. *Nano Lett.* **2013**, *13*, 3262–3268.
246. Alden, J. S.; Tsen, A. W.; Huang, P. Y.; Hovden, R.; Brown, L.; Park, J.; Muller, D. a; McEuen, P. L. Strain Solitons and Topological Defects in Bilayer Graphene. *Proc. Natl. Acad. Sci. U. S. A.* **2013**, *110*, 11256–11260.
247. Warner, J. H.; Lin, Y.; He, K.; Koshino, M.; Suenaga, K. Atomic Level Spatial Variations of Energy States along Graphene Edges. *Nano Lett.* **2014**, *14*, 6155–6159.
248. Meyer, J. C.; Eder, F.; Kurasch, S.; Skakalova, V.; Kotakoski, J.; Park, H. J.; Roth, S.; Chuvilin, A.; Eyhusen, S.; Benner, G.; et al. Accurate Measurement of Electron Beam Induced Displacement Cross Sections for Single-Layer Graphene. *Phys. Rev. Lett.* **2012**, *108*, 196102.
249. Girit, C. O.; Stormer, H. L.; Kim, P.; Novoselov, K. S.; Cohen, M. L.; Louie, S. G.; Wang, X.; Zhang, L.; Lee, S.; Dai, H.; et al. Graphene at the Edge. *Science (Washington, DC, U. S.)* **2009**, *323*, 1705–1708.
250. Lehtinen, O.; Vats, N.; Algara-siller, G.; Knyrim, P.; Kaiser, U. Implantation and Atomic-Scale Investigation of Self-Interstitials in Graphene. *Nano Lett.* **2015**, *15*, 235–241.
251. Liu, Z.; Lin, Y.-C.; Lu, C.-C.; Yeh, C.-H.; Chiu, P.-W.; Iijima, S.; Suenaga, K. In Situ Observation of Step-Edge in-Plane Growth of Graphene in a STEM. *Nat. Commun.* **2014**, *5*, 4055.
252. Erickson, K.; Erni, R.; Lee, Z.; Alem, N.; Gannett, W.; Zettl, A. Determination of the Local Chemical Structure of Graphene Oxide and Reduced Graphene Oxide. *Adv. Mater.* **2010**, *22*, 4467–4472.
253. Gómez-Navarro, C.; Meyer, J. C.; Sundaram, R. S.; Chuvilin, A.; Kurasch, S.; Burghard, M.; Kern, K.; Kaiser, U. Atomic Structure of Reduced Graphene Oxide. *Nano Lett.* **2010**, *10*, 1144–1148.
254. Meyer, J. C.; Chuvilin, A.; Algara-Siller, G.; Biskupek, J.; Kaiser, U. Selective Sputtering and Atomic Resolution Imaging of Atomically Thin Boron Nitride Membranes. *Nano Lett.* **2009**, *9*, 2683–2689.
255. Alem, N.; Erni, R.; Kisielowski, C.; Rossell, M.; Gannett, W.; Zettl, A. Atomically Thin Hexagonal Boron Nitride Probed by Ultrahigh-Resolution Transmission Electron Microscopy. *Phys. Rev. B: Condens. Matter Mater. Phys.* **2009**, *80*, 155425.
256. Alem, N.; Erni, R.; Kisielowski, C.; Rossell, M. D.; Hartel, P.; Jiang, B.; Gannett, W.; Zettl, A. Vacancy Growth and Migration Dynamics in Atomically Thin Hexagonal Boron Nitride under Electron Beam Irradiation. *Phys. Status Solidi RRL* **2011**, *5*, 295–297.
257. Alem, N.; Ramasse, Q. M.; Seabourne, C. R.; Yazyev, O. V.; Erickson, K.; Sarahan, M. C.; Kisielowski, C.; Scott, A. J.; Louie, S. G.; Zettl, A. Subangstrom Edge Relaxations Probed by Electron Microscopy in Hexagonal Boron Nitride. *Phys. Rev. Lett.* **2012**, *109*, 205502.
258. Bhimanapati, G. R.; Kozuch, D.; Robinson, J. Large-Scale Synthesis and Functionalization of Hexagonal Boron Nitride Nanosheets. *Nanoscale* **2014**, *6*, 11671–11675.
259. Zhou, W.; Oxley, M. P.; Lupini, A. R.; Krivanek, O. L.; Pennycook, S. J.; Idrobo, J.-C. Single Atom Microscopy. *Microsc. Microanal.* **2012**, *18*, 1342–1354.

260. Bell, D.; Erdman, N. *Low Voltage Electron Microscopy: Principles and Applications*; John Wiley & Sons and RMS - Royal Microscopical Society, Somerset, NJ, 2012.
261. Lovejoy, T. C.; Ramasse, Q. M.; Falke, M.; Kaeppel, a.; Terborg, R.; Zan, R.; Dellby, N.; Krivanek, O. L. Single Atom Identification by Energy Dispersive X-Ray Spectroscopy. *Appl. Phys. Lett.* **2012**, *100*, 154101.
262. Suenaga, K.; Okazaki, T.; Okunishi, E.; Matsumura, S. Detection of Photons Emitted from Single Erbium Atoms in Energy-Dispersive X-Ray Spectroscopy. *Nat. Photonics* **2012**, *6*, 545–548.
263. Suenaga, K.; Koshino, M. Atom-by-Atom Spectroscopy at Graphene Edge. *Nature* **2010**, *468*, 1088–1090.
264. Zhou, W.; Lee, J.; Nanda, J.; Pantelides, S. T.; Pennycook, S. J.; Idrobo, J.-C. Atomically Localized Plasmon Enhancement in Monolayer Graphene. *Nat. Nanotechnol.* **2012**, *7*, 161–165.
265. Zhou, W.; Kapetanakis, M. D.; Prange, M. P.; Pantelides, S. T.; Pennycook, S. J.; Idrobo, J. C. Direct Determination of the Chemical Bonding of Individual Impurities in Graphene. *Phys. Rev. Lett.* **2012**, *109*, 206803.
266. Zhou, W.; Pennycook, S. J.; Idrobo, J. C. Localization of Inelastic Electron Scattering in the Low-Loss Energy Regime. *Ultramicroscopy* **2012**, *119*, 51–56.
267. Lin, Y.-C.; Dumcenco, D. O.; Huang, Y.-S.; Suenaga, K. Atomic Mechanism of the Semiconducting-to-Metallic Phase Transition in Single-Layered MoS2. *Nat. Nanotechnol.* **2014**, *9*, 391–396.
268. Krivanek, O. L.; Chisholm, M. F.; Nicolosi, V.; Pennycook, T. J.; Corbin, G. J.; Dellby, N.; Murfitt, M. F.; Own, C. S.; Szilagyi, Z. S.; Oxley, M. P.; et al. Atom-by-Atom Structural and Chemical Analysis by Annular Dark-Field Electron Microscopy. *Nature* **2010**, *464*, 571–574.
269. Zhou, W.; Zou, X.; Najmaei, S.; Liu, Z.; Shi, Y.; Kong, J.; Lou, J.; Ajayan, P. M.; Yakobson, B. I.; Idrobo, J. C. Intrinsic Structural Defects in Monolayer Molybdenum Disulfide. *Nano Lett.* **2013**, *13*, 2615–2622.
270. Zou, X.; Liu, Y.; Yakobson, B. I. Predicting Dislocations and Grain Boundaries in Two-Dimensional Metal-Disulfides from the First Principles. *Nano Lett.* **2013**, *13*, 253–258.
271. Najmaei, S.; Liu, Z.; Zhou, W.; Zou, X.; Shi, G.; Lei, S.; Yakobson, B. I.; Idrobo, J.-C.; Ajayan, P. M.; Lou, J. Vapour Phase Growth and Grain Boundary Structure of Molybdenum Disulphide Atomic Layers. *Nat. Mater.* **2013**, *12*, 754–759.
272. Hong, J.; Hu, Z.; Probert, M.; Li, K.; Lv, D.; Yang, X.; Gu, L.; Mao, N.; Feng, Q.; Xie, L.; et al. Exploring Atomic Defects in Molybdenum Disulphide Monolayers. *Nat. Commun.* **2015**, *6*, 6293.
273. Lee, J.; Yang, Z.; Zhou, W.; Pennycook, S. J.; Pantelides, S. T.; Chisholm, M. F. Stabilization of Graphene Nanopore. *Proc. Natl. Acad. Sci. U. S. A.* **2014**, *111*, 7522–7526.
274. Yang, Z.; Yin, L.; Lee, J.; Ren, W.; Cheng, H. M.; Ye, H.; Pantelides, S. T.; Pennycook, S. J.; Chisholm, M. F. Direct Observation of Atomic Dynamics and Silicon Doping at a Topological Defect in Graphene. *Angew. Chem., Int. Ed.* **2014**, *53*, 8908–8912.
275. Guo, J.; Lee, J.; Contescu, C. I.; Gallego, N. C.; Sokrates, T.; Pennycook, S. J.; Moyer, B. a; Chisholm, M. F. Crown Ethers in Graphene. *Nat. Commun.* **2014**, *5*, 5389.
276. Lin, J.; Pantelides, S. T.; Zhou, W. Vacancy-Induced Formation and Growth of Inversion Domains in Transition-Metal Dichalcogenide Monolayer. *ACS Nano* **2015**, *9*, 5189–5197.
277. Lin, J.; Cretu, O.; Zhou, W.; Suenaga, K.; Prasai, D.; Bolotin, K. I.; Cuong, N. T.; Otani, M.; Okada, S.; Lupini, A. R.; et al. Flexible Metallic Nanowires with Self-Adaptive Contacts to Semiconducting Transition-Metal Dichalcogenide Monolayers. *Nat. Nanotechnol.* **2014**, *9*, 436–442.
278. Krivanek, O. L.; Lovejoy, T. C.; Dellby, N.; Aoki, T.; Carpenter, R. W.; Rez, P.; Soignard, E.; Zhu, J.; Batson, P. E.; Lagos, M. J.; et al. Vibrational Spectroscopy in the Electron Microscope. *Nature* **2014**, *514*, 209–212.
279. Tizei, L. H. G.; Lin, Y.-C.; Mukai, M.; Sawada, H.; Lu, A.-Y.; Li, L.-J.; Kimoto, K.; Suenaga, K. Exciton Mapping at Subwavelength Scales in Two-Dimensional Materials. *Phys. Rev. Lett.* **2015**, *114*, 107601.
280. Bimberg, D. Cathodoluminescence Atomic Scale Images of Monolayer Islands at GaAs/GaAlAs Interfaces. *J. Vac. Sci. Technol., B: Microelectron. Process. Phenom.* **1987**, *5*, 1191.
281. Rosner, S. J.; Carr, E. C.; Ludowise, M. J.; Girolami, G.; Erikson, H. I. Correlation of Cathodoluminescence Inhomogeneity with Microstructural Defects in Epitaxial GaN Grown by Metalorganic Chemical-Vapor Deposition. *Appl. Phys. Lett.* **1997**, *70*, 420.
282. Chen, Z.; Zou, J.; Liu, G.; Li, F.; Wang, Y.; Wang, L.; Yuan, X.; Sekiguchi, T.; Cheng, H.; Lu, G. Q. Novel Boron Nitride Hollow Nanoribbons. *ACS Nano* **2008**, *2*, 2183–2191.
283. Chuang, H.; Tan, X.; Ghimire, N. J.; Perera, M. M.; Chamlagain, B.; Cheng, M. M.; Yan, J.; Mandrus, D.; Toma, D. High Mobility WSe2 P - and N -Type Field-Effect Transistors Contacted by Highly Doped Graphene for Low-Resistance Contacts. *Nano Lett.* **2014**, *14*, 3594.
284. Chuang, S.; Battaglia, C.; Azcatl, A.; McDonnell, S.; Kang, J. S.; Yin, X.; Tosun, M.; Kapadia, R.; Fang, H.; Wallace, R. M.; et al. MoS2 P-Type Transistors and Diodes Enabled by High Work Function MoOx Contacts. *Nano Lett.* **2014**, *14*, 1337.
285. Das, S.; Appenzeller, J. Where Does the Current Flow in Two-Dimensional Layered Systems? *Nano Lett.* **2013**, *13*, 3396.
286. Das, S.; Gulotty, R.; Sumant, A. V.; Roelofs, A. All Two-Dimensional, Flexible, Transparent, and Thinnest Thin Film Transistor. *Nano Lett.* **2014**, *14*, 2861.
287. Kappera, R.; Voiry, D.; Yalcin, S. E.; Branch, B.; Gupta, G.; Mohite, A. D.; Chhowalla, M. Phase-Engineered Low-Resistance Contacts for Ultrathin MoS2 Transistors. *Nat. Mater.* **2014**, *13*, 1128–1134.
288. Mos, P. M.; Yamaguchi, H.; Blancon, J.; Kappera, R.; Lei, S.; Najmaei, S.; Mohite, A. D. Spatially Resolved Photoexcited Charge-Carrier Dynamics in Phase-Engineered Monolayer MoS2. *ACS Nano* **2015**, *9*, 840–849.
289. Das, S.; Chen, H. Y.; Penumatcha, A. V.; Appenzeller, J. High Performance Multilayer MoS2 Transistors with Scandium Contacts. *Nano Lett.* **2013**, *13*, 100–105.
290. Larentis, S.; Fallahazad, B.; Tutuc, E. Field-Effect Transistors and Intrinsic Mobility in Ultra-Thin MoSe2 Layers. *Appl. Phys. Lett.* **2012**, *101*, 223104.
291. Das, S.; Appenzeller, J. WSe2 Field Effect Transistors with Enhanced Ambipolar Characteristics WSe2 Field Effect Transistors with Enhanced Ambipolar Characteristics. *Appl. Phys. Lett.* **2013**, *103*, 103501.
292. Hwang, W. S.; Remskar, M. Transistors with Chemically Synthesized Layered Semiconductor WS2 Exhibiting 10^5 Room Temperature Modulation and Ambipolar Behavior. *Appl. Phys. Lett.* **2012**, *101*, 013107.
293. Wang, J.; Rhodes, D.; Feng, S.; Nguyen, M. A. T.; Watanabe, K.; Taniguchi, T.; Mallouk, T. E.; Terrones, M.; Balicas, L.; Zhu, J. Gate-Modulated Conductance of Few-Layer WSe2 Field-Effect Transistors in the Subgap Regime: Schottky Barrier Transistor and Subgap Impurity States. *Appl. Phys. Lett.* **2015**, *106*, 152104.
294. Gong, C.; Colombo, L.; Wallace, R. M.; Cho, K. The Unusual Mechanism of Partial Fermi Level Pinning at Metal-MoS2 Interfaces The Unusual Mechanism of Partial Fermi Level Pinning at Metal-MoS2 Interfaces. *Nano Lett.* **2014**, *14*, 1714–1720.
295. Jacobs-gedrim, R. B.; Shanmugam, M.; Jain, N.; Durcan, C. a. Extraordinary Photoresponse in Two-Dimensional In2Se3 Nanosheets. *ACS Nano* **2014**, *8*, 514–521.
296. Kang, M.; Rathi, S.; Lee, I.; Lim, D.; Wang, J.; Li, L.; Khan, M. A.; Kim, G.-H. Electrical Characterization of Multilayer HfSe2 Field-Effect Transistors on SiO2 Substrate. *Appl. Phys. Lett.* **2015**, *106*, 143108.
297. Late, D. J.; Liu, B.; Luo, J.; Yan, A.; Matte, H. S. S. R.; Grayson, M.; Rao, C. N. R.; Dravid, V. P. GaS and GaSe Ultrathin Layer Transistors. *Adv. Mater.* **2012**, *24*, 3549–3554.
298. Song, H. S.; Li, S. L.; Gao, L.; Xu, Y.; Ueno, K.; Tang, J.; Cheng, Y. B.; Tsukagoshi, K. High-Performance Top-Gated

Monolayer SnS2 Field-Effect Transistors and Their Integrated Logic Circuits. *Nanoscale* **2013**, *5*, 9666–9670.
299. Akinwande, D.; Petrone, N.; Hone, J. Two-Dimensional Flexible Nanoelectronics. *Nat. Commun.* **2014**, *5*, 5678.
300. Komsa, H. P.; Kotakoski, J.; Kurasch, S.; Lehtinen, O.; Kaiser, U.; Krasheninnikov, A. V. Two-Dimensional Transition Metal Dichalcogenides under Electron Irradiation: Defect Production and Doping. *Phys. Rev. Lett.* **2012**, *109*, 035503.
301. Mcdonnell, S.; Addou, R.; Buie, C.; Wallace, R. M.; Hinkle, C. L. Defect-Dominated Doping and Contact Resistance in MoS2. *ACS Nano* **2014**, *8*, 2880–2888.
302. Tongay, S.; Suh, J.; Ataca, C.; Fan, W.; Luce, A.; Kang, J. S.; Liu, J.; Ko, C.; Raghunathanan, R.; Zhou, J.; et al. Defects Activated Photoluminescence in Two-Dimensional Semiconductors: Interplay between Bound, Charged, and Free Excitons. *Sci. Rep.* **2013**, *3*, 2657.
303. Das, S.; Demarteau, M.; Roelofs, A. Ambipolar Phosphorene Field Effect Transistor. *ACS Nano* **2014**, *8*, 11730–11738.
304. Das, S.; Dubey, M.; Roelofs, A. High Gain, Low Noise, Fully Complementary Logic Inverter Based on Bi-Layer WSe2 Field Effect Transistors. *Appl. Phys. Lett.* **2014**, *105*, 083511.
305. Das, S.; Zhang, W.; Thoutam, L. R.; Xiao, Z.; Hoffmann, A.; Demarteau, M.; Roelofs, A. A Small Signal Amplifier Based on Ionic Liquid Gated Black Phosphorous Field Effect Transistor. *IEEE Electron Device Lett.* **2015**, *36*, 621–623.
306. Tan, Z.; Tian, H.; Feng, T.; Zhao, L.; Xie, D.; Yang, Y.; Xiao, L. A Small-Signal Generator Based on a Multi-Layer Graphene/Molybdenum Disulfide Heterojunction. *Appl. Phys. Lett.* **2013**, *263506*, 263506.
307. Zhu, W.; Yogeesh, M. N.; Yang, S.; Aldave, S. H.; Kim, J.; Sonde, S. S.; Tao, L.; Lu, N.; Akinwande, D. Flexible Black Phosphorus Ambipolar Transistors, Circuits and AM Demodulator. *Nano Lett.* **2015**, *15*, 1883–1890.
308. Lee, H. S.; Min, S. W.; Park, M. K.; Lee, Y. T.; Jeon, P. J.; Kim, J. H.; Ryu, S.; Im, S. MoS2 Nanosheets for Top-Gate Nonvolatile Memory Transistor Channel. *Small* **2012**, *8*, 3111–3115.
309. Chang, H. Y.; Yang, S.; Lee, J.; Tao, L.; Hwang, W. S.; Jena, D.; Lu, N.; Akinwande, D. High-Performance, Highly Bendable MoS2 Transistors with High-K Dielectrics for Flexible Low-Power Systems. *ACS Nano* **2013**, *7*, 5446–5452.
310. Huo, N.; Yang, S.; Wei, Z.; Li, S.-S.; Xia, J.-B.; Li, J. Photoresponsive and Gas Sensing Field-Effect Transistors Based on Multilayer WS2 Nanoflakes. *Sci. Rep.* **2014**, *4*, 5209.
311. Sarkar, D.; Liu, W.; Xie, X.; Anselmo, A. C.; Mitragotri, S.; Banerjee, K. MoS2 Field-Effect Transistor for Next-Generation Label-Free Biosensors. *ACS Nano* **2014**, *8*, 3992–4003.
312. Wang, L.; Wang, Y.; Wong, J. I.; Palacios, T.; Kong, J.; Yang, H. Y. Functionalized MoS2 Nanosheet-Based Field-Effect Biosensor for Label-Free Sensitive Detection of Cancer Marker Proteins in Solution. *Small* **2014**, *10*, 1101–1105.
313. Pospischil, A.; Furchi, M. M.; Mueller, T. Solar-Energy Conversion and Light Emission in an Atomic Monolayer P-N Diode. *Nat. Nanotechnol.* **2014**, *9*, 257–261.
314. Kaxiras, E.; Kong, J.; Wang, H. Graphene/MoS2 Hybrid Technology for Large-Scale Two- Dimensional Electronics. *Nano Lett.* **2014**, *14*, 3055–3063.
315. Baugher, B. W. H.; Churchill, H. O. H.; Yang, Y.; Jarillo-Herrero, P. Optoelectronic Devices Based on Electrically Tunable P-N Diodes in a Monolayer Dichalcogenide. *Nat. Nanotechnol.* **2014**, *9*, 262–267.
316. Jariwala, D.; Sangwan, V. K.; Wu, C.-C.; Prabhumirashi, P. L.; Geier, M. L.; Marks, T. J.; Lauhon, L. J.; Hersam, M. C. Gate-Tunable Carbon Nanotube-MoS2 Heterojunction P-N Diode. *Proc. Natl. Acad. Sci. U. S. A.* **2013**, *110*, 18076–18080.
317. Lopez-Sanchez, O.; Lembke, D.; Kayci, M.; Radenovic, A.; Kis, A. Ultrasensitive Photodetectors Based on Monolayer MoS2. *Nat. Nanotechnol.* **2013**, *8*, 497–501.
318. Ross, J. S.; Klement, P.; Jones, A. M.; Ghimire, N. J.; Yan, J.; Mandrus, D. G.; Taniguchi, T.; Watanabe, K.; Kitamura, K.; Yao, W.; et al. Electrically Tunable Excitonic Light-Emitting Diodes Based on Monolayer WSe2 P-N Junctions. *Nat. Nanotechnol.* **2014**, *9*, 268–272.
319. Zhang, W.; Chiu, M.; Chen, C.-H.; Chen, W.; Li, L.; Wee, A. T. S. Role of Metal Contacts in High-Performance Phototransistors Based on WSe2Monolayers. *ACS Nano* **2014**, *8*, 8653–8661.
320. Youngblood, N.; Chen, C.; Koester, S. J.; Li, M. Waveguide-Integrated Black Phosphorus Photodetector with High Responsivity and Low Dark Current. *Nat. Photonics* **2015**, *9*, 249–252.
321. Jang, M. S.; Brar, V. W.; Sherrott, M. C.; Lopez, J. J.; Kim, L.; Kim, S.; Choi, M.; Atwater, H. a. Tunable Large Resonant Absorption in a Midinfrared Graphene Salisbury Screen. *Phys. Rev. B: Condens. Matter Mater. Phys.* **2014**, *90*, 165409.
322. Atwater, H. a; Polman, A. Plasmonics for Improved Photovoltaic Devices. *Nat. Mater.* **2010**, *9*, 205–213.
323. Yu, Z.; Raman, A.; Fan, S. Fundamental Limit of Nanophotonic Light Trapping in Solar Cells. *Proc. Natl. Acad. Sci. U. S. A.* **2010**, *107*, 17491–17496.
324. Grote, R. R.; Brown, S. J.; Driscoll, J. B.; Osgood, R. M.; Schuller, J. a. Morphology-Dependent Light Trapping in Thin-Film Organic Solar Cells. *Opt. Express* **2013**, *21*, A847.
325. Liang, W. Y. Optical Anisotropy in Layer Compounds. *J. Phys. C: Solid State Phys.* **1973**, *6*, 551–565.
326. Schuller, J. a; Karaveli, S.; Schiros, T.; He, K.; Yang, S.; Kymissis, I.; Shan, J.; Zia, R. Orientation of Luminescent Excitons in Layered Nanomaterials. *Nat. Nanotechnol.* **2013**, *8*, 271–276.
327. Akselrod, G. M.; Ming, T.; Argyropoulos, C.; Hoang, T. B.; Lin, Y.; Ling, X.; Smith, D. R.; Kong, J.; Mikkelsen, M. H. Leveraging Nanocavity Harmonics for Control of Optical Processes in 2D Semiconductors. *Nano Lett.* **2015**, *15*, 3578.
328. Butun, S.; Tongay, S.; Aydin, K. Enhanced Light Emission from Large-Area Monolayer MoS2 Using Plasmonic Nanodisc Arrays. *Nano Lett.* **2015**, *15*, 3578.
329. Gan, X.; Gao, Y.; Fai Mak, K.; Yao, X.; Shiue, R. J.; Van Der Zande, A.; Trusheim, M. E.; Hatami, F.; Heinz, T. F.; Hone, J.; et al. Controlling the Spontaneous Emission Rate of Monolayer MoS2 in a Photonic Crystal Nanocavity. *Appl. Phys. Lett.* **2013**, *103*, 181119.
330. Wu, S.; Buckley, S.; Schaibley, J. R.; Feng, L.; Yan, J.; Mandrus, D. G.; Hatami, F.; Yao, W.; Vučković, J.; Majumdar, A.; et al. Monolayer Semiconductor Nanocavity Lasers with Ultralow Thresholds. *Nature* **2015**, *520*, 69–72.
331. Caldwell, J. D.; Kretinin, A.; Chen, Y.; Giannini, V.; Fogler, M. M.; Francescato, Y.; Ellis, C. T.; Tischler, J. G.; Woods, C. R.; Giles, A. J.; et al. Sub-Diffraction, Volume-Confined Polaritons in the Natural Hyperbolic Material, Hexagonal Boron Nitride. *Nat. Commun.* **2014**, *5*, 5221.
332. Dai, S.; Ma, Q.; Andersen, T.; Mcleod, a. S.; Fei, Z.; Liu, M. K.; Wagner, M.; Watanabe, K.; Taniguchi, T.; Thiemens, M.; et al. Subdiffractional Focusing and Guiding of Polaritonic Rays in a Natural Hyperbolic Material. *Nat. Commun.* **2015**, *6*, 6963.
333. Cortes, C. L.; Newman, W.; Molesky, S.; Jacob, Z. Corrigendum: Quantum Nanophotonics Using Hyperbolic Metamaterials (2012 J. Opt.14063001). *J. Opt.* **2014**, *16*, 129501.
334. Piazza, Z. a; Hu, H.-S.; Li, W.-L.; Zhao, Y.-F.; Li, J.; Wang, L.-S. Planar Hexagonal B(36) as a Potential Basis for Extended Single-Atom Layer Boron Sheets. *Nat. Commun.* **2014**, *5*, 3113.
335. Wen, X. D.; Cahill, T. J.; Hoffmann, R. Exploring Group 14 Structures: 1D to 2D to 3D. *Chem. - Eur. J.* **2010**, *16*, 6555–6566.
336. Cahangirov, S.; Topsakal, M.; Aktürk, E.; Šahin, H.; Ciraci, S. Two- and One-Dimensional Honeycomb Structures of Silicon and Germanium. *Phys. Rev. Lett.* **2009**, *102*, 236804.
337. Balendhran, S.; Walia, S.; Nili, H.; Sriram, S.; Bhaskaran, M. Elemental Analogues of Graphene: Silicene, Germanene, Stanene, and Phosphorene. *Small* **2015**, *11*, 640–652.

338. Xu, Y.; Yan, B.; Zhang, H. J.; Wang, J.; Xu, G.; Tang, P.; Duan, W.; Zhang, S. C. Large-Gap Quantum Spin Hall Insulators in Tin Films. *Phys. Rev. Lett.* **2013**, *111*, 136804.
339. Ding, Y.; Wang, Y. Density Functional Theory Study of the Silicene-like SiX and XSi3 (X = B, C, N, Al, P) Honeycomb Lattices: The Various Buckled Structures and Versatile Electronic Properties. *J. Phys. Chem. C* **2013**, *117*, 18266.
340. Matthes, L.; Pulci, O.; Bechstedt, F. Massive Dirac Quasiparticles in the Optical Absorbance of Graphene, Silicene, Germanene, and Tinene. *J. Phys.: Condens. Matter* **2013**, *25*, 395305.
341. Aufray, B.; Kara, A.; Vizzini, Ś.; Oughaddou, H.; Leandri, C.; Ealet, B.; Le Lay, G. Graphene-like Silicon Nanoribbons on Ag(110): A Possible Formation of Silicene. *Appl. Phys. Lett.* **2010**, *96*, 183102.
342. Feng, B.; Ding, Z.; Meng, S.; Yao, Y.; He, X.; Cheng, P.; Chen, L.; Wu, K. Evidence of Silicene in Honeycomb Structures of Silicon on Ag(111). *Nano Lett.* **2012**, *12*, 3507–3511.
343. Jamgotchian, H.; Colignon, Y.; Hamzaoui, N.; Ealet, B.; Hoarau, J. Y.; Aufray, B.; Bibérian, J. P. Growth of Silicene Layers on Ag(111): Unexpected Effect of the Substrate Temperature. *J. Phys.: Condens. Matter* **2012**, *24*, 172001.
344. Meng, L.; Wang, Y.; et al. Buckled silicene formation on Ir(111). *Nano Lett* **2013**, *13* (2), 685–690.
345. Dávila, M. E.; Xian, L.; Cahangirov, S.; Rubio, A.; Lay, G. L. Germanene: A Novel Two-Dimensional Germanium Allotrope Akin to Graphene and Silicene. *New J. Phys.* **2014**, *16*, 095002.
346. Bampoulis, P.; Zhang, L.; Safaei, A.; van Gastel, R.; Poelsema, B.; Zandvliet, H. J. W. Germanene Termination of Ge2Pt Crystals on Ge(110). *J. Phys.: Condens. Matter* **2014**, *26*, 442001.
347. Park, J. H.; Suzuki, T.; Kurosawa, M.; Miyao, M.; Sadoh, T. Nucleation-Controlled Gold-Induced-Crystallization for Selective Formation of Ge(100) and (111) on Insulator at Low-Temperature (???250 ??c). *Appl. Phys. Lett.* **2013**, *103*, 082102.
348. Kaloni, T. P.; Modarresi, M.; Tahir, M.; Roknabadi, M. R.; Schreckenbach, G.; Freund, M. S. Electrically Engineered Band Gap in Two-Dimensional Ge, Sn, and Pb: A First-Principles and Tight-Binding Approach. *J. Phys. Chem. C* **2015**, *119*, 11896–11902.
349. De Padova, P.; Quaresima, C.; Ottaviani, C.; Sheverdyaeva, P. M.; Moras, P.; Carbone, C.; Topwal, D.; Olivieri, B.; Kara, A.; Oughaddou, H.; et al. Evidence of Graphene-like Electronic Signature in Silicene Nanoribbons. *Appl. Phys. Lett.* **2010**, *96*, 261905.
350. Li, L.; Wang, Y.; et al. Buckled germanene formation on Pt (111). *Adv. Mater.* **2014**, *26* (28), 4820–4824.
351. Liu, C. C.; Jiang, H.; Yao, Y. Low-Energy Effective Hamiltonian Involving Spin-Orbit Coupling in Silicene and Two-Dimensional Germanium and Tin. *Phys. Rev. B: Condens. Matter Mater. Phys.* **2011**, *84*, 195430.
352. Houssa, M.; Pourtois, G.; Afanas'Ev, V. V.; Stesmans, A. Electronic Properties of Two-Dimensional Hexagonal Germanium. *Appl. Phys. Lett.* **2010**, *96*, 082111.
353. Lebègue, S.; Eriksson, O. Electronic Structure of Two-Dimensional Crystals from Ab Initio Theory. *Phys. Rev. B: Condens. Matter Mater. Phys.* **2009**, *79*, 115409.
354. Miró, P.; Audiffred, M.; Heine, T. An Atlas of Two-Dimensional Materials. *Chem. Soc. Rev.* **2014**, *43*, 6537–6554.
355. Liu, C. C.; Feng, W.; Yao, Y. Quantum Spin Hall Effect in Silicene and Two-Dimensional Germanium. *Phys. Rev. Lett.* **2011**, *107*, 076802.
356. Cai, B.; Zhang, S.; Hu, Z.; Hu, Y.; Zou, Y.; Zeng, H. Tinene: A Two-Dimensional Dirac Material with a 72 meV Band Gap. *Phys. Chem. Chem. Phys.* **2015**, *17*, 12634–12638.
357. Zhu, F.-F.; Chen, W.-J.; Xu, Y.; Gao, C.-L.; Guan, D.-D.; Liu, C.-H.; Qian, D.; Zhang, S.-C.; Jia, J.-F. Epitaxial Growth of Two-Dimensional Stanene. *Nat. Mater.* **2015**, *14*, 1020.
358. Buscema, M.; Groenendijk, D. J.; Blanter, S. I.; Steele, G. A.; van der Zant, H. S. J.; Castellanos-Gomez, A. Fast and Broadband Photoresponse of Few-Layer Black Phosphorus Field-Effect Transistors. *Nano Lett.* **2014**, *14*, 3347–3352.
359. Koenig, S. P.; Doganov, R. A.; Schmidt, H.; Castro Neto, A. H.; Özyilmaz, B. Electric Field Effect in Ultrathin Black Phosphorus. *Appl. Phys. Lett.* **2014**, *104*, 103106.
360. Li, L.; Yu, Y.; Ye, G. J.; Ge, Q.; Ou, X.; Wu, H.; Feng, D.; Chen, X. H.; Zhang, Y. Black Phosphorus Field-Effect Transistors. *Nat. Nanotechnol.* **2014**, *9*, 372–377.
361. Liu, H.; Neal, A. T.; Zhu, Z.; Luo, Z.; Xu, X.; Tománek, D.; Ye, P. D. Phosphorene: An Unexplored 2D Semiconductor with a High Hole Mobility. *ACS Nano* **2014**, *8*, 4033–4041.
362. Xia, F.; Wang, H.; Jia, Y. Rediscovering Black Phosphorus as an Anisotropic Layered Material for Optoelectronics and Electronics. *Nat. Commun.* **2014**, *5*, 4458.
363. Morita, A. Semiconducting Black Phosphorus. *Appl. Phys. A: Solids Surf.* **1986**, *39*, 227–242.
364. Qiao, J.; Kong, X.; Hu, Z.-X.; Yang, F.; Ji, W. High-Mobility Transport Anisotropy and Linear Dichroism in Few-Layer Black Phosphorus. *Nat. Commun.* **2014**, *5*, 4475.
365. Tran, V.; Soklaski, R.; Liang, Y.; Yang, L. Layer-Controlled Band Gap and Anisotropic Excitons in Few-Layer Black Phosphorus. *Phys. Rev. B: Condens. Matter Mater. Phys.* **2014**, *89*, 235319.
366. Wang, X.; Jones, A. M.; Seyler, K. L.; Tran, V.; Jia, Y.; Zhao, H.; Wang, H.; Yang, L.; Xu, X.; Xia, F. Highly Anisotropic and Robust Excitons in Monolayer Black Phosphorus. *Nat. Nanotechnol.* **2015**, *10*, 517–521.
367. He, J.; He, D.; Wang, Y.; Cui, Q.; Bellus, M. Z.; Chiu, H.-Y.; Zhao, H. Exceptional and Anisotropic Transport Properties of Photocarriers in Black Phosphorus. *ACS Nano* **2015**, *9*, 6436–6442.
368. Chen, X.; Wu, Y.; Wu, Z.; Han, Y.; Xu, S.; Wang, L.; Ye, W.; Han, T.; He, Y.; Cai, Y.; et al. High-Quality Sandwiched Black Phosphorus Heterostructure and Its Quantum Oscillations. *Nat. Commun.* **2015**, *6*, 7315.
369. Wang, H.; Wang, X.; Xia, F.; Wang, L.; Jiang, H.; Xia, Q.; Chin, M. L.; Dubey, M.; Han, S. Black Phosphorus Radio-Frequency Transistors. *Nano Lett.* **2014**, *14*, 6424–6429.
370. Wood, J. D.; Wells, S. A.; Jariwala, D.; Chen, K.-S.; Cho, E.; Sangwan, V. K.; Liu, X.; Lauhon, L. J.; Marks, T. J.; Hersam, M. C. Effective Passivation of Exfoliated Black Phosphorus Transistors against Ambient Degradation. *Nano Lett.* **2014**, *14*, 6964–6970.
371. Anasori, B.; Xie, Y.; Beidaghi, M.; Lu, J.; Hosler, B. C.; Hultman, L.; Kent, P. R. C.; Gogotsi, Y.; Barsoum, M. W. Two-Dimensional, Ordered, Double Transition Metals Carbides (MXenes). *ACS Nano* **2015**, *9*, 9507.
372. Maiti, U. N.; Lee, W. J.; Lee, J. M.; Oh, Y.; Kim, J. E. J. Y.; Kim, J. E. J. Y.; Shim, J.; Han, T. H.; Kim, S. O. Carbon: 25th Anniversary Article: Chemically Modified/Doped Carbon Nanotubes & Graphene for Optimized Nanostructures & Nanodevices (Adv. Mater. 1/2014). *Adv. Mater.* **2014**, *26*, 2–2.
373. Ma, R.; Sasaki, T. Nanosheets of Oxides and Hydroxides: Ultimate 2D Charge-Bearing Functional Crystallites. *Adv. Mater.* **2010**, *22*, 5082–5104.
374. Naguib, M.; Kurtoglu, M.; Presser, V.; Lu, J.; Niu, J.; Heon, M.; Hultman, L.; Gogotsi, Y.; Barsoum, M. W. Two-Dimensional Nanocrystals Produced by Exfoliation of Ti3AlC2. *Adv. Mater.* **2011**, *23*, 4248–4253.
375. Naguib, M.; Mashtalir, O.; Carle, J.; Presser, V.; Lu, J.; Hultman, L.; Gogotsi, Y.; Barsoum, M. W. Two-Dimensional Transition Metal Carbides. *ACS Nano* **2012**, *6*, 1322–1331.
376. Naguib, M.; Halim, J.; Lu, J.; Cook, K. M.; Hultman, L.; Gogotsi, Y.; Barsoum, M. W. New Two-Dimensional Niobium and Vanadium Carbides as Promising Materials for Li-Ion Batteries. *J. Am. Chem. Soc.* **2013**, *135*, 15966–15969.
377. Barsoum, M. W.; Golczewski, J.; Seifert, H. J.; Aldinger, F. F Abrication and Electrical and Thermal Properties of Ti2InC, Hf2InC and (Ti,Hf)2InC. *J. Alloys Compd.* **2002**, *340*, 173–179.
378. Naguib, M.; Presser, V.; Tallman, D.; Lu, J.; Hultman, L.; Gogotsi, Y.; Barsoum, M. W. On the Topotactic Transformation of Ti2AlC into a Ti-C-O-F Cubic Phase by Heating in Molten Lithium Fluoride in Air. *J. Am. Ceram. Soc.* **2011**, *94*, 4556–4561.

379. Barsoum, M. W. The Topotactic Transformation of Ti3SiC2 into a Partially Ordered Cubic Ti(C0.67Si0.06) Phase by the Diffusion of Si into Molten Cryolite. *J. Electrochem. Soc.* **1999**, *146*, 3919.
380. Hoffman, E. N.; Yushin, G.; Barsoum, M. W.; Gogotsi, Y. Synthesis of Carbide-Derived Carbon by Chlorination of Ti 2AlC. *Chem. Mater.* **2005**, *17*, 2317–2322.
381. Hoffman, E. N.; Yushin, G.; El-Raghy, T.; Gogotsi, Y.; Barsoum, M. W. Micro and Mesoporosity of Carbon Derived from Ternary and Binary Metal Carbides. *Microporous Mesoporous Mater.* **2008**, *112*, 526–532.
382. Naguib, M.; Presser, V.; Lane, N.; Tallman, D.; Gogotsi, Y.; Lu, J.; Hultman, L.; Barsoum, M. W. Synthesis of a New Nanocrystalline Titanium Aluminum Fluoride Phase by Reaction of Ti2AlC with Hydrofluoric Acid. *RSC Adv.* **2011**, *1*, 1493.
383. Mashtalir, O.; Naguib, M.; Mochalin, V. N.; Dall'Agnese, Y.; Heon, M.; Barsoum, M. W.; Gogotsi, Y. Intercalation and Delamination of Layered Carbides and Carbonitrides. *Nat. Commun.* **2013**, *4*, 1716.
384. Lukatskaya, M. R.; Mashtalir, O.; Ren, C. E.; Dall'Agnese, Y.; Rozier, P.; Taberna, P. L.; Naguib, M.; Simon, P.; Barsoum, M. W.; Gogotsi, Y. Cation Intercalation and High Volumetric Capacitance of Two-Dimensional Titanium Carbide. *Science* **2013**, *341*, 1502–1505.
385. Come, J.; Naguib, M.; Rozier, P.; Barsoum, M. W.; Gogotsi, Y.; Taberna, P.-L.; Morcrette, M.; Simon, P. A Non-Aqueous Asymmetric Cell with a Ti2C-Based Two-Dimensional Negative Electrode. *J. Electrochem. Soc.* **2012**, *159*, A1368–A1373.
386. Wang, X.; Kajiyama, S.; Iinuma, H.; Hosono, E.; Oro, S.; Moriguchi, I.; Okubo, M.; Yamada, A. Pseudocapacitance of MXene Nanosheets for High-Power Sodium-Ion Hybrid Capacitors. *Nat. Commun.* **2015**, *6*, 6544.
387. Naguib, M.; Come, J.; Dyatkin, B.; Presser, V.; Taberna, P. L.; Simon, P.; Barsoum, M. W.; Gogotsi, Y. MXene: A Promising Transition Metal Carbide Anode for Lithium-Ion Batteries. *Electrochem. Commun.* **2012**, *16*, 61–64.
388. Xie, X.; Chen, S.; Ding, W.; Nie, Y.; Wei, Z. An Extraordinarily Stable Catalyst: Pt NPs Supported on Two-Dimensional Ti3C2 $\times$ 2 (X = OH, F) Nanosheets for Oxygen Reduction Reaction. *Chem. Commun.* **2013**, *49*, 10112–10114.
389. Wang, Y.; Li, Z.; Wang, J.; Li, J.; Lin, Y. Graphene and Graphene Oxide: Biofunctionalization and Applications in Biotechnology. *Trends Biotechnol.* **2011**, *29*, 205–212.
390. Jakus, A. E.; Secor, E. B.; Rutz, A. L.; Jordan, S. W.; Hersam, M. C.; Shah, R. N. Three-Dimensional Printing of High-Content Graphene Scaffolds for Electronic and Biomedical Applications. *ACS Nano* **2015**, *9*, 4636–4648.
391. Sheehan, P. E.; Stine, R.; Robinson, J. T.; Hernandez, S. C.; Whitener, K. E.; Walton, S. G. Chemically Modifying Graphene for Surface Functionality. *Prepr. - Am. Chem. Soc., Div. Energy Fuels* **2013**, *58*, 3.
392. Chen, Q.; Smith, J. M.; Park, J.; Kim, K.; Ho, D.; Rasool, H. I.; Zettl, A.; Alivisatos, a. P. 3D Motion of DNA-Au Nanoconjugates in Graphene Liquid Cell Electron Microscopy. *Nano Lett.* **2013**, *13*, 4556–4561.
393. Wang, B.; Eichfield, S. M.; Wang, D.; Robinson, J. A.; Haque, M. A. In Situ Degradation Studies of Two-Dimensional WSe2-Graphene Heterostructures. *Nanoscale* **2015**, *7*, 14489–14495.
394. Zhao, J.; Deng, Q.; Bachmatiuk, A.; Sandeep, G.; Popov, A.; Eckert, J.; Rümmeli, M. H. Free-Standing Single-Atom-Thick Iron Membranes Suspended in Graphene Pores. *Science* **2014**, *343*, 1228–1232.
395. Komsa, H.; Teng, P.; Yeh, C.; Huang, F.; Lin, Y.; Suenaga, K. Three-Fold Rotational Defects in Two-Dimensional Transition Metal Dichalcogenides̈ . *Nat. Commun.* **2015**, *6*, 6736.
396. Lee, C.; Li, Q.; Kalb, W.; Liu, X.-Z.; Berger, H.; Carpick, R. W.; Hone, J. Frictional Characteristics of Atomically Thin Sheets. *Science* **2010**, *328*, 76–80.
397. Chou, H.; Ismach, A.; Ghosh, R.; Ruoff, R. S.; Dolocan, A. Revealing the Planar Chemistry of Two-Dimensional Heterostructures at the Atomic Level. *Nat. Commun.* **2015**, *6*, 7482.
398. Fleurence, A.; Friedlein, R.; Ozaki, T.; Kawai, H.; Wang, Y.; Yamada-Takamura, Y. Experimental Evidence for Epitaxial Silicene on Diboride Thin Films. *Phys. Rev. Lett.* **2012**, *108*, 245501.
399. Howell, S. L.; Jariwala, D.; Wu, C.-C.; Chen, K.-S.; Sangwan, V. K.; Kang, J.; Marks, T. J.; Hersam, M. C.; Lauhon, L. J. Investigation of Band-Offsets at Monolayer−Multilayer MoS_2 Junctions by Scanning Photocurrent Microscopy. *Nano Lett.* **2015**, *15*, 2278–2284.
400. Tosun, M.; Fu, D.; Desai, S. B.; Ko, C.; Seuk Kang, J.; Lien, D.-H.; Najmzadeh, M.; Tongay, S.; Wu, J.; Javey, A. MoS2 Heterojunctions by Thickness Modulation. *Sci. Rep.* **2015**, *5*, 10990.
401. Wang, Y. et al. Monolayer $PtSe_2$, a New Semiconducting Transition-Metal-Dichalcogenide, Epitaxially Grown by Direct Selenization of Pt. *Nano Lett.* **2015**, *15* (6), 4013–4018.
402. Chiu, M.-H.; Zhang, C.; Shiu, H.-W.; Chuu, C.-P.; Chen, C.-H.; Chang, C.-Y. S.; Chen, C.-H.; Chou, M.-Y.; Shih, C.-K.; Li, L.-J. Determination of Band Alignment in the Single-Layer MoS2/WSe2 Heterojunction. *Nat. Commun.* **2015**, *6*, 7666.
403. Lee, C.-H.; Lee, G.-H.; van der Zande, A. M.; Chen, W.; Li, Y.; Han, M.; Cui, X.; Arefe, G.; Nuckolls, C.; Heinz, T. F.; et al. Atomically Thin P-N Junctions with van Der Waals Heterointerfaces. *Nat. Nanotechnol.* **2014**, *9*, 676–681.
404. Wu, W.; Wang, L.; Li, Y.; Zhang, F.; Lin, L.; Niu, S.; Chenet, D.; Zhang, X.; Hao, Y.; Heinz, T. F.; et al. Piezoelectricity of Single-Atomic-Layer MoS2 for Energy Conversion and Piezotronics. *Nature* **2014**, *514*, 470–474.
405. Mak, K. F.; McGill, K. L.; Park, J.; McEuen, P. L. Valleytronics. The Valley Hall Effect in MoS2 Transistors. *Science* **2014**, *344*, 1489–1492.
406. Zeng, H.; Dai, J.; Yao, W.; Xiao, D.; Cui, X. Valley Polarization in MoS2Monolayers by Optical Pumping. *Nat. Nanotechnol.* **2012**, *7*, 490–493.
407. Chen, H.; Niu, Q.; Zhang, Z.; MacDonald, A. H. Gate-Tunable Exchange Coupling between Cobalt Clusters on Graphene. *Phys. Rev. B: Condens. Matter Mater. Phys.* **2013**, *87*, 144410.
408. Parkin, S. S. P.; Friend, R. H. 3 D Transition-Metal Intercalates of the Niobium and Tantalum Dichalcogenides. II. Transport Properties. *Philos. Mag. B* **1980**, *41*, 95–112.
409. Parkin, S. S. P.; Friend, R. H. 3 D Transition-Metal Intercalates of the Niobium and Tantalum Dichalcogenides. I. Magnetic Properties. *Philos. Mag. B* **1980**, *41*, 65–93.
410. Ghimire, N. J.; McGuire, M. A.; Parker, D. S.; Sipos, B.; Tang, S.; Yan, J. Q.; Sales, B. C.; Mandrus, D. Magnetic Phase Transition in Single Crystals of the Chiral Helimagnet Cr1/3NbS2. *Phys. Rev. B: Condens. Matter Mater. Phys.* **2013**, *87*, 104403.
411. Cao, T.; Li, Z.; Louie, S. G. Tunable Magnetism and Half-Metallicity in Hole-Doped Monolayer GaSe. *Phys. Rev. Lett.* **2015**, *114*, 236602.
412. Wu, S.; Dai, X.; Yu, H.; Fan, H.; Hu, J.; Yao, W. Magnetisms in P-Type Monolayer Gallium Chalcogenides (GaSe, GaS). **2014**, *arXiv Prepr. arXiv1409.4733*.
413. Casto, L. D.; Clune, A. J.; Yokosuk, M. O.; Musfeldt, J. L.; Williams, T. J.; Zhuang, H. L.; Lin, M. W.; Xiao, K.; Hennig, R. G.; Sales, B. C.; et al. Strong Spin-Lattice Coupling in CrSiTe3. *APL Mater.* **2015**, *3*, 041515.
414. Williams, T. J.; Aczel, A. A.; Lumsden, M. D.; Nagler, S. E.; Stone, M. B.; Yan, J. Q.; Mandrus, D. Magnetic Correlations in the Quasi-2D Semiconducting Ferromagnet $CrSiTe_3$. **2015**, *arXiv1503.08199*.
415. Brec, R. Review on Structural and Chemical Properties of Transition Metal Phosphorous Trisulfides MPS3. *Solid State Ionics* **1986**, *22*, 3–30.
416. Li, X.; Cao, T.; Niu, Q.; Shi, J.; Feng, J. Coupling the Valley Degree of Freedom to Antiferromagnetic Order. *Proc. Natl. Acad. Sci. U. S. A.* **2013**, *110*, 3738–3742.
417. Li, X.; Yang, J. CrXTe3 (X = Si, Ge) Nanosheets: Two Dimensional Intrinsic Ferromagnetic Semiconductors. *J. Mater. Chem. C* **2014**, *2*, 7071.

418. Sivadas, N.; Daniels, M. W.; Swendsen, R. H.; Okamoto, S.; Xiao, D. Magnetic Ground State of Semiconducting Transition-Metal Trichalcogenide Monolayers. *Phys. Rev. B: Condens. Matter Mater. Phys.* **2015**, *91*, 235425.
419. Rodin, A. S.; Carvalho, A.; Castro Neto, A. H. Strain-Induced Gap Modification in Black Phosphorus. *Phys. Rev. Lett.* **2014**, *112*, 176801.